UNIVERSITÀ
DI SIENA
1240

University of Siena

Department of Biotechnology, Chemistry and Pharmacy

Doctoral School in Biochemistry and Molecular Biology – BIBIM 2.0
Cycle XXXIV

Coordinator of PhD School: Prof. Lorenza Trabalzini

N-acetyl-L-cysteine ethyl ester (NACET) as a potential therapeutic strategy for the prevention and treatment of Age-related Macular Degeneration

Tutor:
Prof. Federico Galvagni

PhD candidate:
Giulia Realini

Academic year: 2021/2022

Table of contents

1 ABSTRACT

Age-related macular degeneration (AMD) is a multifactorial progressive chronic ocular disease. Genetics, environmental insults, and age-related issues are risk factors for the development of the disease. Dysfunction of retinal pigment epithelium (RPE) is involved in AMD and oxidative stress in RPE is one of the major causes of the etiopathogenesis of AMD. Therefore, the introduction of antioxidants may represent one of the most effective ways to delay the onset of AMD. Glutathione (GSH) is a key player in the detoxification of xenobiotics, their metabolites and of reactive oxygen species (ROS) and consequently many drugs are currently in use as GSH enhancers. N-acetyl-L-cysteine ethyl ester (NACET) is a lipophilic and cell permeable GSH prodrug that has been proposed to delay AMD progression. Here, we reported an RNA-seq transcriptome analysis of human Retinal Pigment Epithelial cells (ARPE-19) and described for the first time that NACET induces transcriptional activation of nuclear factor erythroid 2-related factor 2 (NRF2) target genes. NRF2 is a transcription factor that allows the maintenance of redox homeostasis by binding to the antioxidant responsive elements (ARE) in the upstream promoter region of many antioxidative genes and thereby inducing their transcription. By means of HPLC analysis, RT-qPCR, Western blot analysis, CRISPR-Cas9 gene editing and luciferase assay, we validated the transcriptome analysis and demonstrated that NACET increases the intracellular level of free cysteine and promotes transcriptional activation of NRF2 target genes through inhibition of NRF2 degradation. Moreover, using transcriptional profiling of retina of young and old mice orally treated with NACET, we showed that NACET rescued 57 genes impaired by aging, many of which have been correlated with retinal dysfunctions. Our study suggests that NACET, as cysteine and GSH precursor and as NRF2 activator, may be a useful tool for the treatment of oxidative stress-related retinal diseases. Although we tested NACET focusing on AMD, we also verified that NACET-induced NRF2 activation is not cell-context dependent, suggesting that NACET may be a promising agent for prevention/treatment of any pathology where oxidative stress is involved.

2 INTRODUCTION

2.1 The visual sense organ

Vision is one of the most important sensory systems responsible for the perception of visual stimuli. The visual system allows to discriminate location, shape, size, colour, reliefs, movements of what is observed. The mechanism that allows the vision of what surrounds us is very complex, in fact, the visual process involves an elaborated system of structures, each of which is designed for a specific function. The process of sight and visual perception converts environmental information in the form of light into electrical signal, to analyses and interprets it. The visual system includes the anterior segment of the eye, which serve to focus light on the retina (in order composed of the cornea, the aqueous humor, and the lens) and the posterior segment, which receives and transforms the light signals into electrical signal (in order composed of the vitreous body, the retina, and the optic nerve). Finally, it includes the optic tracts and optic radiations, transmitting neural signals through the optic nerve to a specific area of the brain, the visual cortex, and several additional nuclei of the brain (Figure 1A-B). Highly specialized cells called photoreceptors (PRs) are present on the retina (about 6 million cones and 120 million rods) and transform light stimuli into nerve impulses. Cones respond to high levels of light intensity, while rods respond to low levels of intensity bright. These nerve impulses are then transmitted to the visual cortex, responsible for decoding them (Hejtmancik & Nickerson, 2015; Lee Ann, 2012; Nissen & Röpke, 2005; Sung & Chuang, 2010).

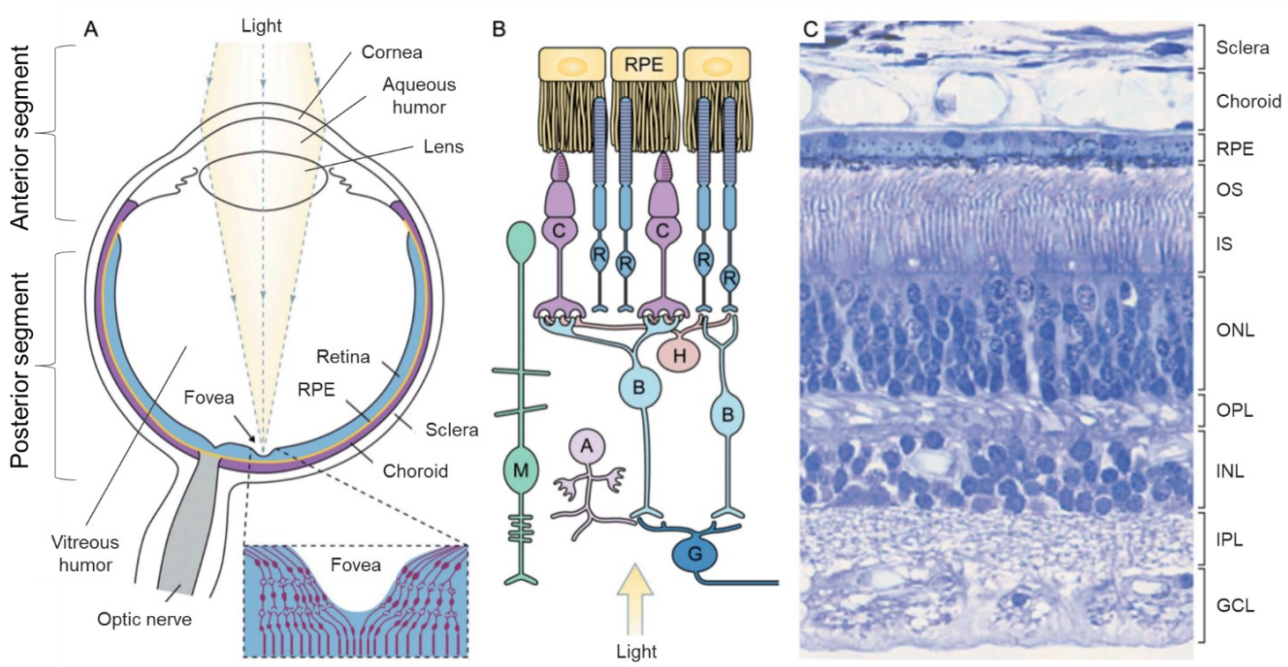

Figure 1. Overview of the visual sense organ. (A) Diagrams of the eye; an enlarged diagram of the fovea is shown in the box. Retina forms the inner lining of most of the posterior part of the eye. The RPE is sandwiched between the retina and choroids, a vascularized and pigmented connective tissue. (B) Diagram of the organization of retinal cells. R, rod; C, cone; B, bipolar cell; H, horizontal cell; A, amacrine cell; G, ganglion cells; M, Müller cell. (C) An H&E-stained

transverse section of human retina. Retina has laminated layers. The nuclei of the photoreceptors constitute the outer nuclear layer (ONL). The nuclei of the bipolar cells, amacrine cells, horizontal cells, and Müller glial cells are found in the inner nuclear layer (INL), and the nuclei of ganglion cells form the ganglion cell layer (GCL). The outer plexiform layer (OPL) contains the processes and synaptic terminals of photoreceptors, horizontal cells, and bipolar cells. The inner plexiform layer (IPL) contains the processes and terminals of bipolar cells, amacrine cells, and ganglion cells. The processes of Müller glial cells fill all space in the retina that is not occupied by neurons and blood vessels. Figure adapted from Sung & Chuang, 2010.

Each component of the visual system is critical for correct vision. This implies that each part of the visual system and each molecule in the various metabolic and functional pathways must function correctly and interact seamlessly in carrying out visual perception. Indeed, the homeostasis biological systems of the cells in the visual system have to protect and preserve vision over the lifetime of the individual to prevent age-related eye disorders, such as cataract, diabetic retinopathy (DR) and age-related macular degeneration (AMD) (Hejtmancik & Nickerson, 2015; Lee Ann, 2012; Nissen & Röpke, 2005; Sung & Chuang, 2010).

2.1.1 Retina

The third and inner coat of the eye is the retina, which is the light-sensitive part of the eye. It includes the macula, the area at the posterior pole responsible for central high-resolution visual acuity, that contains most of photoreceptors located within the retina. Under light microscopy, the retina shows to have 10 distinct layers (Figure 1C), which are rather three layers of neuronal cell bodies and a single layer of pigmented epithelium, between which lie their processes and synapses. The 10 so-called retinal layers are:

1. Inner limiting membrane (ILM): is a basement membrane secreted by Müller cells, it forms the boundary to the vitreous.
2. Nerve fibre layer (NF): contains the axons of the ganglion cell.
3. Ganglion cell layer (GCL): consists of the cell bodies of the ganglion cells.
4. Inner plexiform layer (IPL): is formed by the synapses between amacrine cells, ganglion cells and bipolar cells.
5. Inner nuclear layer (INL): contains the nuclei of amacrine cells, bipolar cells, horizontal cells, and glial Müller cells.
6. Outer plexiform layer (OPL): is composed of the processes and synaptic terminals of photoreceptor cells (rods and cones), horizontal cells and bipolar cells.
7. Outer nuclear layer (ONL): consists of photoreceptors cell bodies.
8. External limiting membrane (ELM): is not a real membrane, but an optical phenomenon caused by the junctions between the photoreceptor inner segments and the Müller cells.
9. Inner segment (IS) / outer segment (OS): is the photoreceptor layer, consists of inner and outer segments of rods and cones.

10. Retinal pigment epithelium (RPE): is the outermost layer of the retina, the closest to the choroid, composed of a single layer of epithelial cells.

Bruch's membrane (BrM) is an extracellular matrix located between the RPE and the choroid, it plays an essential role as structural and functional support to the RPE. The BrM acts as a barrier between the choriocapillaris and RPE and helps in the diffusion of molecules across the retina. Dysfunctions of Bruch's membrane have been found in AMD and other ocular diseases and are caused mostly by deposit formation, extracellular matrix degeneration, and angiogenesis (Lee Ann, 2012; Murali et al., 2020; Nissen & Röpke, 2005; Sung & Chuang, 2010).

2.1.2 Retinal pigment epithelium

RPE is a single-cell layer of polarized pigmented hexagonal cells, that lies between the neural retina and the choroid (Figure 2). Each cell of RPE consists of a basal non-pigmented part containing the nucleus adjacent to the choroid and an apical pigmented portion which extends between the rods. The RPE has a variety of functions. It is responsible for absorption of scattered light by the abundant melanin granules, improving the quality of the optical system and reducing the photo-oxidative energy. The RPE cells have tight junctions between their lateral surfaces, functioning as a selective blood-retinal barrier that controls the transports from the choriocapillaris to the retina. RPE supplies nutrients, ions, and metabolites to PRs, controls ion homeostasis and removes waste products from the retina. Because PRs are constantly exposed to photo-oxidative stress, another important function of RPE is the phagocytosis of the outer segments of photoreceptors. All these RPE functions are essential for retinal homeostasis, and consequently dysfunctions of the RPE are found in AMD, DR and retinitis pigmentosa (RP) (Caceres & Rodriguez-Boulan, 2020; Lee Ann, 2012; Lehmann et al., 2014).

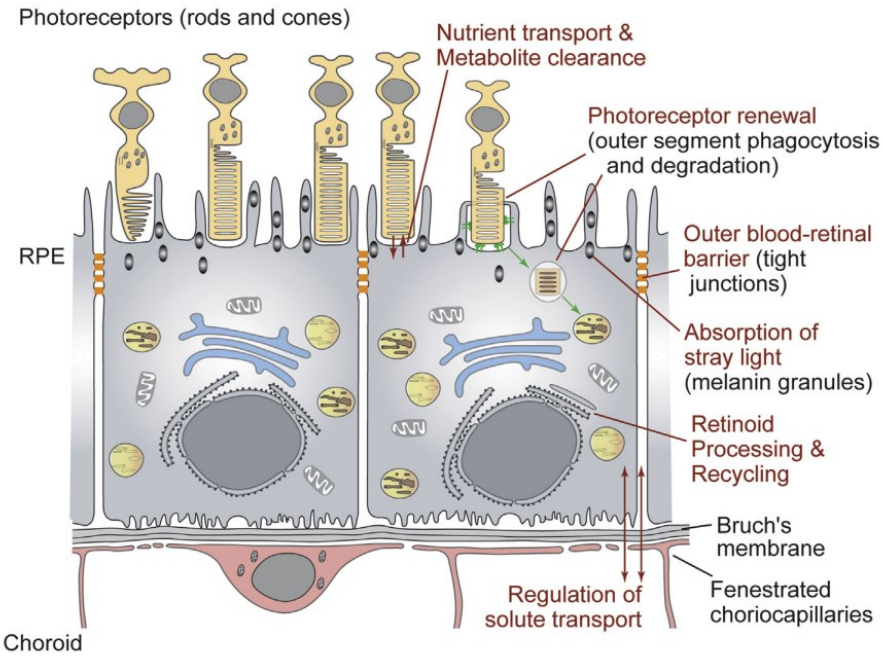

Figure 2. Schematic representation of the support functions of RPE. From Lehmann et al., 2014.

2.2 Age-related Macular Degeneration

AMD is a progressive chronic ocular disease, characterized by a gradual deterioration of the macula, the area of retina responsible for central and sharp vision (Kauppinen, 2020). This pathology is the third leading cause of irreversible blindness worldwide and the primary leading cause of vision loss in the Western world. As the term implies, it affects elderly individuals and its incidence and prevalence are set to rise due to global demographic shift towards an ageing society (Miller et al., 2017) (Lim et al., 2012) (Chakravarthy et al., 2010). The sclerosis of the vessels located under the retina (choroid), the accumulation of lipids and the alterations of the metabolism of the RPE contribute to the macular degenerative process. In these conditions the physiological metabolism of the retina is prevented. AMD is classified into two forms: wet (neovascular or exudative) and dry (atrophic or nonexudative). AMD is characterized by the presence of drusen, extracellular depositions accumulating between BrM and the RPE. In wet AMD in addition to these lesions, there is an abnormal blood vessel growth or choroidal neovascularization. In the case of wet AMD, anti-vascular endothelial cell growth factor (anti-VEGF) treatments by intravitreal injections are available as a therapy, while no effective treatments are available for dry AMD, with an increasing prevalence of the disease, leading to retinal atrophy. Dietary intake of antioxidants, such as zinc, vitamin C, vitamin E and beta-carotene is prescribed to patients with dry AMD to reduce the risk of the disease developing into wet form. This lack of prevention and treatment for dry AMD, that leads to photoreceptor dysfunction, death, and vision loss, underscores the importance of gaining a better knowledge regarding its pathobiology (Handa et al., 2019; Taylor et al., 2016).

2.3 Risks factors of AMD

The development of advanced AMD has multifactorial risk factors (Figure 3). Age is the strongest demographic risk factor associated with AMD. The risk of acquiring AMD increases more than threefold in patients older than 75 years compared to patients between 65 and 74 years of age (Al-Zamil & Yassin, 2017; Lambert et al., 2016). Risks factors of AMD include darker iris pigmentation, previous cataract surgery, and hyperopic refraction. About lifestyle: diet high in fat and cholesterol, cigarette smoking, obesity, excessive sunlight exposure, high blood pression and cardiovascular diseases are ocular risk factors (Lim et al., 2012). All these risk factors are linked to the induction of oxidative stress, which is consequently thought to be a major influence in AMD pathophysiology (Heesterbeek et al., 2020; Lim et al., 2012).

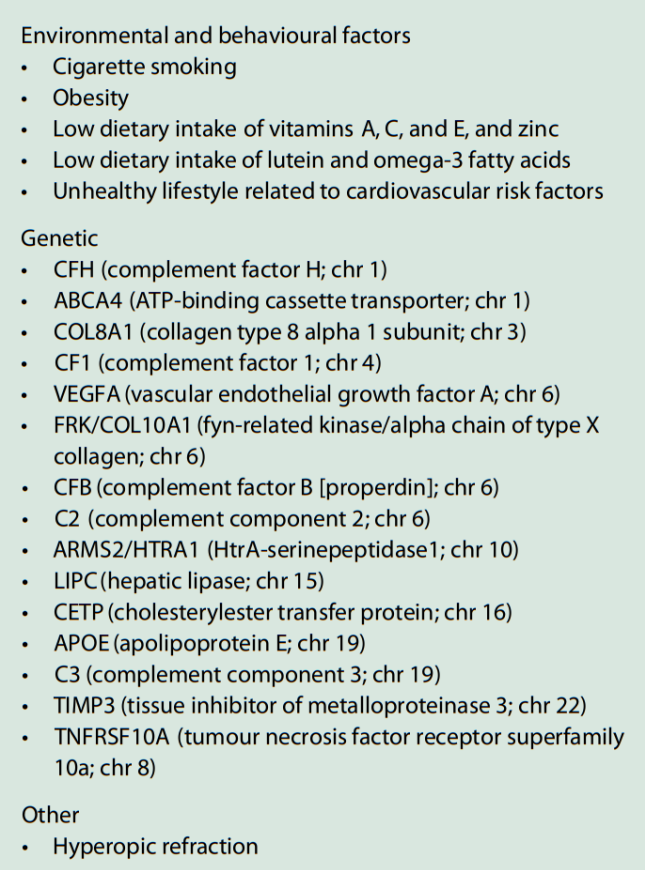

Figure 3. Summary of the risk factors for AMD. From Lim et al., 2012.

There has been strong evidence that genetic factors play an important role in the development of AMD. A large genome-wide study reveals that 52 independently associated common and rare variants, distributed across 34 loci, can explain more than half of the genomic heritability. These variants are mostly involved in the complement system (e.g. CFH), extracellular matrix remodelling (e.g. ARMS2/HTRA1) and lipid metabolism (e.g. APOE) (Fritsche et al., 2016; Heesterbeek et al., 2020).

2.3.1 Aging and AMD

The human biological fitness is conserved by stress response, maintenance, and repair pathways. These cellular pathways include nutrients and energy signaling, DNA damage response (DDR), mitochondrial quality control (mtQC), telomere shortening, capability to combat oxidative stress and metabolize toxic species. The efficacy of these pathways decreases with aging. Aging can be defined as a progressive time-dependent accumulation of cellular insults or damage, consequently resulting in degeneration and functional decline of the organism. The process of aging is not only associate

with several impaired cellular responses, but also with diverse stress coming from environmental factors. Thus, age-associated changes in the cells may induce senescence and lead to several disorders named as age related disease, such as AMD (Blasiak et al., 2020; Sharma et al., 2014). The accumulation of senescent cells due to persistent stress is a major driver of AMD pathogenesis (Figure 4). Various exogenous and endogenous factors as oxidative stress, DNA damage, inflammatory cytokines, telomere shortening, and metabolic dysfunction can promote cellular senescence, accelerating the expansion of AMD-like changes (Lee et al., 2021).

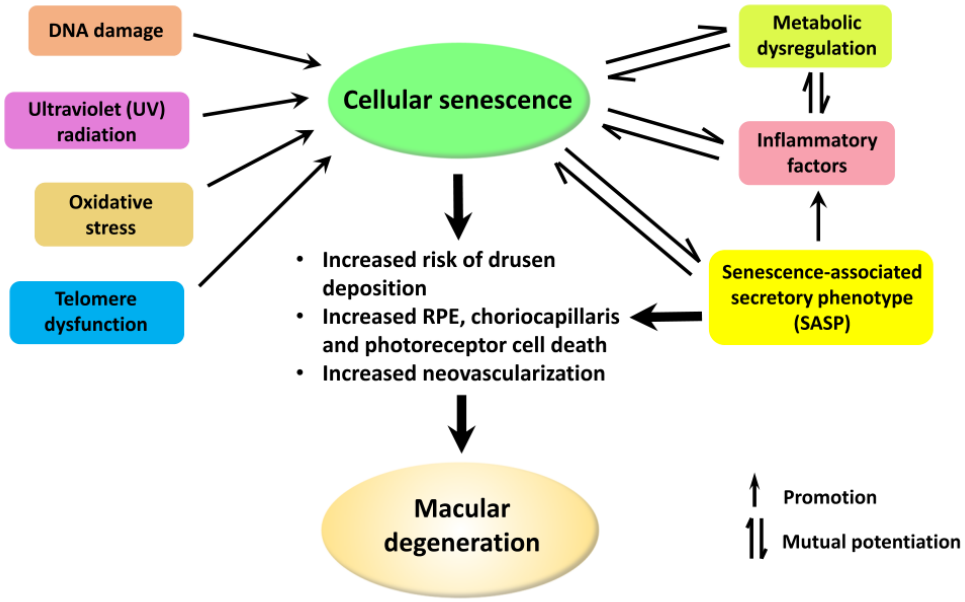

Figure 4. Etiology and consequences of cellular senescence contributing to AMD. Cellular senescence is highly relevant to AMD pathogenesis. From Lee et al., 2021.

Cellular senescence is a cell state characterized by an irreversible arrest of cell division, trigged by stressful insults and a variety of endogenous and exogenous stimuli. This state of stable cell-cycle arrest is accompanied by a secretory features, macromolecular damage, and altered metabolism. The Senescence-Associated Secretory Phenotype, also called SASP, entails the secretion of proinflammatory signals in the tissue microenvironment and contributes to age-related conditions. Senescence may be induced by many factors important for AMD pathogenesis and results in SASP, that releases growth factors, cytokines, chemokines, proteases, and other molecules inducing inflammation and other AMD-related effects. These effects can be induced in the affected cell and neighbouring cells, leading to progression of AMD phenotype (Figure 5) (Blasiak, 2020; Cuollo et al., 2020; Gorgoulis et al., 2019; Lee et al., 2021).

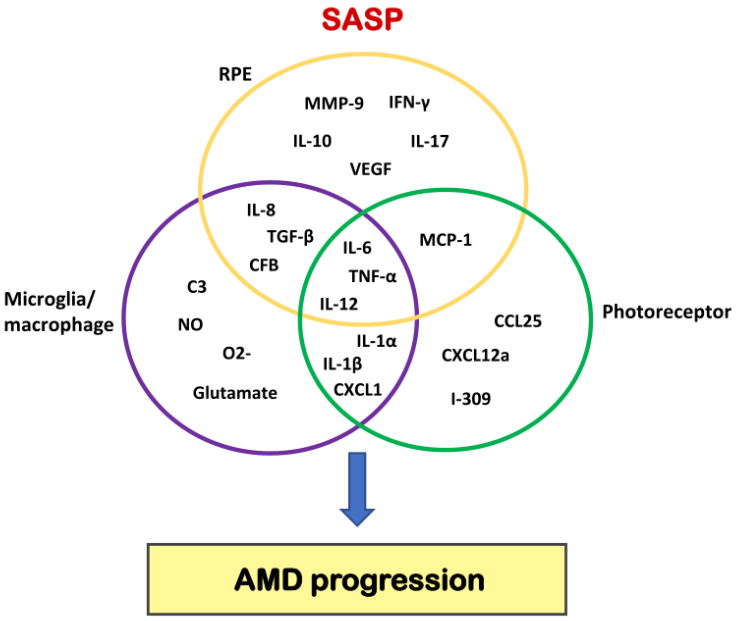

Figure 5. SASP during progression of AMD. Numerous SASP factors, such as IL-6, IL-12, TNF-α, IFN-γ, and IL-8, are released from the senescent retinal cells. ROS, in tandem with damaged DNA, further promote the age-related decline in RPE and photoreceptors resulting in a feedforward cycle of damage. Signaled by the SASP-chemokines released into the tissue environment, immune cells extravasate from the blood vessels, infiltrate the retina, and release SASP components, contributing to a chronic inflammation and other AMD-related pathologies. Adapted from Lee et al., 2021.

SASP arising from chronic senescence is a master and protracted source of the chronic inflammation typical in aging (Lee et al., 2021). In fact, aging is frequently associated with a dysregulation of the immune system, leading to a chronic low grade systemic pro-inflammatory state of the organism, a process that has been called "inflammaging" (Franceschi et al., 2000). It's well known that inflammaging is associated with an over-abundance of reactive oxygen species (ROS), which can induce oxidative stress, that cause damage on the primary cellular components including lipids, proteins, and DNA and increase inflammation (Zuo et al., 2019). It is evident that oxidative stress and the consequent activation of pro-inflammatory pathways is a key component in the pathogenesis of many age-related diseases, such as AMD (Finkel & Holbrook, 2000; Lee et al., 2021; Reuter et al., 2010).

2.3.2 Oxidative Stress and AMD

Cells are constantly exposed to environmental (xenobiotics, drugs, and UV) and endogenous (reactive oxygen species (ROS), hydroperoxides and quinone) stressors. Oxidative stress is defined as an imbalance between production of free radicals and reactive metabolites, so-called oxidants or ROS, and their elimination by protective mechanisms, referred to as antioxidants. If unchecked, oxidative stress leads to damage of important biomolecules and cells, with potential impact on the whole organism and diseases of many organs, including eyes (retinal damage and cataract) (Niture et al., 2014; Reuter et al., 2010). The RPE cells in young individuals alleviate stressors generation by the

elimination of dysfunctional mitochondria, via mitophagy, and by increasing antioxidant system. The antioxidant defences consist of enzymes and non-enzymatic molecules. Amongst the latter are included low molecular-weight compounds, as vitamins C and E, β-carotene, and glutathione. Most of the enzymatic antioxidant defences (i.e., superoxide dismutase, catalase, and the enzymes responsible for glutathione metabolism) are regulated by the transcription factor nuclear factor erythroid 2-related factor 2 (NRF2). The retina is one of the highest oxygen-consuming tissues in the human body. In addition, photons striking the retina not only activate the visual pigments but can also form ROS, eventually affecting nearby molecules. The elevated metabolic activity together with the exposure to visible light makes the retina one of the highest oxidative environments in the body (Marazita et al., 2016). This combination together with the aging process, increase the amount of ROS generated by RPE, arising the oxidative stress. Thus, natural and synthetic Nrf2-activating compounds have been tested as potential therapeutic agents for AMD (Bellezza, 2018).

2.4 NACET as Cysteine pro-drug

Oxidative stress plays a major role in the etiopathogenesis of retinal diseases, including AMD and DR. Therefore, it is easy to understand how important the introduction of antioxidants could be to delay the onset of oxidative stress-related diseases and reduce the risk of their progression (Tosi et al., 2021). Several drugs are currently in use as glutathione (GSH) enhancers, which is the ubiquitous antioxidant that regulates ROS. Since cysteine (Cys) is the limiting substrate in GSH synthesis (Figure 6), the most common way to increase GSH levels in cells is to provide them with Cys or with a source of this molecule.

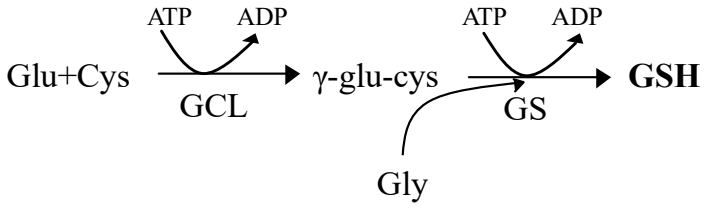

Figure 6. GSH is synthesized by an ATP-dependent two-step process. The first step is catalysed by glutamate-cysteine ligase (GCL), which is composed of catalytic and modifier subunits (GCLC and GCLM). This step conjugates cysteine with glutamate, generating γ-glutamylcysteine. The second step is catalysed by GSH synthase (GS), which adds glycine to γ-glutamylcysteine to form γ-glutamylcysteinylglycine or GSH. Adapted from Marí et al., 2010.

Several cysteine derivatives have been proposed to this aim. To achieve high in-vivo efficacy of an antioxidant, it is essential that the agent be able to penetrate the tissues and cells, and lipophilicity governs cellular penetrance. Out of many antioxidant candidates, N-acetyl-L-cysteine (NAC) is the most widely used, even though it has low lipophilicity and bioavailability, which can be increased by the esterification of the carboxyl group to produce N-acetyl cysteine ethyl ester (NACET). It has been demonstrated that differently from NAC, NACET effectively raises the intracellular levels of

cysteine, γ-glutamylcysteine and GSH, because it freely crosses the plasma membrane and inside the cell, it is de-esterified to the more hydrophilic NAC, which, in turn, is trapped into the cell and slowly transformed into cysteine. The higher availability of cysteine is matched by an increase in GSH synthesis (Figure 7) (Giustarini et al., 2012, 2018; Kularatne et al., 2020).

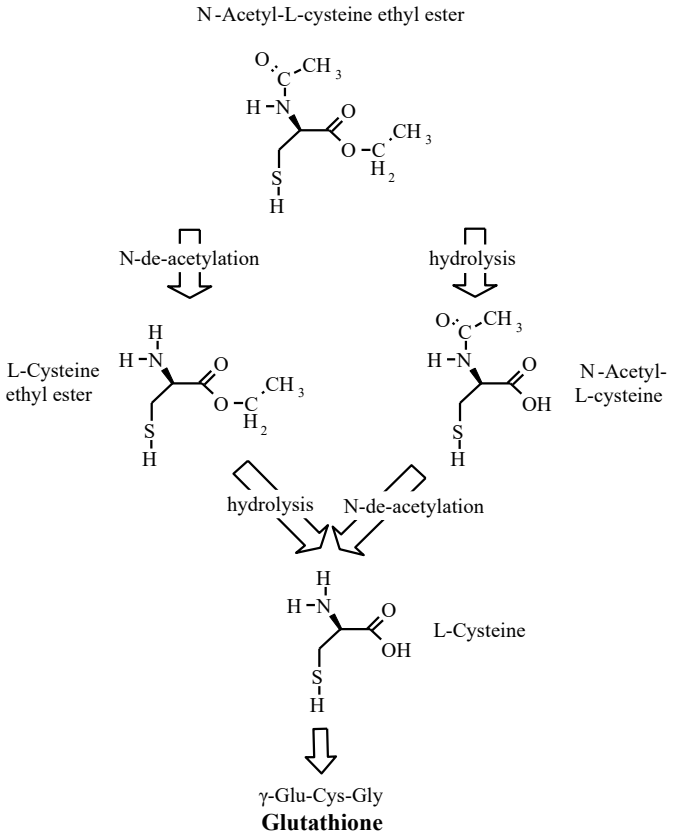

Figure 7. Structural formulas of N-acetylcysteine ethyl ester (NACET), of its products of N-de-acetylation cysteine ethyl ester (CET) and hydrolysis NAC. The final common metabolite, Cys, is supplied for the synthesis of the tripeptide glutathione (GSH). Adapted from Giustarini et al., 2012

Recently, it has been demonstrated that NACET increases the viability in oxidative stressed RPE cells more effectively than NAC by directly and more rapidly reacting with oxidizing agents. Moreover, pre-treatment with NACET, but not NAC, predisposes RPE cells to oxidative stress resistance and increases the intracellular reduced GSH. Furthermore, NACET increases GSH levels in rats' eyes after oral administration (Tosi et al., 2021). Therefore, the use of NACET to treat stress-related retinal disorders, such as AMD, might be promising.

2.5 NRF2 signaling pathway

2.5.1 NRF2

The transcription factor NRF2 is a master regulator of the cellular xenobiotic and oxidative stress response. NRF2 is encoded by *NFE2L2* gene, it belongs to the Cap 'n' Collar (CNC) transcription factor subfamily and contains a basic leucine zipper DNA binding domain (b-Zip) at the C terminus.

NRF2 contains six highly conserved domains named Nrf2-ECH homology (Neh) domains (Figure 8). The bZip in Neh1 domain allows NRF2 to heterodimerize with small musculoaponeurotic fibrosarcoma (sMaf) proteins The heterodimer complex binds the Antioxidant Response Elements (ARE) sequence and promotes the expression of downstream antioxidant and detoxifying genes. Neh2 domain, through ETGE and DLG motifs, interacts with the repressor Kelch-like-ECH-associated protein 1 (KEAP1), which promotes NRF2 ubiquitination and proteasomal degradation. The Neh3 domain binds to the chromo-ATPase/helicase DNA-binding protein family member CHD6, which functions as an Nrf2 transcriptional coactivator. Neh4 and Neh5 domains function as two transactivation domains by interacting with CREB-binding protein (CBP). Neh6 contains a degron for KEAP1-independent NRF2 degradation through the interaction with β-transducin repeat-containing protein (β-TrCP), which is in complex with the S-phase kinase-associated protein 1 (Skip1)-Cul1-Rbx1 E3 ubiquitin ligase. Finally, the Neh7 domain is involved in the repression of NRF2 transcriptional activity interacting with retinoid X (RXRs) and retinoic acid (RARs) receptors, which prevent the binding of the transcription co-activators to the Neh4 and Neh5 domains (Jaramillo & Zhang, 2013; H. Lin et al., 2020; S. Wu et al., 2019).

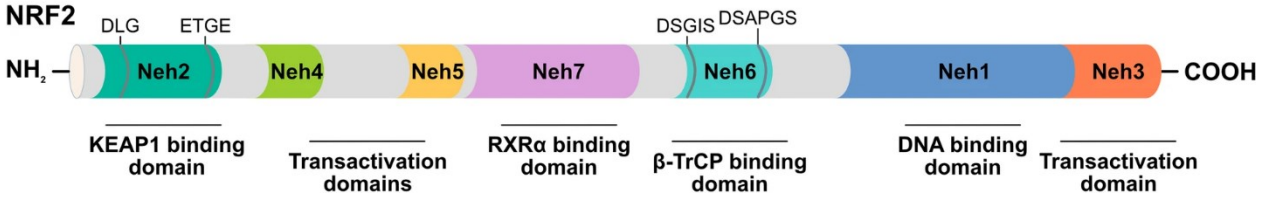

Figure 8. Domain structure of the human NRF2 proteins. Functional domains, relevant motifs (DLG, ETGE, DSGIS, DSAPGS). Neh1–7: NRF2-ECH homology 1–7. From Bono et al., 2021.

2.5.2 KEAP1-dependend NRF2 regulation

KEAP1, the main intracellular regulator of NRF2, contains the broad complex-tramtrack-bric a brac (BTB) domain that directly binds to Cul3-based E3 ligase and mediates the KEAP1 homodimerization, which is required for its NRF2 inhibitory function (Figure 9). The intervening region (IVR) domain functions as a sensor to recognize and react with electrophiles. Finally, the two

glycine repeat (DGR) domains and C-terminal region (CTR) mediates the interaction with the ETGE and DLG motifs in Neh2 domain of NRF2 (Bellezza et al., 2018; H. Lin et al., 2020).

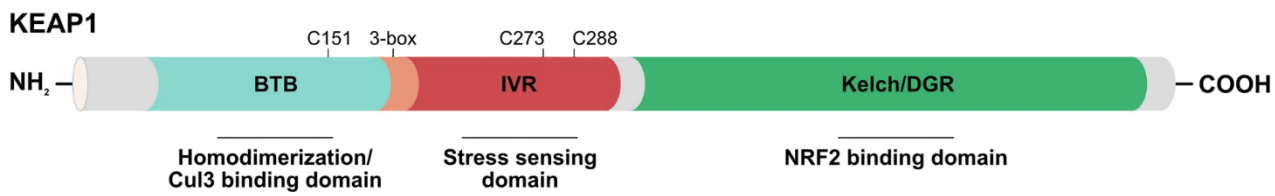

Figure 9. Domain structure of the human KEAP1 proteins. Functional domains, relevant motifs, 3-box and the most important cysteine residues (C151, C273, C288) involved in stress sensing are displayed. BTB: Broad complex/Tramtrack/Bric à Brac, IVR: intervening region, DGR: double glycine region. From Bono et al., 2021.

Under basal condition, KEAP1 homodimerizes through the BTB domain and constitutively interacts with NRF2. KEAP1 also binds E3 ubiquitin ligase Cullin-3 (CUL3) to form a complex that ubiquitinates NRF2 and promotes its 26S proteasomal degradation. Therefore, KEAP1-mediated high turnover keeps NRF2 basal levels very low and NRF2 has a short half-life of approximately 10–30 min. Upon exposure to oxidative stress or xenobiotic compounds, the reactive cysteine residues of KEAP1 are modified, leading to a conformational change of its structure that prevents NRF2 degradation. In this way, de novo-synthesized NRF2 accumulates and translocates into the nucleus, forms heterodimer with sMAFs and binds to ARE/ electrophile responsive elements, thereby promoting the transcription of multiple target genes. NRF2 regulates the expression of genes involved in several processes, such as antioxidant response, drug detoxification, cellular metabolism, and inflammation. Once the cellular stress is recovered, NRF2 is dissociates from the ARE sequence, KEAP1 enters into the nucleus and escorts NRF2 out to the cytoplasmic Cul3-E3 ubiquitin ligase

machinery for degradation (Figure 10) (Cloer et al., 2019; Tonelli et al., 2018; S. Wu et al., 2019; W. L. Wu & Papagiannakopoulos, 2020).

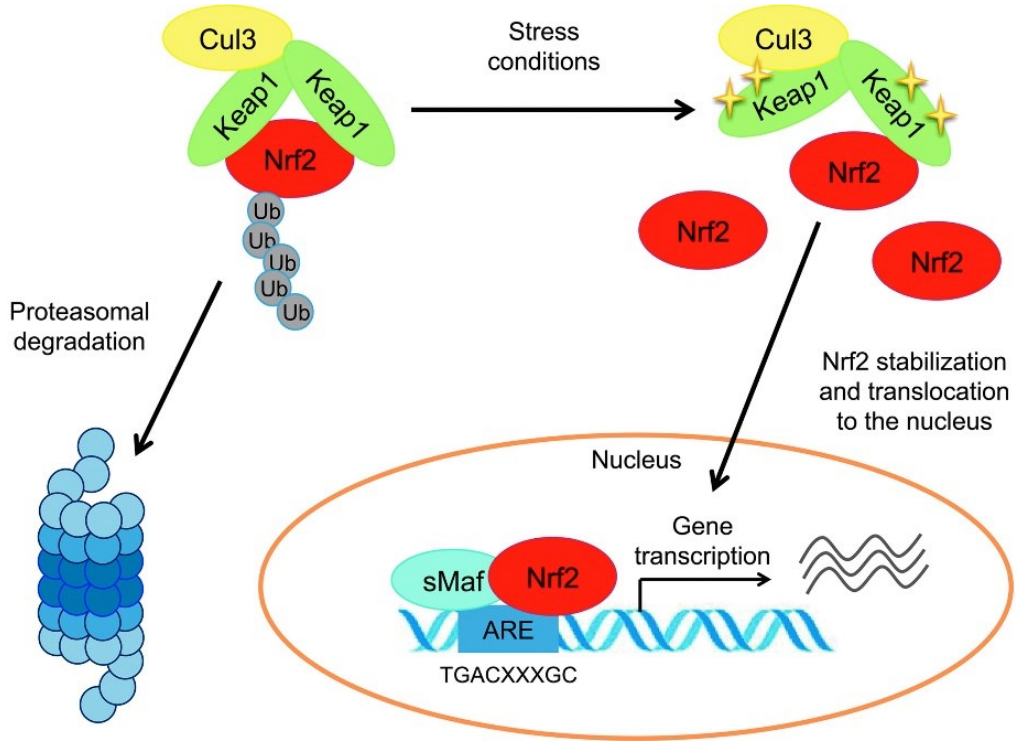

Figure 10. Representation of Nrf2 activation and response. Under unstressed conditions, Keap1 interacts with Nrf2, which is constantly ubiquitylated by the Cul3 E3 ubiquitin ligase and subsequently degraded by the proteasome. In response to stress, Keap1 is inactivated, resulting in Nrf2 stabilization and release. Nrf2 enters the nucleus where it heterodimerizes with the transcriptional activator small Maf proteins and induces expression of target genes that contain the ARE motif. From Tonelli et al., 2018.

2.5.3 KEAP1-independent NRF2 regulation

Recent advances have identified novel mechanism regulating NRF2 degradation. In addition to the very well-known regulation by KEAP1, three kinds of E3 ubiquitin ligases have been found to participate in the KEAP1-independent degradation of NRF2: β-transducin repeat-containing protein (β-TrCP), DDB1 and Cullin4 associated factor 11 (DCAF11, also referred to as WDR23), and HMG-CoA reductase degradation 1 homolog (Hrd1). β-TrCP recognizes and ubiquitylates the Neh6 domain of NRF2 phosphorylated by glycogen synthase kinse-3 (GSK-3), leading to proteasome degradation of NRF2 by Skp1-Cul1/Rbx1 complex. Ligands of tyrosine kinase, G protein-coupled, metabotropic, and ionotropic receptors that activate phosphatidyl inositol 3-kinase (PI3K)/ATK and canonical WNT are signaling pathways that participate to NRF2 regulation by GSK-3/β-TrCP (Figure 11). DCAF11 and DDB1-Cul4/Roc1 bind to the Neh2 domain of NRF2 to mediate its degradation (Figure 12). Finally, a recent study demonstrated that the multipass Endoplasmic reticulum (ER) membrane protein Hrd1, also called synoviolin, is up-regulated in response to ER stress and mediates the degradation of NRF2 (Cuadrado, 2015; Lo et al., 2017; Park et al., 2019; T. Wu et al., 2014).

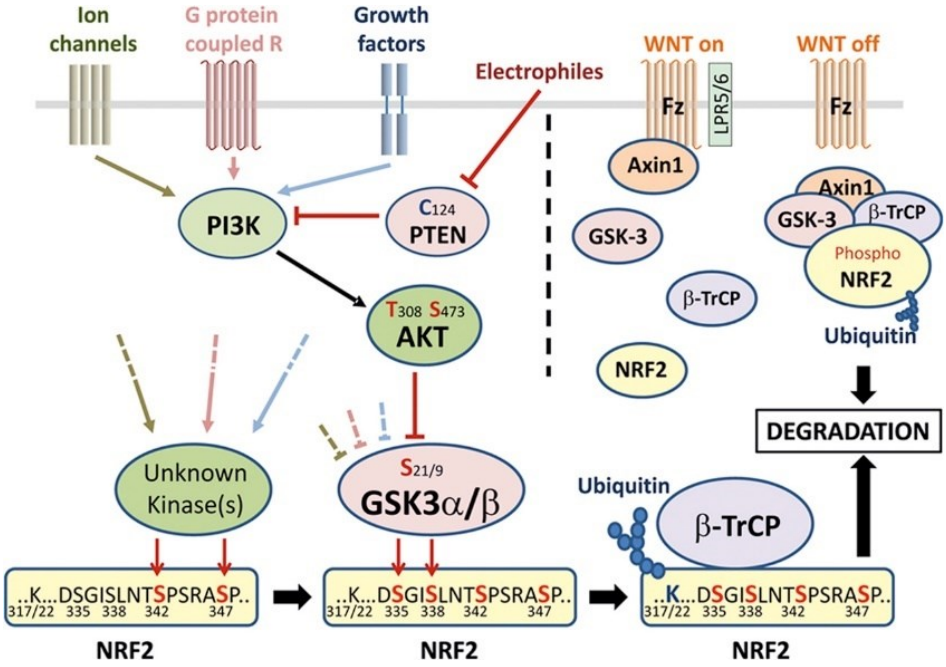

Figure 11. Signaling pathways that participate in regulation of the GSK3/βTrCP/Nrf2 axis. Ion channels, G protein coupled receptors, growth factors and electrophiles share the regulation of the survival pathway represented by PI3K/AKT. An unknown kinase(s) primes the Neh6 domain of Nrf2 for further phosphorylation by GSK3 at S335 and S338, creating a degradation domain that is recognized by β-TrCP and leads to Cullin1/Rbx1 ubiquitination. In the absence of WNT-3A, a pool of Nrf2 is found in a complex with Axin1, GSK-3, and β-TrCP and sent to proteasome degradation. In the presence of WNT-3A, this complex is disassembled and Nrf2 is stabilized. From (Cuadrado, 2015).

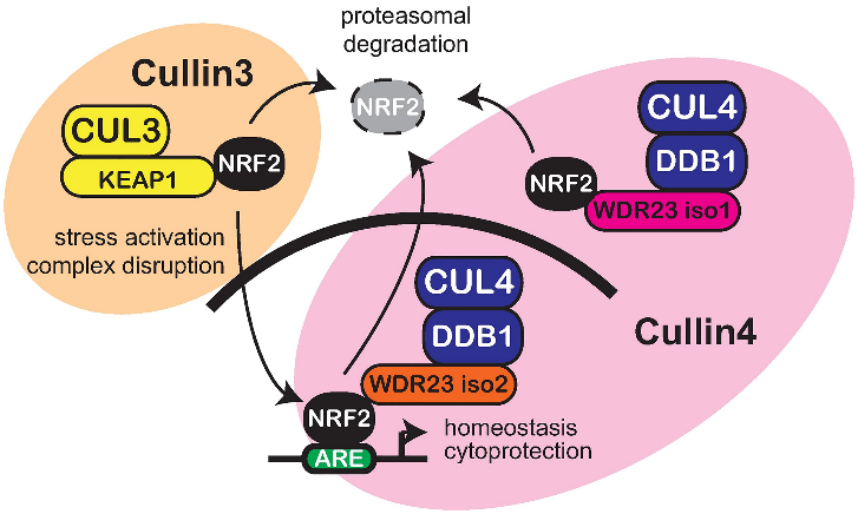

Figure 12. WDR23 and KEAP1 pathways coordinate NRF2 regulation. Model for the shared regulation of NRF2 by the cytoplasmic Cullin3 E3-ubiquitin ligase complex (CUL3-KEAP1) and the nuclear and the cytoplasmic Cullin4 E3-ubiquitin ligase complexes (CUL4-DDB1-WDR23). From (Lo et al., 2017).

2.5.4 NRF2-ARE signaling pathway

The NRF2-sMaf complex binds, in a sequence-specific manner, to the antioxidant response element (ARE), that are *cis*-regulatory element in the promoter region of several genes encoding cytoprotective and detoxification proteins. The core sequence of ARE includes 5'- TGACNNNGC-

3'. NRF2 is a pleiotropic transcription factor that induces the expression of genes involved in glutathione metabolism, NADPH regeneration, thioredoxin metabolism (e.g., thioredoxin-1, or TXN1), drug biotransformation and efflux multidrug resistance–associated proteins (e.g., ATP Binding Cassette Subfamily C Member 1, or ABCC1), and enzymes involved in iron accumulation and ferroptosis (e.g., Heme Oxygenase 1, or HMOX) (Figure 13) (Tonelli et al., 2018; W. L. Wu & Papagiannakopoulos, 2020).

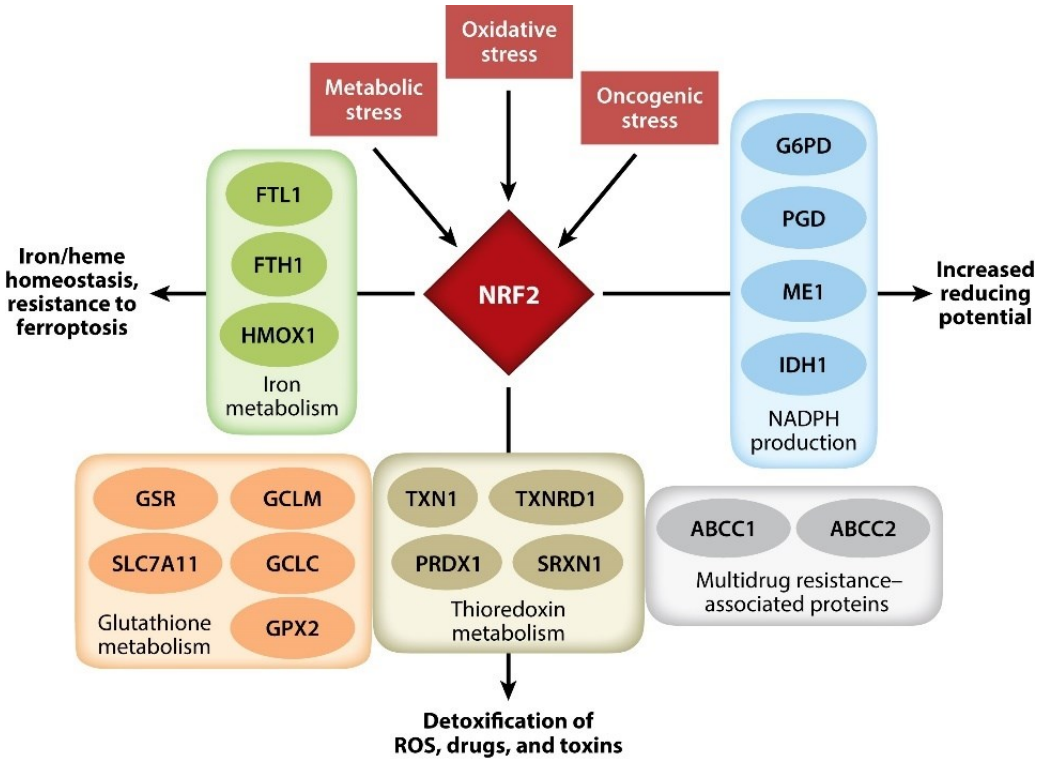

Figure 13. Downstream targets regulated by Nrf2. Oxidative stress, metabolic stress, and various oncogenic stress signals activate NRF2 response. NRF2 is a pleiotropic transcription factor that induces the expression of: Glutathione (GSR, GCLC, GCLM, GPX2, and SLC7A11), multidrug resistance–associated proteins (ABCC1 and ABCC2), and thioredoxin (TXN1, PRDX1, TXNRD1, and SRXN1) metabolism proteins mediate detoxification of ROS, drugs, and toxins. The glucose-dependent pentose phosphate pathway enzymes (G6PD), 6-phosphogluconate dehydrogenase (PGD) and the central carbon metabolism enzymes ME1 and IDH1 increase the reducing capacity of cells by regenerating NADPH. Heme degradation by HMOX1 and iron sequestration by FTL1 and FTH1 maintain heme and iron homeostasis, preventing iron accumulation and ferroptosis. From W. L. Wu & Papagiannakopoulos, 2020.

2.5.5 The antiporter system Xc^-

A well-known gene regulated by NRF2 is SLC7A11, that codes for the 'transporter proper' subunit xCT in the cystine/glutamate exchange system Xc^-. The Xc^- is a member of the heteromeric amino acid transporters (HATs) and is composed of two chains linked by a disulphide bridge: the heavy chain 4F2hc subunit (SLC3A2), which anchors the antiporter to the membrane, and the light chain xCT subunit (SLC7A11), which is responsible for the cystine-glutamate exchange (Figure14) (Martis et al., 2020). The capability of cells to synthesize GSH depends mainly on cysteine availability. The system Xc^- mediates the Na^+ -independent exchange of extracellular cystine into cells coupled to the

efflux of intracellular glutamate. Cystine is rapidly reduced intracellularly to cysteine, which represents the rate-limiting factor of GSH synthesis. Therefore, the system Xc^- is a critical regulator of cellular homeostasis, maintaining extracellular cysteine/cystine redox balance, GSH synthesis and controlling of extracellular glutamate levels. Thus, strategies to induce the expression of this exchanger have a direct impact to the RPE cells biology and on their ability to respond to oxidative stress, hence its therapeutic potential in preventing or slowing down the progression of oxidative damage-related ocular pathologies (Ananth et al., 2020; Martis et al., 2020).

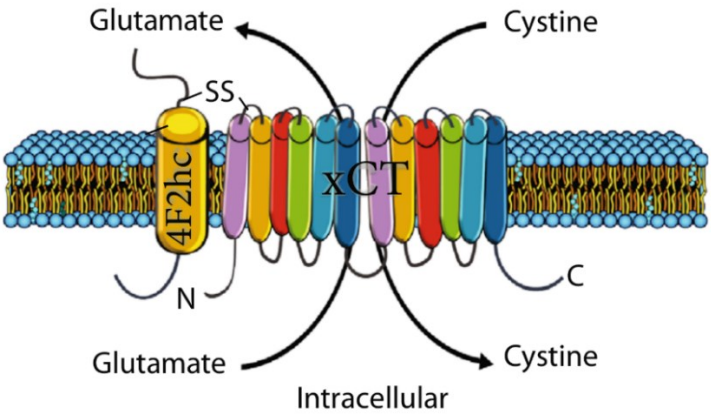

Figure 14. Structure of system Xc^-. Formed by two subunits: 4F2hc and xCT linked by a disulphide bond (SS). 4F2hc spans the membrane once and is responsible for anchoring the antiporter to the membrane. xCT contains 12 transmembrane domains with the C- and N-terminal located intracellularly. From Martis et al., 2020.

Many studies have demonstrated that induction of xCT expression by agents, such as nitric oxide, resulted in increased cystine uptake and increased GSH levels in whole cultured retinas from the mouse and rat, isolated rat Müller cells, rat retinal ganglion (RGC) cells, and human RPE cells (Bridges et al., 2001; Dun et al., 2006; J. Wang et al., 2015). xCT gene has an ARE sequence in its promoter region and it is consequently under the regulation of NRF2 (Figure 15), in fact, the inhibition of NRF2, which reduces xCT expression, led to a reduction in GSH levels in the cultured Müller cells (Carpi-Santos & Calaza, 2018; J. Wang et al., 2015).

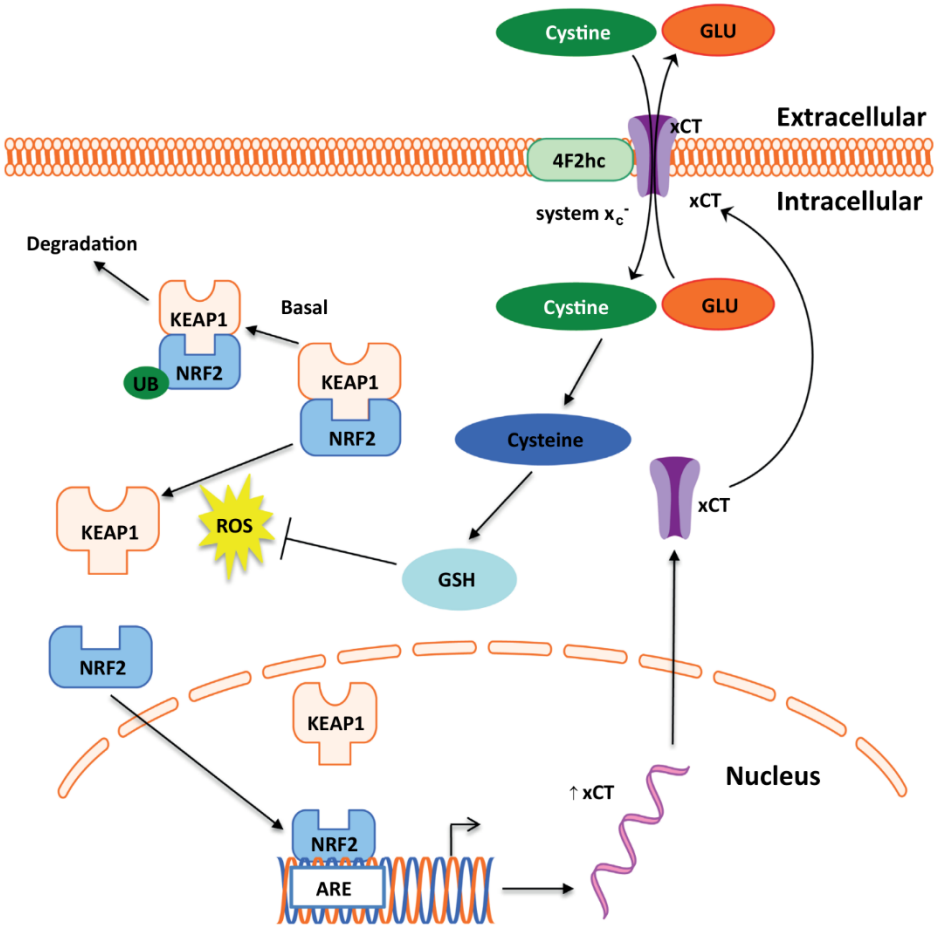

Figure 15. Representation of the KEAP1/NRF2 pathway regulating xCT expression and system Xc^- activity. SLC7A11/xCT is a direct transcriptional target of the activated NRF2. System Xc^- increases the delivery of cystine, the rate-limiting substrate in GSH biosynthesis, to contrast the stressor that has induced the KEAP1-dependent NRF2 activation. From Habib et al., 2015.

3 MATERIAL AND METHODS

3.1 Chemicals

NAC (C5H9NO3S, MW 163,19 g/mol) and NACET (C7H13NO3S, MW 191.2 g/mol) were kindly provided by Professors Daniela Giustarini and Ranieri Rossi and were prepared from powder to a final 20 mM concentration in MilliQ water, then 0.22 µm filtered. For NACET chemical characterization see Giustarini et al., 2012. Powdered BSO (L-buthionine-sulfoximine) (SignaAldrich) were prepared to a final 100 µM concentration in MilliQ water, then 0.22 µm filtered. Hydrogen peroxide was purchased from Fluka and diluted in MilliQ water just prior to use.

3.2 Mice

For the *in vivo* analysis, we collaborated with the Dr. Francesco Neri, group leader at Leibniz Institute on Aging - Fritz Lipmann Institute (FLI). Young (8-20 weeks old) and old (80-110 weeks old) C57BL/6J mice were used to treat with NACET-supplemented water. To achieve an oral dosage of 50mg/kg body weight/day of NACET, a solution 0.25 mg/ml NACET (CAS: 59587-09-6, Cat. N.: O32426, AChemBlock) has been used, which has been prepared fresh every two day and administered to mice in place of drinking water, to use in the placebo group. This concentration is based on the average water consumption per mouse (5 ml/day measured in our animal facility). After 5 days mice have been sacrificed by CO2 euthanasia, then we proceed with the dissection of the eyes to collect the retinas as follow (Figure 16). Enucleation (1-2): apply pressure to the skull dorsally and ventrally from the eye, until the eye begins to bulge out slightly. Using forceps, grasp the optic nerve at the back of the eye by wedging them between the eyeball and eye socket and remove gently the eye. Place eye in dissecting dish filled with PBS under a dissecting scope. Hemisecting (3): stabilize the eye by grasping the optic nerve or ocular muscles with forceps. Create a pilot hole at the cornea–sclera boundary and cut along the cornea/sclera boundary with microdissection scissors to remove the cornea and iris and remove the lens using forceps (4). Isolation of the retina by removing the optic nerve and sclera (5): to remove the optic nerve, cut the optic nerve at the base near the sclera. To remove the sclera, use forceps to tease apart the sclera from the retina and peel it off. Finally washing rinse it off with PBS (Protocol adapted from Simmons & Fuerst, 2018).

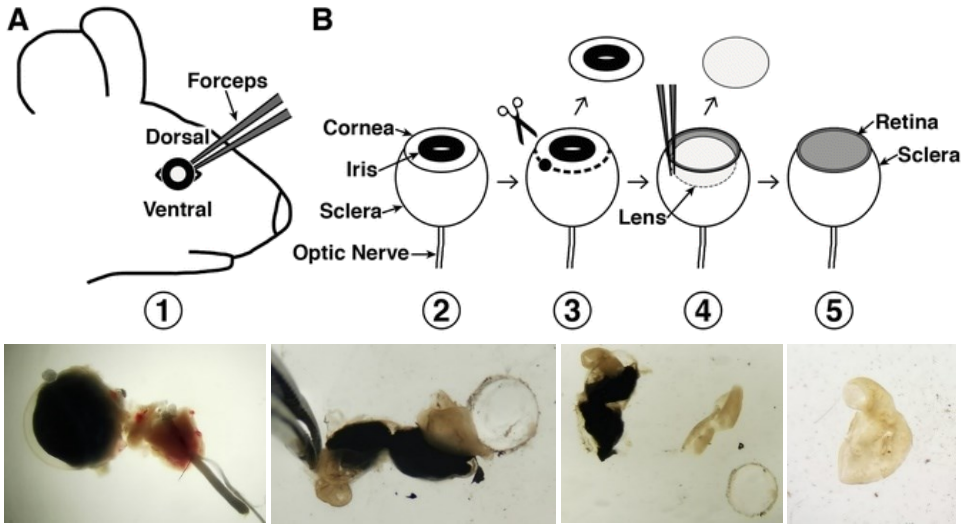

Figure 16. Diagram (A-B) and photos (C) showing the process of removing and dissecting the eye. (A) Enucleation (steps 1-2). Apply pressure below the eye socket and grasp the optic nerve with forceps and gently remove eye. Place eye in dissecting dish filled with PBS. (B) Hemisecting (steps 3-5). Poke a pilot hole at the cornea/sclera boundary and use microdissection scissors to cut the cornea and iris (step 3). Next, remove the lens with forceps (step 4). Gently detach the retina from the hemisected eye-sclera (step 5). Diagram A-B from Simmons & Fuerst, 2018.

One of the retinas of each mouse were used to measure the concentration of Cys and GSH, through High Performance Liquid Chromatography (HPLC) analysis, while the other retina has been used for RNA-seq analysis.

3.3 Cell culture

The ARPE-19, a spontaneously arising retinal pigment epithelia (RPE) cell line, was used for these experiments. ARPE-19 is widely used to study retinal cell biology, pathological conditions, and pharmacology (Dunn et al., 1996).

The cells were seeded in DMEM-F12 medium (Dulbecco's modified Eagle's medium: Ham's Nutrient Mixture F12, EuroClone®), supplemented with 2 mM L-Glutamine, 100 µg/ml streptomycin, 100 U/ml penicillin and 10% (v/v) fetal bovine serum (FBS), at 37°C in a humidified atmosphere containing 5% (v/v) CO_2.

3.4 NFE2L2 Crispr/Cas9 editing

The plasmid LentiCRISPR v2 (pLCv2) (Addgene, plasmid #52961) (Figure 17) was used to obtain NEF2L2 editing in the ARPE-19 cell line. It contains two expression cassettes for the hSpCas9 and the chimeric guide RNA. The vector was digested using BsmBI (NEB) and a pair of annealed synthetic oligonucleotides was cloned into the single guide RNA scaffold. The oligonucleotides were designed based on a target site sequence of 23 pb.

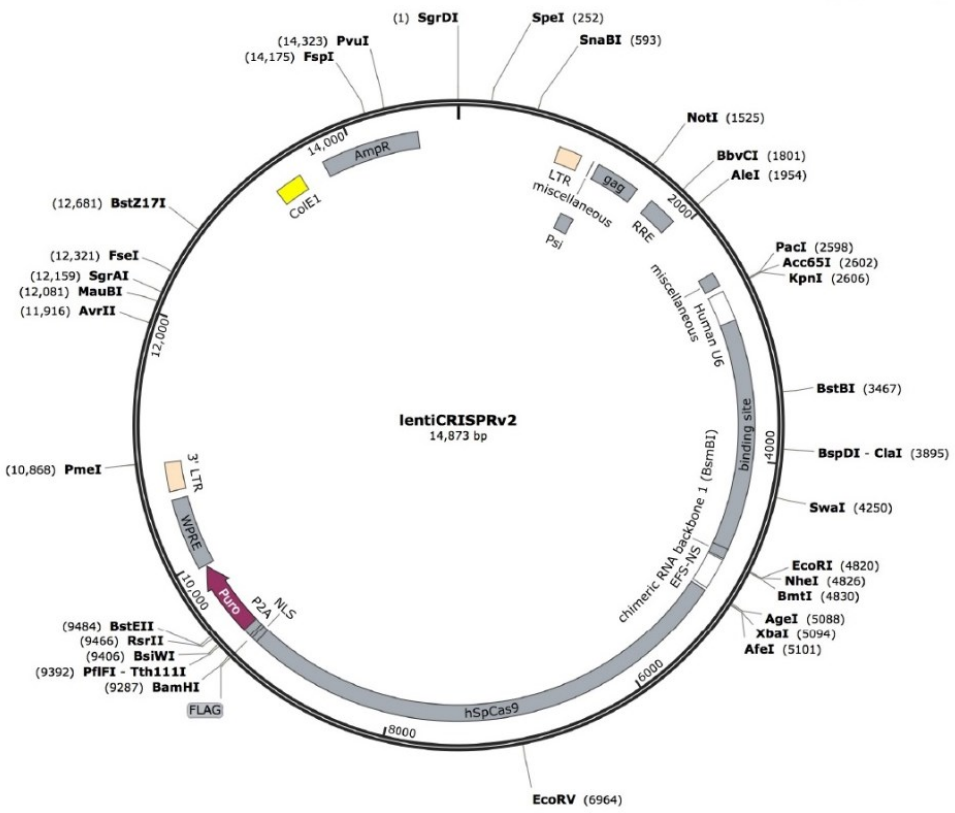

Figure 17. The 14873 bp long LentiCRISPR v2 (pLCv2) presents the restriction sites for BsmBI located at 2852 bp and 4737 bp, for the removal of the "filler" DNA sequences and its substitution with the target sequence of interest to generate the gRNA. The "filler" DNA sequences is located between the U6 promoter for the synthesis of the gRNA and the gRNA scaffold sequence necessary for Cas9 binding. This vector carries the Cas9 gene under the control of the EF1alpha core promoter, the ampicillin and puromycin resistance gene (Amp R and Puro R) and the sequences for lentiviral particle packaging (3' LTR and 5'LTR).

The online tool named CHOPCHOP (https://chopchop.cbu.uib.no/) was used to design the sgRNAs (sgRNA-1 and 2). The sequences of the oligonucleotide couples obtained by the software are listed below. The target sequence is not underlined, while the underlined sequences form the two overhangs necessary to clone in the correct orientation the double stranded oligonucleotides in the pLCv2 vector digested by BsmBI.

Two couples of oligonucleotides have been identified as sgRNA:

sgRNA-1 forward: 5' CACCGCATACCGTCTAAATCAACAGGGG 3'

sgRNA-1 reverse: 5' AAACCCCCTGTTGATTTAGACGGTATGC 3'

sgRNA-2 forward: 5' CACCGCATTAATTCGGGATATACGTAGG 3'

sgRNA-2 reverse: 5' AAACCCTACGTATATCCCGAATTAATGC 3'

To anneal the oligonucleotide pairs (100 pmol of each oligonucleotide in 1X NEB buffer 2; 5 mM NaCl, 1 mM Tris-HCl, 1 mM MgCl2, 0.1 mM DTT, pH 7.9) were loaded in a thermocycler and the

following denaturing/annealing program was run: 95° C for 5 min and then ramp down to 25 °C at 5°C/min. In order to ligate the annealed oligonucleotides in the digested vector, 200 ng of pLCv2 (previously run in agarose gel and purified by Qiagen QIAquick Gel Extraction Kit) and 100 pg of annealed oligonucleotides were incubated overnight at 16 °C in 1x T4 DNA Ligase Reaction Buffer (50 mM Tris-HCl, pH 7.5; 10 mM MgCl2; 1 mM ATP; 10 mM DTT) with 1 µl T4 of DNA ligase enzyme (NEB). Finally, the ligation products were concentrated by standard ethanol precipitation (0.3 M Sodium Acetate pH 5.2, 1.5 µl of Glicogen and 2 volumes of Ethanol absolute) and resuspended in 15 µl of sterile MilliQ water. To allow plasmidic DNA amplification, the ligation products were transformed in competent Escherichia Coli bacteria cells by electroporation using the following parameters: 2000 V, 25 µF, 200 Ω in Gene Pulser electroporation cuvette, gap width 0.1 cm, (Bio-Rad). After electroporation the bacteria were incubated at 37 °C in rotation for 1 hour, then the solution from each tube was spread on a LB agar plate, containing 100 µg/ml ampicillin, and incubated at 37°C overnight. The day after, bacterial colonies were picked and inoculated into a 3ml LB medium culture containing 100 µg/ml ampicillin, at 37°C for 16 hours; NucleoSpin® Plasmid (Macherey-Nagel) mini kit for plasmid DNA was used to purify the plasmid DNA according to manufacturer's instruction and the proper sgRNA insertion was checked by Sanger sequencing.

3.5 Dual-luciferase assay

The dual luciferase assay was performed with the Dual Luciferase Reporter (DLR) Assay System kit (Promega Corp., Madison, WI). All reagents were prepared according with manufacturer instruction: Passive Lysis Buffer 5x (PLB) was prepared in a 1:5 ratio with MilliQ water, Firefly luciferase reagent (LARII) was ready to use and Firefly quenching-Renilla luciferase reagent (STOP & Glo) was prepared by adding 1 volume of 50X Stop & Glo Substrate to 50 volumes of Stop & Glo Buffer. DLR assay system relies on two different reporter genes, Renilla and Firefly luciferase, to evaluate regulated gene expression. The Firefly luciferase gene pGL4.37 (lucP/ARE/Hygro) vector (Promega) was used to evaluate the NRF2 activity. pRL-SV40 vector (Promega), for the expression of Renilla luciferase under the control of a constitutive promoter, was used as internal control of transfection efficiency.

3.5.1 ARPE-19 transfection

$2.0x10^6$ of control (ctrl.) and edited (NRF2 ΔC) ARPE-19 cells were centrifuged three times for 5 minutes, at 190xg with DMEM/F12 supplemented with 2.5% (v/v) FBS and 0.25% (w/v) bovine serum albumin (BSA). Then the cells were resuspended in 200µl of the same DMEM/F12 used for washing, added and gently mixed with 1.7 µg of pRL-SV40 vector and 3 µg of pGL4.37 (lucP/ARE/Hygro) vector. Each mix was put into an electroporation cuvette (Gene Pulser

electroporation cuvette, Gap Width 0.2 cm, Bio-Rad). Electroporation was performed by using the following parameters: 290 V, 1,000 µF, 200 Ω. After the electroporation, the cuvette content was first added in a tube with pre-warmed complete DMEM/F12 and then plated in six-wells dishes, 24 hours later the medium was changed, and the reported induction started. After the reported treatment, cells were washed twice with PBS and lysed in 1x PLB, then, by means of a scraper, cells were mechanically removed from the plate and collected in 1.5 ml centrifuge tube. Finally, the samples were sheared using Diagenode's Bioruptor 300 at HIGH setting, 5 cycles of 30 seconds and centrifuged at 16200xg, for 5 minutes at 4°C, the supernatant was recovered and stored at -20°C.

3.5.2 Luminescence measurement

After lysis, 10 µl of PLB lysed sample was used for luminescence measurements by means of Turner Designs model TD-20/20 luminometer by adding 50 µl of the Firefly luciferase reagent (LARII). Subsequently, the Renilla luciferase luminescence was measured by addition of 50 µl of the Firefly quenching-Renilla luciferase reagent (Stop & Glo) (Figure 18). The data are represented as the ratio of Firefly to Renilla luciferase activity (Fluc/Rluc).

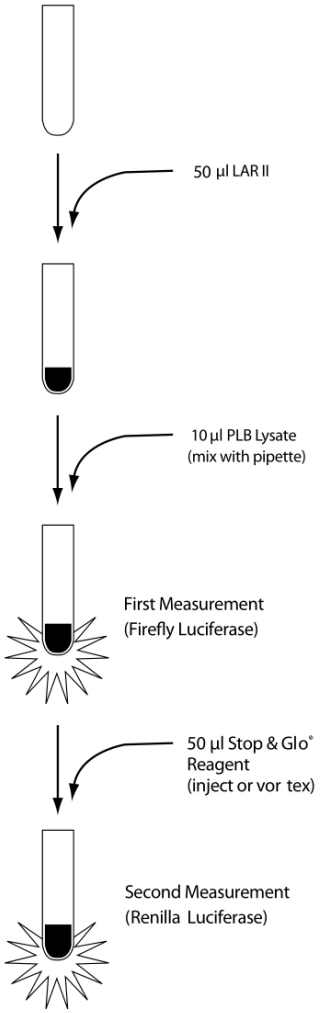

Figure 18. DLR™ Assay system. Adapted from Dual Luciferase® Reporter Assay System (Promega) technical manual.

3.6 Lentiviral Infection in ARPE-19 cells

To generate ARPE-19 cells edited for NFEL2L or ARPE-19 cells overexpressing SLC7A11, we carried out infections by means of defective Lentiviral particles.

3.6.1 Lenti-X 293T transfection

For viral packaging plasmids pRSV-Rev, pMDLG/pRRE, and pMD2.VSVG were cotransfected with the expression plasmid (pLCv2-sgRNA 1 or 2, or pLenti CMV-SLC7A11-sh926R-FLAG-IRES-Hygro). To transfect Lenti-X 293T cell line, the TransIT-VirusGen Transfection kit (Mirus) was used according with the manufacturer instructions. For each transfection 1.5 µg of pMD2.VSVG, 2.4 µg of pMDLG/pRRE and 1.2 µg of pRSV-Rev were mixed, and added to 5.1 µg of transfer plasmid DNA (pLCv2-sgRNA 1, 2, pLCv2-without sgRNA, and pLenti CMV-SLC7A11-sh926R-FLAG-IRES-Hygro). Then the mix (virus packaging-DNA) were transferred in a sterile tube containing 1 ml of Optimem (GIBCO), finally 30 µl of Transit reagent were added and gently mixed. To allow the formation of transfection complexes, the mixture was incubated 20 minutes at room temperature, and subsequently added drop-by-drop on 80% confluent Lenti-X 293T cell line. An extra sample was transfected with GFP-expressing plasmid (pCCLsin.PPT.hPGK.GFPpre) to check the transfection and transduction efficiency by means of the fluorescence signal. At 24 and 48 h post-transfection, supernatants of Lenti-X 293T cells containing the lentiviral particles were transferred in a 50 ml centrifuge tube. The medium was filtered by using 0.45 µm filters, aliquoted and stored at -80°C.

3.6.2 ARPE-19 transduction

ARPE-19 cells were plated on six-well plates at a concentration of $9.6x10^4$ cell per well. After 24h the culture medium was replaced with 1 ml of complete DMEM/F12, 1 ml of supernatant containing lentiviral particles and 2 µg polybrene (Hexadimethrine bromide), per well. After 24 hours, medium was changed, and after other 48h, puromycin selection was started for ARPE-19 cell carrying pLCv2-sgRNA 1 or 2.

3.6.3 Puromycin selection

Since the pLCv2-sgRNA 1 and 2 plasmids contain the puromycin resistant gene, we selected cells with integrated plasmids by puromycin treatment (2µg/ml). The drug was added at each medium change or cell passage. In such way, only cells that have integrated in the genome the pLCv2-sgRNA 1 or 2, expressing the resistance, survived and grew during and after the treatment. After 2 weeks of selection, western blot was performed to check the editing efficiency. Cells transduced with lentiviral particles expressing sgRNA1 did not show any evident editing of NFE2L2 and consequent variation in the molecular weight of NRF2. In sgRNA2 transduced cells, an evident alteration of the molecular weight of NRF2 was observed, even though not in 100% of the cells (Figure 19A). Thus, we performed a a clonal selection. Cells were seeded by limiting dilution in six 96 well plates to obtain single clone colonies. This process required 3 months. Single clone cell extracts were analysed by western blot (Figure 19B) and a single biallelic edited clone (C1) was identified. Since now, the edited clone C1 will be referred as NRF2 ΔC. ARPE-19 cells transduced with pLCv2-without sgRNA (ARPE-19-A1) were puromycin selected, grown as a pool, and used as negative control.

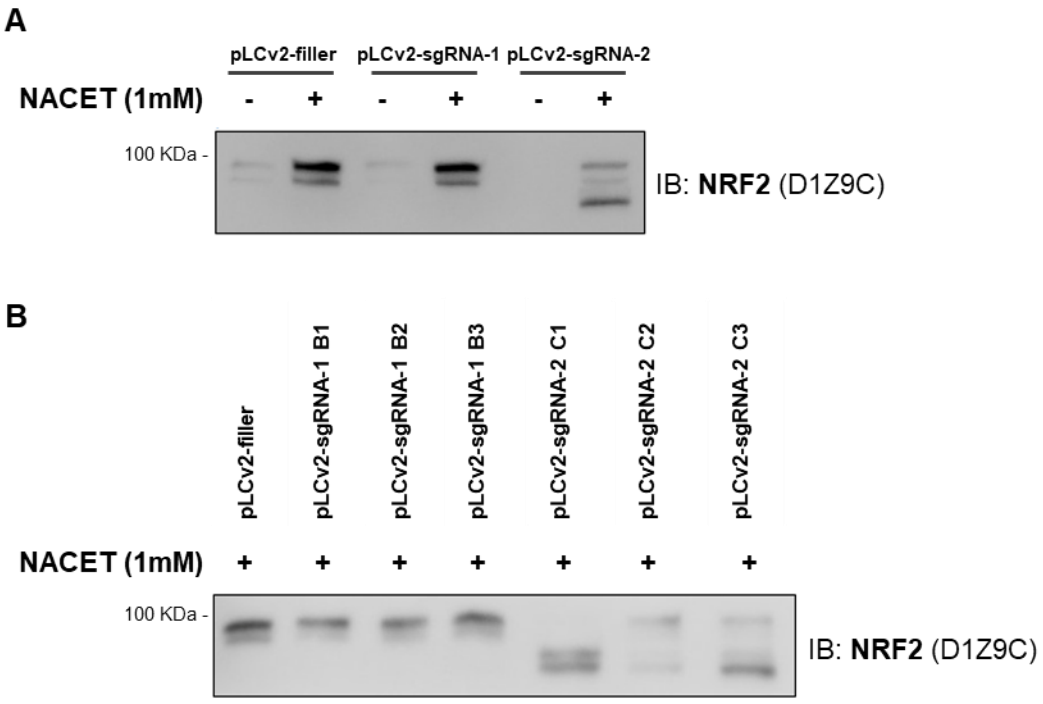

Figure 19. NFE2L2 CRISPR/CAS9 editing. A) Pooled pLCv2-filler, pLCv2-sgRNA-1 and pLCv2-sgRNA-2 transduced ARPE-19 cells were treated with 1mM of NACET to induce NRF2, and whole cell extracts were analyzed by western blot. B) Western blot of NACET induced ARPE-19 clones obtained by limiting dilution of pooled transduced cells.

3.7 Immunofluorescence

Cells were grown in 8 Lab-Tek II® Chamber Slide™ system (Nunc®, 154534). The seeding density for ARPE19 was 15000 cells/well. After 24h cells were treated with 1mM NACET at 2/4/6/8/24

hours before the fixation. Cells were fixed using 4% paraformaldehyde in PBS for 10 min at room temperature, then washed three times with ice-cold PBS. Cells were permeabilized with PBS containing 0.1% Triton X-100 and rinsed in PBS three times for 5 min. Cells were blocked using a PBS solution with 0.1% Tween 20, 1% BSA and 5% donkey serum for 30 min and incubated in the diluted primary antibody (Table 1) in 1% BSA in PBST in a humidified chamber overnight at 4°C. After three 5 min washes in PBS, cells were incubated with the secondary antibody (table 1) in 1% BSA in PBST for 1 h at room temperature in the dark and rinsed again three times in PBS for 5 min each in the dark. During the second wash 0.1 µg/ml DAPI was added to PBS. The slides were mounted with coverslip using DePeX (SERVA). The images were taken using a Zeiss Apotome 3 and analysed with ImageJ software, to obtain the mean fluorescence intensity of cells expressing a nuclear protein of interest (Shihan et al., 2021), calculating the average of intensity value for green fluorescence per nucleus, in ≥ 3 images for each time-treatment and counting a number greater than 150 nuclei.

Primary antibody	**Company**	**Dilution**
Anti-NRF2	Abcam, EP1808Y, rabbit mAb	1:500 in 1%BSA in PBST
Anti-NRF2 (phospho S40)	Abcam, EP1809Y, rabbit mAb	1:500 in 1%BSA in PBST
Anti-α-Tubulin	Sigma, T5168, mouse mAb	1:500 in 1%BSA in PBST
Secondary antibody		
Anti-Rabbit IgG (H+L)	ThermoFisher, A21206, Alexa Flour 488, donkey pAb	1:1000 in 1%BSA in PBST
Anti-Mouse IgG (H+L)	ThermoFisher, A10037, Alexa Flour 568, donkey pAb	1:1000 in 1%BSA in PBST

Table 1. Primary and secondary antibodies used in Immunofluorescence analysis.

3.8 RNA extraction and isolation

Total RNA was extracted and isolated from ARPE-19 using EuroGOLD TriFast™ (EuroClone). TriFast™ includes phenol and guanidinium thiocyanate in a monophasic solution. After addition of chloroform the homogenate separates into three phases upon centrifugation. The aqueous phase containing the RNA, whereas the interphase and the organic phase containing the DNA and the proteins, respectively.

- The medium was removed from the culture plates.
- The cells were lysed directly in a culture dish by addition of 1 ml TriFast™ to a 3.5 cm diameter dish and then the cell lysate was passed several times through a pipette.
- The cells were scraped from plat using a cell scraper and the lysate was transferred to a conical 1,5ml tube.
- For allow the dissociation of the nucleoprotein complexes the samples were kept for 5 minutes at room temperature.
- To remove insoluble material from homogenates, it was centrifuged at 12000 xg for 10 minutes at 4°C and the supernatant was transferred to a fresh tube.

- 200 µl chloroform were added per 1 ml of TriFast™, samples were shaken by hand vigorously for 15 seconds, incubated for 5-15 minutes at room temperature and centrifuge at 12000 xg for 10-15 minutes at 4°C.
- Then the aqueous phase (colorless top layer) was transferred to a fresh tube. RNA remains exclusively into the aqueous phase whereas DNA and the proteins are in the interphase and lower phenol phase.
- 300 µl of chloroform was added. The samples were centrifuged at 12.000 xg for 15 minutes at 4°C and the aqueous phase was transferred to a fresh tube.
- The RNA was precipitated with 500 µl of isopropanol, shaken vigorously for 5-10 seconds and incubated at room temperature for 5-10 minutes.
- Samples were then centrifuged at 12000 xg for 8 minutes at 4-25°C, then the supernatant was carefully removed without disturbing the pellet.
- 1 ml of 75% ethanol was added to each sample to wash the RNA pellets.
- The samples were centrifugated at 7500 xg for 5 minutes at 4-25°C, then the ethanol was removed, and the RNA pellet was briefly air dried.
- The RNA was resuspended in 20-50 µl of water and the RNA pellet was dissolved by passing the solution through a pipette tip several times.

3.9 mRNA sequencing library preparation and data analysis

RNA quantity and quality were evaluated by Nanodrop 8000 (ThermoFisher Scientific) and Fragment Analyzer (Advanced Analytical) using the Standard Sensitivity RNA Analysis Kit; 15nt DNF-471-0500 (Advanced Analytical). RNA samples were further processed for mRNA-seq library preparation according to the manufacturer's instructions (TruSeq^{R}RNA Sample preparation v2, Illumina) and for the subsequent data analysis, which have been kindly performed by Dr. Mahdi Rasa.

Fastq files quality check was performed using FastQC v0.11.5. The fastq files were mapped to the mm9 genome for mouse samples or hg19 genome for ARPE19 cell line using TopHat v2.1.0 (Trapnell et al., 2012) with the following parameters --bowtie1 --no-coverage-search -a 5. The number of reads covered by each gene was calculated by HTSeq-Count 0.11.2 (Anders et al., 2015) with -s no -a 0 -t exon -m intersection-nonempty parameters. Before further analysis, all of the rRNA genes were removed from the count data. For calculating differentially expressed genes and normalized count, DESeq2 R package v1.20.0 (Love et al., 2014) was used with the default parameters. For PCA plot, the normalized count was used and the genes were filtered using the following criteria, count>10 in at least 6 samples, IQR of the log transform count >= 1.5. After filtering, the log 10 transformed count was used in prcomp R function with center = TRUE, scale. = TRUE parameters. PC1 and PC2 were

used for the plotting. For functional and pathway analysis as well as upstream regulators analysis, IPA (Ingenuity Pathway Analysis v45868156) software has been used (Krämer et al., 2014) with differentially expressed genes (padj<0.05,DESeq2). All of the plotting (bar plot, heatmap, Venn diagram and volcano plot) was done using R and relevant packages.

3.10 RT-qPCR

To evaluate the expression of target genes, we performed Real-Time Reverse Transcription Quantitative Polymerase Chain Reaction (RT-qRT-PCR). Real-Time qPCR is a technique that enables the amplification and the simultaneous quantification of DNA products generated during each cycle of PCR process, using the intercalation of double-stranded DNA-binding dyes. It is often combined with the Reverse Transcriptase (qRT-PCR), in order to quantitatively detect RNA expression, through the creation of complementary DNA (cDNA) transcripts from RNA.

The SYBR® Green PCR Master Mix and SYBR® Green RT-PCR Reagents Kit (Thermo Fisher) have been used, as follows:

- 10 µl 2x Brilliant SYBR® Green RT-PCR Master Mix
- 1 µl forward primer 10 µM (Table 2)
- 1 µl reverse primer 10 µM (Table 2)
- 1 µl RT/RNase block
- 2 µl RNA 12.5 ng/µl
- Water to 20 µl

Thermocycling conditions for RT-qPCR:

- Retrotranscription: 50°C for 15 minutes
- Denaturation: 95°C for 3 minutes
- 50 cicles:
    - Denaturation: 95°C for 15 seconds
    - Annealing: temperature is reported in Table 2, for 17 seconds
    - Extension: 68°C for 17 seconds

RT-qPCR analysis were performed using the Rotor-Gene Q and the Rotor-Gene Q Software (Qiagen).

	FORWARD	REVERSE	T. annealing
NQO1	CGCAGACCTTGTGATATTCCAG	CGTTTCTTCCATCCTTCCAGG	57°C
HMOX1	TGACCCATGACACCAAGGAC	AGTGTAAGGACCCATCGGAGA	58°C
MGST1	TCGTGACAAAGCAAATTGTCTGG	CCATTACCTGGGTGAGGTCAA	63°C
GSR	GCCTTCACGAGTGATCCCAA	CTGCACCAACAATGACGCTG	55°C
GCLM	GGAACCTGCTGAACTGGGG	CCCTGACCAAATCTGGGTTGA	58°C
GCLC	GTTCTTGAAACTCTGCAAGAGAAG	CCTTCAATCATGTAACTCC	55°C
TXN	TGGTGAAGCAGATCGAGAGC	ACATCCTGACAGTCATCCACAT	57°C

SLC7A11	TCCCTACTATGGTCAGAAAG	TTGGGCAGATTGCCAAGATC	57°C
NEF2L2	GCGCAGACATTCCCGTTTG	GACTGGGCTCTCGATGTGAC	56°C
GAPDH	GAAGGTGAAGGTCGGAGTC	GAAGATGGTGATGGGATTTC	57°C

Table 2. Primers and T. annealing used for the RT-qPCR.

3.11 Protein assays

3.11.1 Total protein extraction

The total protein extraction from ARPE19 cells was performed using the RIPA lysis and extraction buffer, as follows:

- The medium was removed, cold PBS 1X was applied to rinse the plat and then RIPA 1X (50 mM Tris-HCl pH 7.2, 100 mM NaCl, 1% (v/v) Triton X100, 1% (w/v) deoxycholic acid, 0.1% (w/v) SDS, 50 NaF, 2 mM EDTA) with sodium orthovanadate 2mM and 1X Protease Inhibitor Mix (Sigma-Aldrich) was added to the well.
- The cells were scraped from plat using a cell scraper, transferred to a conical 1.5ml tube.
- The samples were sonicated for 5 minutes, centrifugated at 12000 xg for 5 minutes at 4°C and then the supernatant was collected and stored at -20°C.

3.11.2 Determination of protein concentration

The protein concentration has been evaluated using the Pierce™ BCA Protein Assay Kit (Thermo Fisher); which is based on bicinchoninic acid (BCA) for the colorimetric detection and quantitation of total protein. This method combines the reduction of Cu^{+2} to Cu^{+1} by protein in an alkaline medium with the colorimetric detection of the Cu^{+1} by bicinchoninic acid. The purple-colored reaction product of this assay is formed by the chelation of two molecules of BCA with one Cu^{+1} ion. This complex exhibits a strong absorbance at 562 nm measured using the spectrophotometer. Protein concentrations generally are determined and reported with reference to standards of the bovine serum albumin (BSA). BSA is the universally accepted reference protein for total protein quantitation. A series of dilutions of known concentration are prepared from the protein and assayed alongside the unknown(s) before the concentration of each unknown is determined based on the standard curve. Focused on the results obtained, relative normalization was performed, based on the lower protein concentration sample, to use the same amount of total protein in the different assays.

3.11.3 Western Blot

The Western blot is a widely used technique that allows to detect specific proteins, using certain antibodies, in a sample of tissue homogenate or extract, previously separated by sodium dodecyl sulfate-polyacrylamide gel electrophoresis (SDS-PAGE). The antibodies can be labelled or commonly can bind a secondary antibody. Once the proteins were quantified, we proceeded with the dilution in 1X sample buffer (SB). For protein separation, based on their molecular weight,

polyacrylamide gels have been used. The samples were heated to 95°C for 5 minutes, before being loaded onto the gel. Upon application of a constant electric field (a voltage of 100 V and 30 mA was applied), the protein, in running buffer (25 mM Tris, 0.2 M glycine and 3.5 μM SDS), migrates towards the anode, each with a different speed depending on its mass. Once electrophoresis was finished, proteins have been transferred from polyacrylamide gel to nitrocellulose membrane (GE Healthcare Life Science), applying an electric field of 100V and 300 mA in the transfer buffer (25 mM Tris, 0.2 M glycine and 20% (v/v) ethanol) for about 2 hours on ice. Thereafter Ponceau S, a colorant which non-specifically binds to proteins present on the membrane, was used to detect possible presence of proteins. Ponceau S was removed from the protein bands by water washing and then the membrane was placing, for 1 hour with gentle shaking, in a PBS solution containing 5% milk (w/v), 0.1% Tween-20 (v/v), for blocking non-specific binding. It follows the incubation with the primary antibodies (Table 3) (e. g. diluted 1:1000 in PBS, 5% milk (w/v), 0.1% Tween-20 (v/v)) under gentle agitation at 4°C overnight. To remove unbound primary antibody the membrane was rinsed twice with PBS, 5% milk (w/v), 0.1% Tween-20 (v/v) for 5 minutes. After washing the membrane, it is exposed to the horseradish peroxidase (HRP)-secondary antibodies, for 1 hour at room temperature under gentle agitation. It follows four washes with PBS and 0.1% Tween and two washes with PBS 1X, each for 4 minutes at room temperature with gentle shaking. Thereafter, 1 ml of Luminata™ Crescendo Western HRP Chemiluminescence Substrate (Thermo Fischer), a premixed ready-to-use chemiluminescent reagents for detection of HRP-based Westerns, was used to cover, for 1 minute, the entire membrane in order to detect the specific antigen-antibody binds. Horseradish peroxidase (HRP) catalyzes the oxidation of luminol in the presence of peroxide, releasing photons (chemiluminescence). ImageQuant™ LAS 4000 (GE Healthcare) was used to produce digital images of the chemiluminescent membrane samples and the bands quantification was made using the ImageQuant LAS 4000 control software.

Antigene	Antibody	Source/Type	Cat #	Working concentration
NRF2	NRF2 (D1Z9C) XP	Rabbit mAb	#12721 - Cell Signaling	1:2000
NRF2	NRF2 (A-10)	Mouse mAb	# sc-365949 - Santa Cruz Biotechnology	1:300
KEAP1	KEAP1(OTI1B4-formerly 1B4)	Mouse mAb	#TA502059 - Origene	1:1000
NQO1	NQO1 Antibody (A180)	Mouse mAb	# sc-32793 - Santa Cruz Biotechnology	1:5000
xCT/SLC7A11	SLC7A11 Antibody (711589)	Rabbit mAb	# 711589 Thermo Fisher Scientific	1:500
GAPDH	Anti-GAPDH (7E4-H6-H6)	Mouse mAb	#STJ99066 – St John's Laboratory	1:3000
b-ACTIN	Anti-β-Actin (AC-15)	Mouse mAb	#A5441 - Sigma-Aldrich	1:5000
Rabbit	Peroxidase-conjugated AffinityPure Goat Anti-Rabbit IgG (H+L)	Goat mAb	# 111-035-003- Jackson Immuno Research	1:5000

Mouse	Peroxidase-conjugated AffinityPure Goat Anti-Mouse IgG (H+L)	Goat mAb	# 115-035-003- Jackson Immuno Research	1:3000

Table 3. Primary and secondary antibodies used in Western blot.

3.12 Analysis of Intracellular Low Molecular Mass Thiols (LMM-SH)

To measure the intracellular levels of NAC, Cys, γ-GluCys, CysGly and GSH from *in vitro* experiments on ARPE-19 cells, the culture medium was removed, and the cells were washed twice with phosphate-buffered saline solution (PBS), pH 7.4, at 4°C, lysed with 0.5 mL of a 4% (w/v) solution of ice-cold TCA containing 1mM K3EDTA and collected after scraping. Samples were either immediately analysed or stored at −80°C until analysed. Measurements were always carried out within 5 days from sample preparation. Thiol analyses were performed by HPLC analysis was kindly performed by Professors Daniela Giustarini and Ranieri Rossi. After labelling of the –SH group with the fluorescent probe monobromobimane (mBrB) (Calbiochem, La Jolla, CA, USA) as previously described (Giustarini et al., 2018). For the *in vivo* experiments, we homogenized the retinas in 9 µl of 4% (w/v) solution of ice-cold TCA containing 1mM K3EDTA per each 1mg of tissue. The same HPLC method was also applied to supernatants of homogenized mice's eyes to measure their LMM-SH content. An Agilent series 1100 HPLC (Agilent Technologies, Milan, Italy) equipped with diode array and a fluorescence detector was used for all determinations. All expression analyses were performed three times independently. For the normalization, protein content was measured by the Bradford assay after protein pellet resuspension in 0.1 N NaOH. Bovine serum albumin was used as standard.

3.13 KEAP1 mass spectrometry analysis

Mass spectrometry analysis was kindly performed by Dr. Laura Salvini (Toscana Life Sciences, Siena). For this analysis, 10 µg of recombinant human KEAP1 (in 20 mM Tris pH 7.5, 500 mM NaCl, 10% (v/v) glicerol, 2 mM GSH, 5% (w/v) trehalose, 5% (w/v) mannitol, 0.01% (v/v) Tween-80; #11981-H29B-100, Sino Biologicals) for every 4 experimental points were diluted to 100 µl of 20 mM Tris pH 8.0 and diafiltrated by means of a Amicon Ultra-0.5 ml device to eliminate GSH. The reaction volume was returned to 80 µl of 20 mM Tris pH 8.0. 2.4 µl of 1 M DTT (final concentration 30 mM) was added to the protein and the mixture was incubated 30 min at room temperature to reduce the –S-S- bridges and free the cysteine residues. Following this step, 180 µl of 20 mM Tris pH 8.0 was added and the diafiltrated to remove the excess of DTT and the reaction volume was returned again to 180 µl of 20 mM Tris pH 8.0. The reaction volume was divided in 4 aliquots (45 µl; 1 µM final concentration of KEAP1), and to each aliquot were added 5 µl of water or cysteine at the concentration of 1 µM (Cys/KEAP1 ratio 0.1), 2.5 µM (ratio 0.25), 5 µM (ratio 0.5), 10 µM (ratio 1),

50 µM (ratio 5), 500 µM (ratio 50). The reaction was incubated 1 h at room temperature, diluted with 20 mM Tris pH 8.0, diafiltrated, rediluted and the protein digested by trypsinization for 3 h. The analyses were performed on a Q-Exactive Plus mass spectrometer (Thermofisher Scientific), equipped with electrospray (ESI) ion source operating in positive ion mode. The instrument is coupled to an UHPLC Ultimate 3000 (Thermofisher Scientific). The chromatographic analyses were performed on a column Acquity UPLC Waters CSH C18 130Å (1 mm X 100 mm, 1,7 µm, Waters) using a linear gradient and the eluents were 0.1% formic acid in water (phase A) and 0.1% formic acid in acetonitrile (phase B). The flow rate was maintained at 100 µl/min and column oven temperature at 50°C. The raw data obtained were analysed using the Biopharma Finder 2.1 software from ThermoFisher Scientific. The elaboration process consisted in the comparison between the peak list obtained "in silico" considering an expected aminoacidic sequence of a certain protein, a particular enzyme and fixed or variable modification.

3.14 Statistical analysis

The data analysis was performed using Prism 6 statistical software (GraphPad Software Inc., San Diego, CA). Evaluation of the data was conducted one-way or two-way ANOVA. The significant differences were estimated using Tukey's multiple comparison test (*, $p < 0.05$; **, $p < 0.01$; ***, $p < 0.001$; ****, $p < 0.0001$). Student's t test was used to confirm significant differences between treatments. Two-tailed probabilities of less than 0.05 were considered significant.

4 RESULTS

4.1 NACET induces NRF2 pathway in ARPE-19 cells

To deeply investigate the role of NACET in prevention of oxidative stress, we performed a transcriptome analysis of ARPE-19 cells after NAC or NACET treatments (Figure 20).

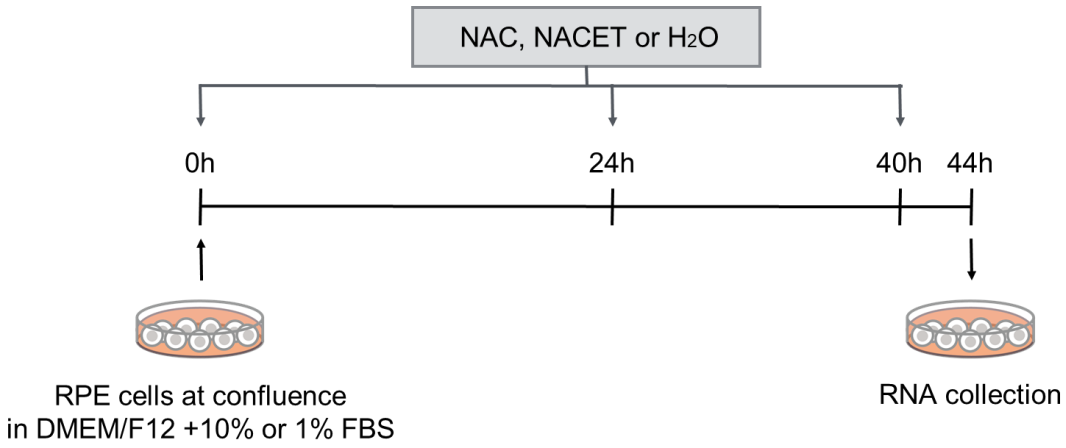

Figure 20. NAC, NACET treatment schedule. Confluent ARPE-19 cells, cultured in DMEM/F12 with 1% or 10% FBS, were treated chronically with 0.4 mM NAC, NACET or H_2O at the indicated time points. Total mRNA was extracted and RNA-seq analysis was performed.

We analysed the differentially expressed genes (DEGs) in ARPE-19 cultured with 1% or 10% of FBS and treated with NAC, NACET or vehicle (H_2O) alone (control). Comparing control ARPE-19 to NAC treated cells, both cultured with 1% FBS, we detected 257 differentially expressed genes (57 up- and 200 down-regulated genes), while in presence of 10% FBS, there were 122 differentially expressed genes and among them, 52 were upregulated and 70 downregulated. After NACET treatment in 1% FBS, we detected 411 DEGs, among them 115 up- and 296 down-regulated, while in presence of 10% FBS, there were 227 DEGs, 108 up- and 119 down-regulated (Table 4).

	1%		10%	
	up	down	up	down
NAC	57	200	52	70
NACET	115	296	108	119

Table 4. Comparison of differentially expressed genes (DEGs) in ARPE-19 treated with NAC or NACET cultured in 1% or 10% FBS.

41 DEGs were upregulated by NACET in a serum independent manner (Figure 21). Surprisingly, data analysis showed that 32 out of 41 genes serum-independently upregulated only by NACET were NRF2 direct targets. Moreover, 21 of them were described to be involved in oxidative stress response (Figure 22). It is well known that NRF2 pathway is activated by exposure to oxidative stress and

therefore the unexpected results - we expected a decrease in oxidative stress response following treatment with an antioxidant such as NACET - prompted us to investigate further this pathway.

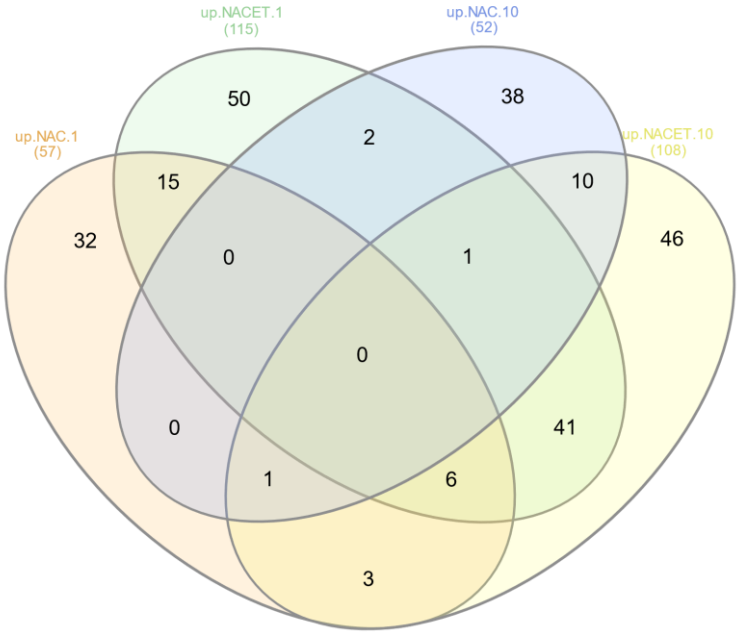

Figure 21. Venn diagram showing the number of upregulated DEGs and the overlap of DEGs among the four comparisons of ARPE-19 treated with NAC or NACET cultured in 1% or 10% FBS.

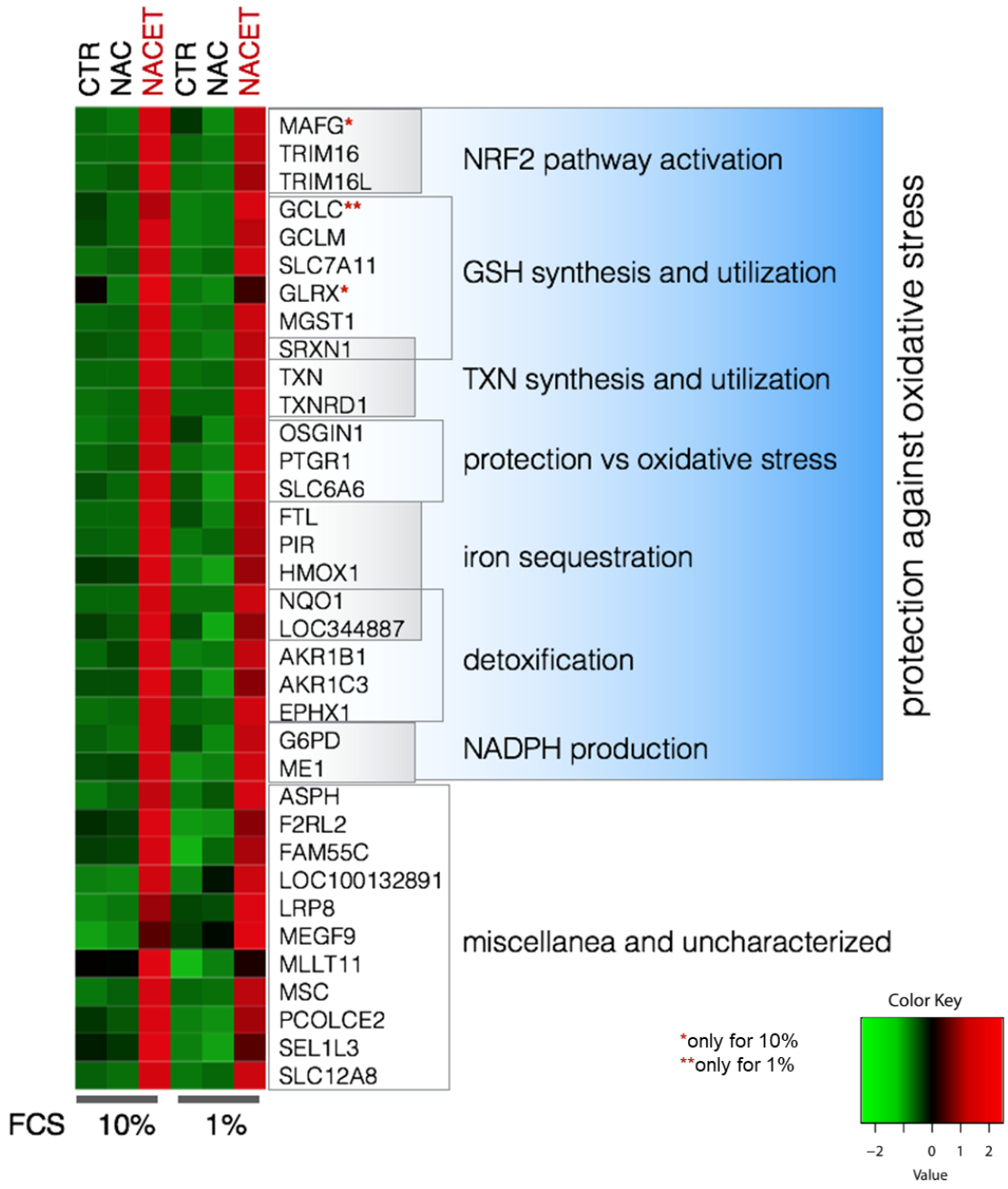

Figure 22. 32 out of 41 genes serum-independently upregulated only by NACET are NRF2 direct targets. Functional categories are indicated on the right. Red asterisks indicate three important known targets of NRF2 for its antioxidant action that are reported even thougth significantly upregulated by NACET only in 10% or 1% FBS condition.

To investigate whether NACET induces NRF2 expression at protein level, we performed a time-course analysis on confluent ARPE-19 cells treated with NACET for the indicated time points (Figure 23). NACET induced a rapid increase of the expression of the NRF2 100 kDa isoform, with a peak of activation between 4 and 6 hours. The 76 kDa isoform, detected by the anti-NRF2 A-10 antibody, has a later activation timing, suggesting a different regulation mechanism. This latter observation was

not investigated deeper. We also analysed the expression levels of KEAP1, the negative regulator of the NRF2-ARE signaling pathway, that showed no variations in its expression.

Moreover, we performed an immunofluorescence analysis on ARPE-19 treated with NACET at 0 (ctrl), 2, 4, 6, 8 and 24 hours. The results showed that NACET leads to an increase of NRF2 protein localization in the nucleus, confirming the previous observation (Figure 24).

As expected from the described activation mechanism of NRF2, the mRNA level of Nuclear Factor Erythroid 2 Like 2 (*NFE2L2*), the gene coding for NRF2, did not show any significant variation, confirming that also the NACET-dependent NRF2 expression induction depends on a post-transcriptional mechanism (Figure 25).

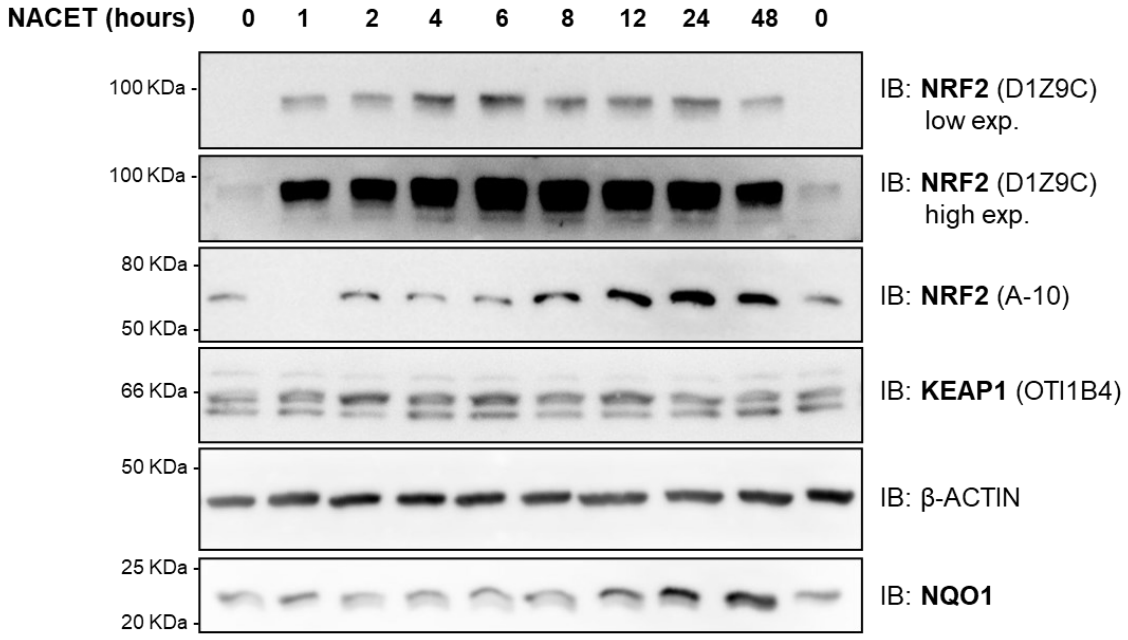

Figure 23. NACET induces NRF2 expression and its target gene, NQO1, at protein level in ARPE-19 cells. Confluent ARPE-19 cells were treated with 1 mM NACET at the indicated time points, and whole cell lysates were analysed by western blot with anti-NRF2 (D1Z9C), anti-NRF2 (A-10), and anti-KEAP1 (OTI1B4) antibodies. β-actin was used as loading control. We reported the low and the high exposition of the immunoblot for NRF2 (D1Z9C), to better appreciate the differences in the induction levels.

A

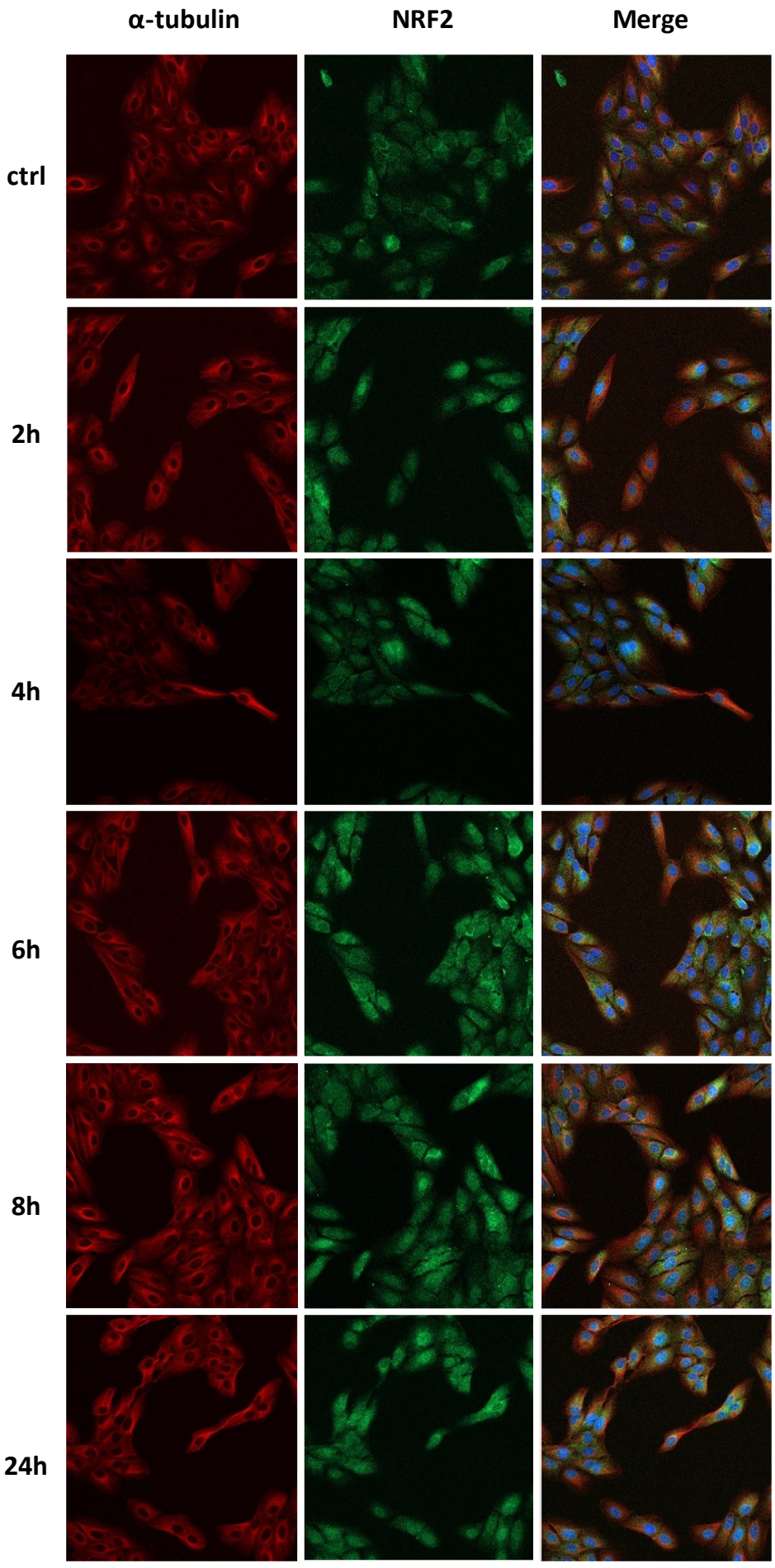

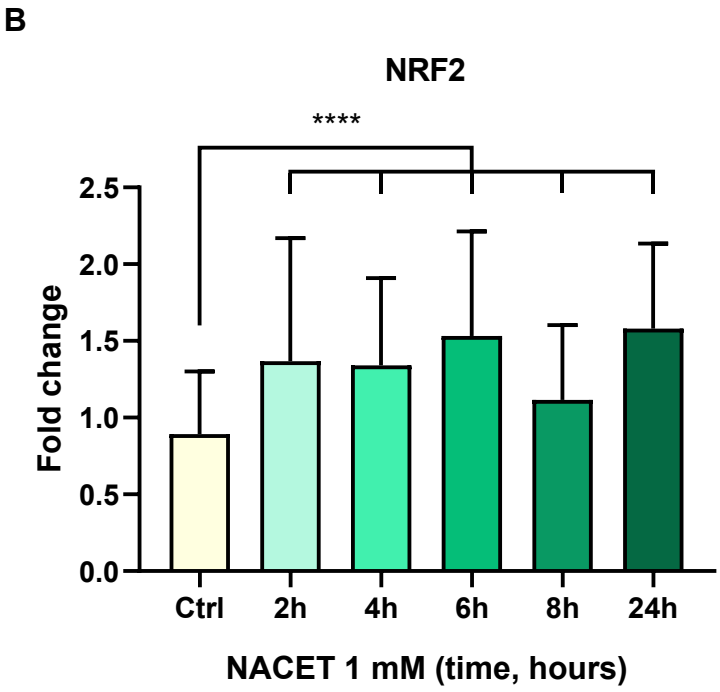

Figure 24. NRF2 protein localization in ARPE-19 cells after NACET treatment. (A) Immunofluorescence staining of α-tubulin, NRF2 and merge images at 0 (Ctrl), 2, 4, 6, 8 and 24 hours after NACET 1 mM treatment. (B) Fold change of nuclear NRF2 after NACET treatments. Results are represented as mean fluorescence intensity of cells expressing nuclear NRF2, in a number greater than 150 nuclei of ≥ 3 images for each time point treatment. Data are shown as mean value ± SD. **** $p < 0.0001$.

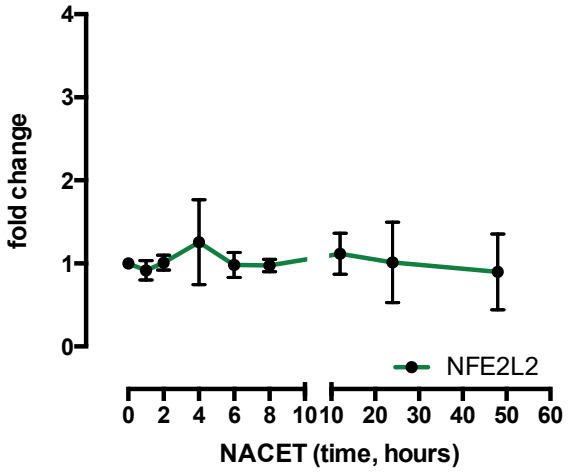

Figure 25. *NFE2L2* mRNA levels does not change after NACET treatment. Confluent ARPE-19 cells were treated with 1 mM NACET, and total mRNA was extracted at the indicated time points. Gene expression was analysed by RT-qPCR and represented as fold change relative to untreated cell condition. NFE2L2 mRNA levels were normalized to the expression of GAPDH as internal control. Results are represented as means ± SD of two independent experiments.

4.2 NACET induces ARE genes in ARPE-19 cells

To validate the data obtained by the transcriptomic analysis, we performed a time-course treatment with 1 mM NACET of ARPE-19 cells and analysed by means of RT-qPCR the expression of a selected set of NRF2 target genes involved in xenobiotic detoxification (NAD(P)H dehydrogenase quinone 1; NQO1), antioxidant response (heme oxygenase 1; HMOX1 and thioredoxin; (TXN), and glutathione synthesis and utilization (glutamate-cysteine ligase modifier subunit; GCLM,

glutamatecysteine ligase catalytic subunit; GCLC, glutathione reductase; GSR, and microsomal glutathione Stransferase 1; MGST1) (Figure 26).

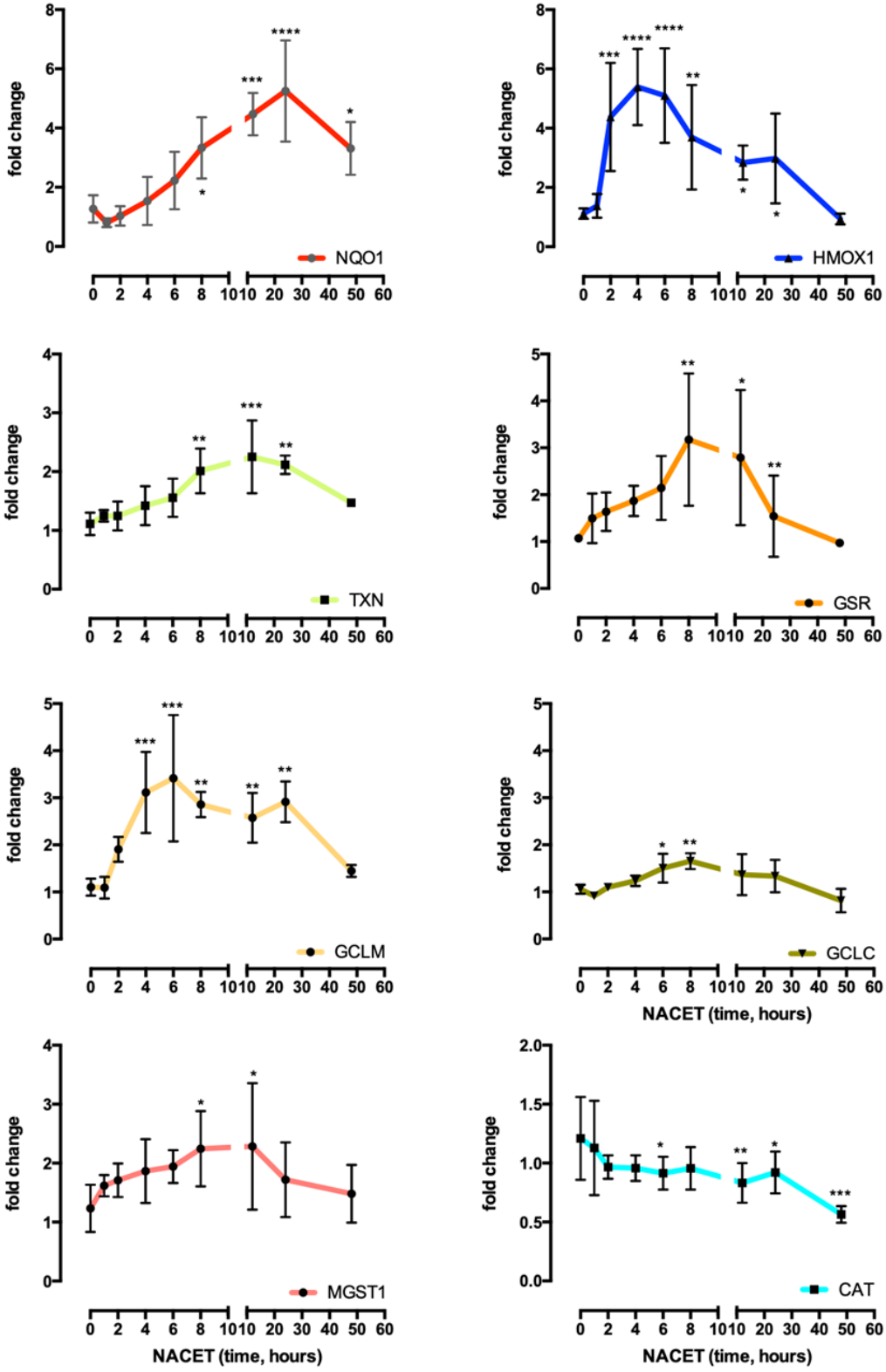

Figure 26. NACET induces NRF2 target gene expression in ARPE-19 cells. Confluent ARPE-19 cells were treated with 1 mM NACET, and total mRNA was extracted at the indicated time points. The expression of selected NRF2 target genes was analysed by RT-qPCR and represented as fold change relative to untreated cell condition. mRNA levels were

normalized to the expression of GAPDH as internal control. Results are represented as means ± SD of four independent experiments * p<0.05, ** p < 0.01, *** p < 0.001 and **** p < 0.0001.

4.3 NRF2 mediate NACET-induced ARE genes transcription

To demonstrate that NRF2 is responsible of the NACET-dependent transcriptional activation of the upregulated genes identified by RNA-seq, we generated an ARPE-19 cell line, genome-edited by CRISPR/Cas9 technology, expressing a non-functional form of NRF2, because deleted of the C-terminal part containing about half DNA/sMaf binding domain and all the CHD6 binding domain (Figure 27).

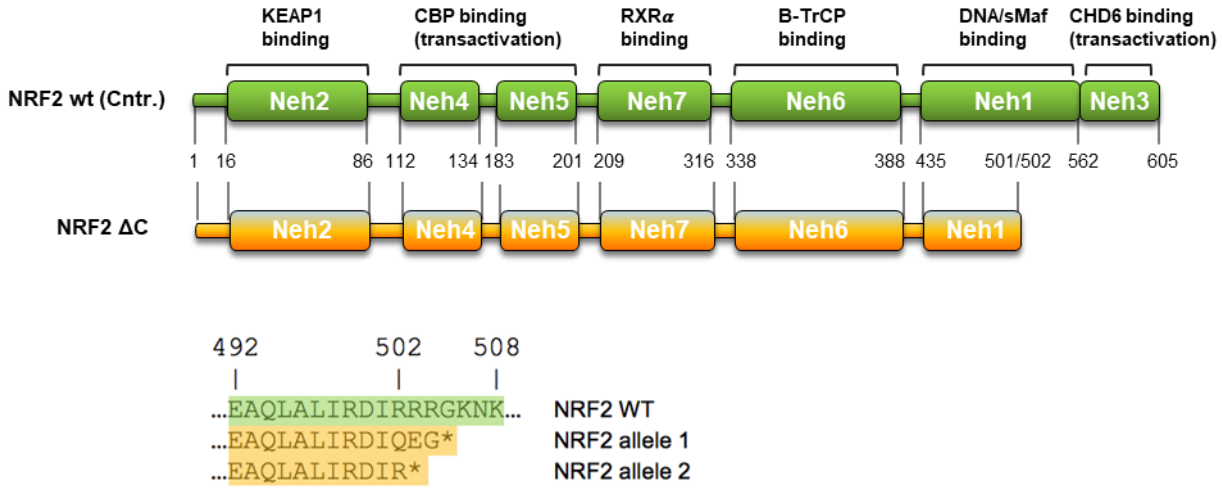

Figure 27. Schematic view of wild type and CRIPR/Cas9 edited NRF2 proteins. The functional domains and the site of mutation inserted by CRISPR/Cas9 are indicated. CRIPR/Cas9 edited NRF2 protein has been named NRF2 ΔC. The number of the amino acid residues are numbered from N-terminal methionine. The last amino acid residue of the edited form is not yet identified.

To obtain that, ARPE-19 were transduced with lentiviral particles for the expression of the endonuclease Cas9 and a guide RNA (gRNA), the latter specific for the exon 5 of NFE2L2 (NM_006164.5). As negative control, other cells were transduced with similar particles, but missing the gRNA sequence in the viral genome. As shown in the western blot of Figure 28A, the edited clone NRF2 ΔC expressed the truncated form of NRF2, while the control (Cntr.), obtained by transduction with control particles, maintained the NACET-dependent induction of full length NRF2 protein. We also verified by western blot analysis that NACET lost the capability to induce the NRF2-target gene NQO1 in edited cells (Figure 28A). The same effect is observed by RT-qRT-PCR for HMOX1, GCLM and GSR, demonstrating in this way that the transcriptional effect of NACET is, at least for the analysed genes, due to NRF2 activation (Figure 28B). To demonstrate the capability of NACET to promote transcriptional activation of target genes through NRF2-ARE binding, we transfected by electroporation NRF2 ΔC and control ARPE-19 cells with a construct carrying luciferase gene under the control of an artificial ARE-containing promoter, and subsequently performed a luciferase assay.

As shown in Figure 28C, we observed an induction of luciferase activity in a directly proportional manner to the NACET concentration used for cell treatment. Moreover, NRF2 ΔC expressing cell extracts, showed almost absent luciferase activity together with insensibility to NACET treatment.

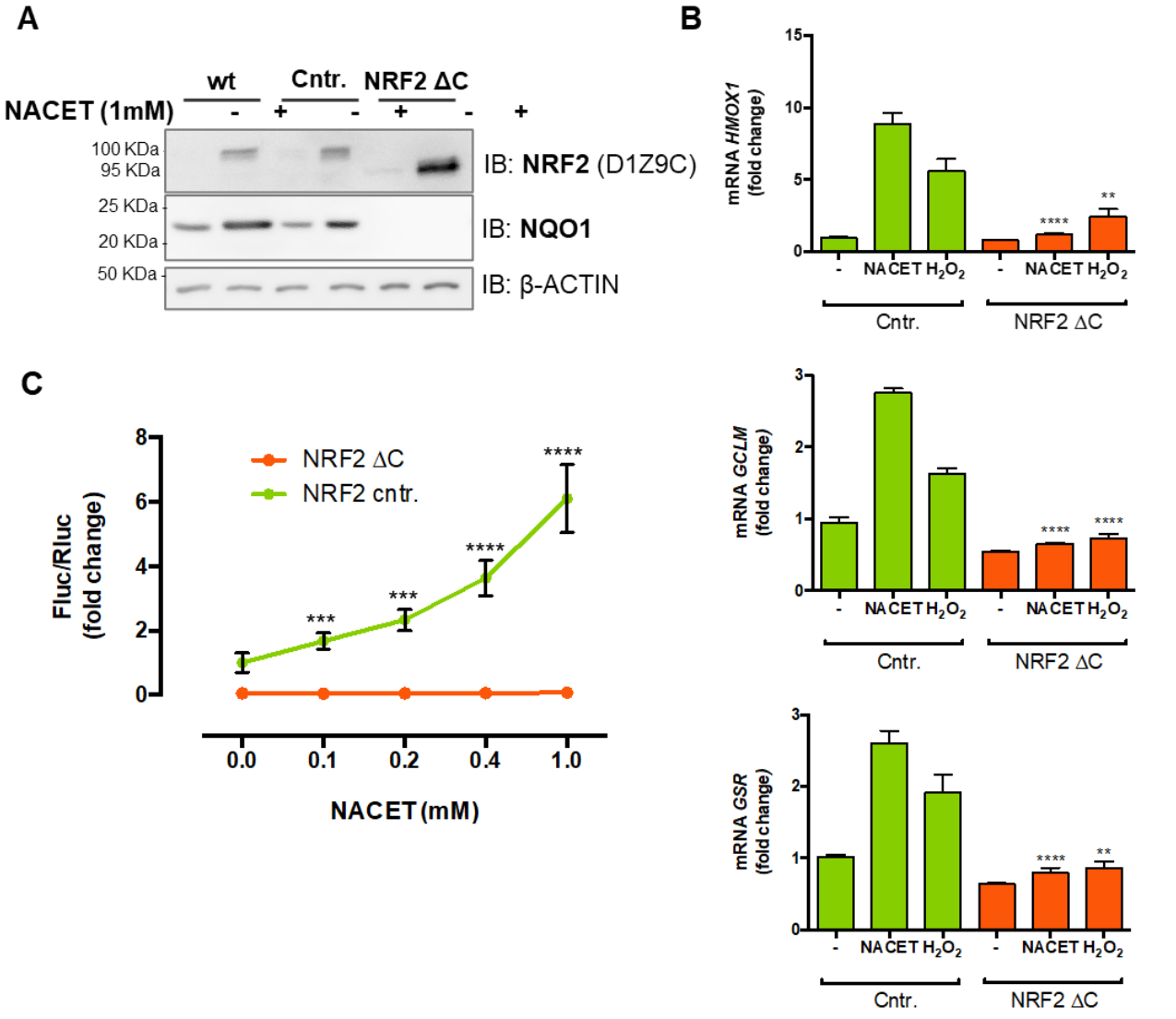

Figure 28. NRF2 is responsible of the NACET-dependent transcriptional activation of the upregulated genes identified by RNA-seq. A) Western blot analysis showing the expression of NRF2, NQO1 and, as loading control, β-actin, in WT, control and NRF2-edited ARPE-19 cells treated and untreated with 1 mM NACET. B) Graph showing the RT-qPCR analysis of the expression of HMOX1, GCLM and GSR after 8 hours of induction with 1 mM NACET or 0.2 mM H_2O_2. H_2O_2, a well-known NRF2 activator, was used as positive control (Covas, et al., 2013). Data are normalized versus GAPDH expression and results are shown as fold induction compared to untreated WT ARPE-19 cells. C) Graph showing the ARE-Luciferase activity assay in treated and untreated control and edited cells.

To further confirm the activation of the NRF2 pathway by NACET and to evaluate whether this activation is peculiar of NACET treatment or the effect of an indirect oxidative stress, we performed a transcriptome analysis in triplicate on ARPE-19 and NRF2 ΔC cells following NACET and H_2O_2 treatments.

Firstly, to determinate the relationship between all samples, we conducted the Principal Component Analysis (PCA) of the transcriptome data. PCA shows biological replicates clustered together (Figure 29). The first principal component (PC1) accounted for 59.4% of the expression variance and separated ARPE-19 from NRF2 ΔC samples based on their differences in NRF2, indicating that the presence/absence of a functional NRF2 explains the variance in this set of samples. The second principal component (PC2) accounted for 14.3% of the expression variance and separated the samples as consequence of the different stimuli, showing a greater separation between transcriptome of H_2O_2 and untreated cells rather than between transcriptome of NACET and untreated cells, indicating a different transcriptional response to the treatments.

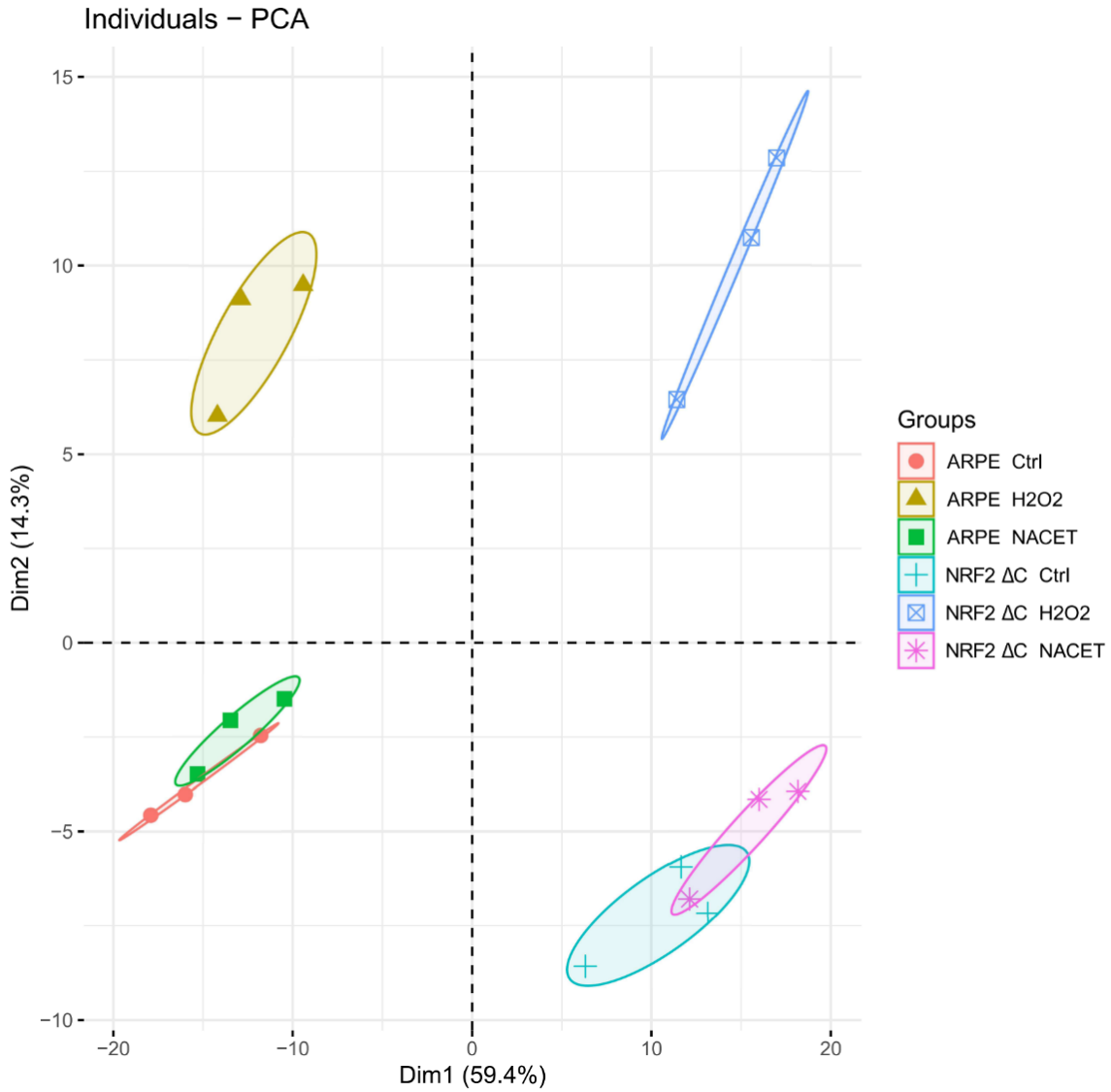

Figure 29. Principal component analysis (PCA) of ARPE-19 and NRF2 ΔC cells following NACET and H2O2 treatments. PCA was performed on 18 samples: 3 Ctrl, 3 NACET, 3 H_2O_2 of ARPE-19 and NRF2 ΔC cells, respectively.

Moreover, we calculated the number of differentially expressed genes (DEGs – adjusted p-value <0.05) and plotted them for the untreated vs NACET treated control cells (Figure 30A) and for the

untreated vs NACET treated NRF2 ΔC cells (Figure 30B). The comparison of the two volcano plots clearly shows that NACET induced a subset of NRF2 dependent genes, such as NQO1, MGST1, HMOX1, GCLC, GCLM and GSR. Upon comparing the DEGs in the NACET treated groups of ARPE-19 and NRF2 ΔC, as expected, there was a decrease in the expression of NRF2 target genes, such as NQO1, MGST1 and HMOX1, confirming that NRF2 is responsible of the NACET-dependent transcriptional activation of these upregulated genes (Figure 31).

This comparative transcriptome analysis unveils that NACET induces only a relatively low gene expression perturbation in comparison to a typical oxidative stress stimulus. In the Figure 32 are show the DEGs in common and uncommon between Ctrl and NACET, both in ARPE-19 and NRF2 ΔC cells. In particular, it is shown that in ARPE-19 are induced 1788 and 520 DEGs exclusively after H_2O_2 and NACET treatment, respectively, while there are only 542 DEGs in common and 31 DEGs in common but having an opposite expression trend. A similar result has been found in NRF2 ΔC cells, with 1814 and 477 DEGs induced exclusively after H_2O_2 and NACET treatment, respectively, and 384 DEGs in common and 41 having an opposite trend. The Ingenuity Pathway Analysis (IPA) of DEGs in common between H_2O_2- and NACET- treated wild type ARPE-19 reveals that tRNA charging and NRF2−mediated oxidative stress response are the most enriched pathways in this comparison (Figure 33 A). In the Figure 33 B, the IPA of the common DEGs between H_2O_2- and NACET- treated NRF2 ΔC cells shows that tRNA charging remains the only significant function. This result underlines the H_2O_2 and NACET treatment are two divergent stimuli sharing almost exclusively NRF2 pathway activation.

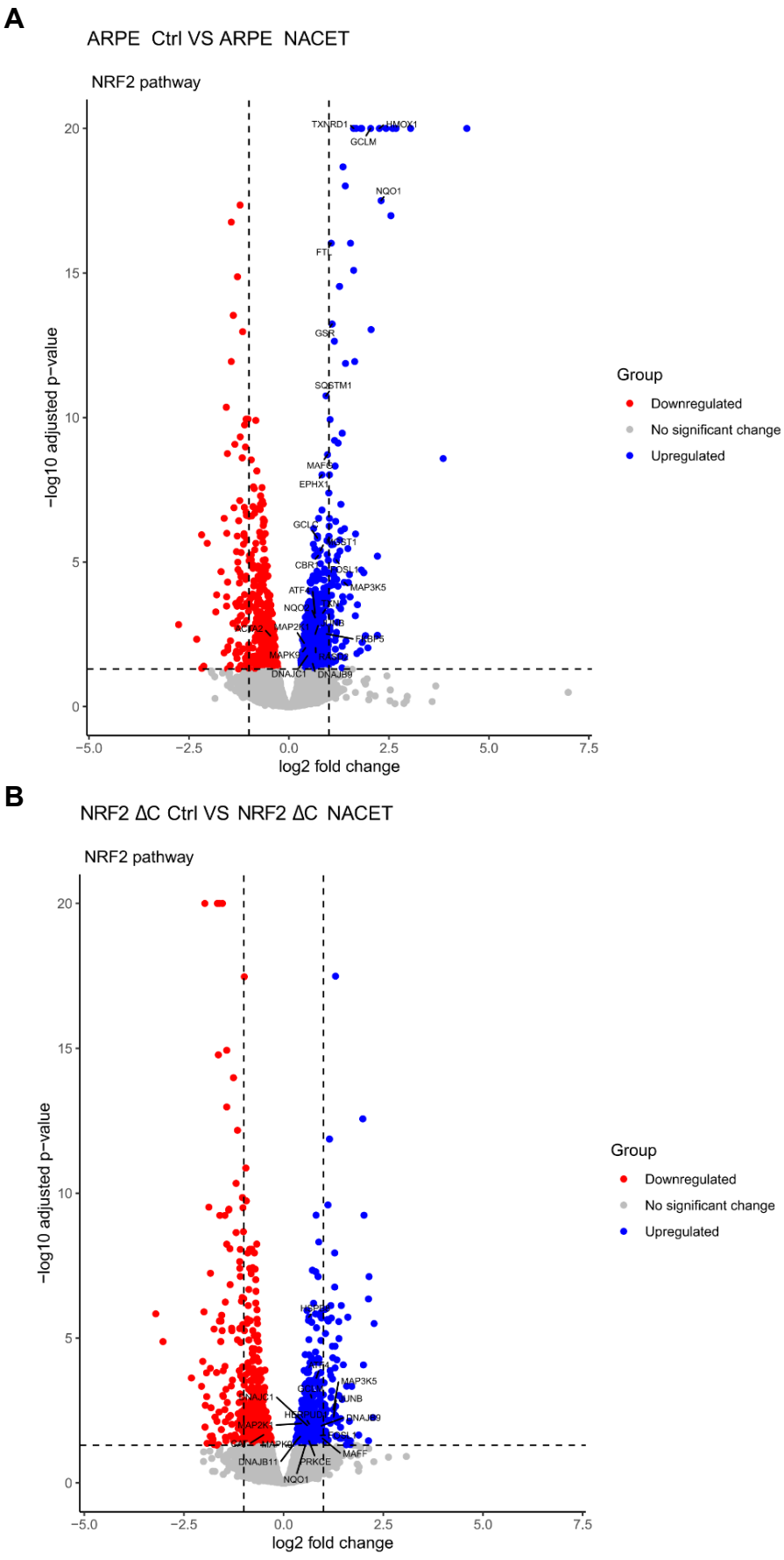

Figure 30. Volcano plot representation of up- and down-regulated genes in the comparison between (A) ARPE-19 Ctrl versus ARPE-19 NACET and (B) NRF2 ΔC Ctrl versus NRF2 ΔC NACET. The group mentioned before “VS" is the base group.

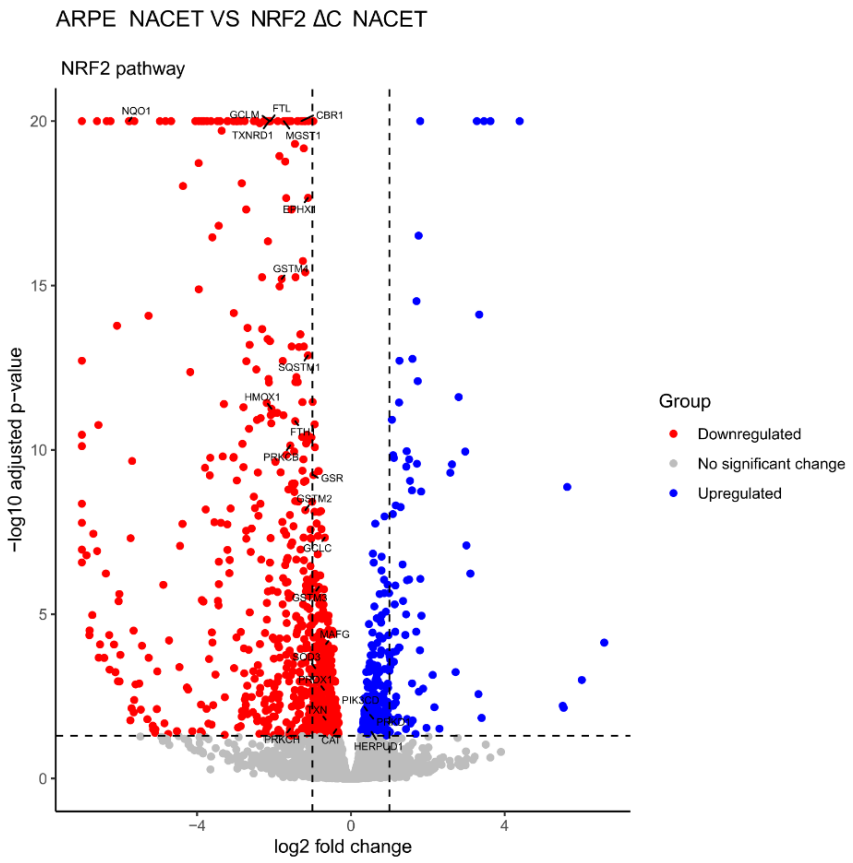

Figure 31 Volcano plot representation of up- and down-regulated genes in the comparison between ARPE-19 NACET versus NRF2 ΔC NACET. The group mentioned before “VS" is the base group.

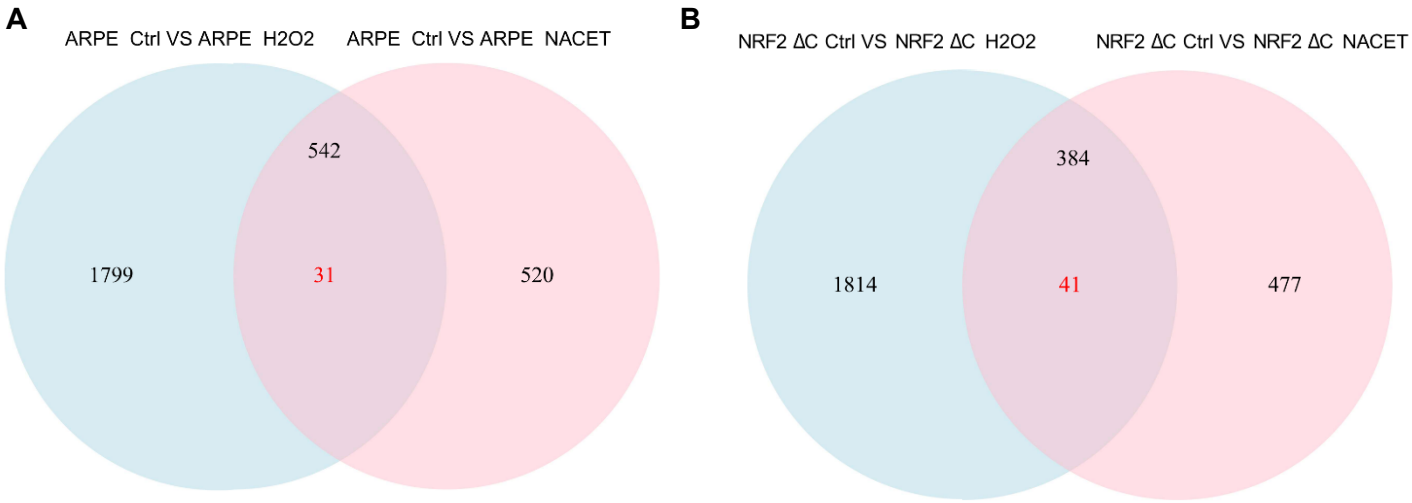

Figure 32. Representation of DEGs in common and uncommon between Ctrl and NACET treatments, both in ARPE-19 and NRF2 ΔC cells. (A) Venn diagram summarizes the overlap of DEGs found in ARPE Ctrl versus ARPE H_2O_2 compared to ARPE Ctrl versus ARPE NACET. (B) Venn diagram summarizes the overlap of DEGs found in NRF2 ΔC Ctrl versus NRF2 ΔC H_2O_2 compared to NRF2 ΔC Ctrl versus NRF2 ΔC NACET. In red: common DEGs with an opposite expression trend. The group mentioned before “VS" is the base group.

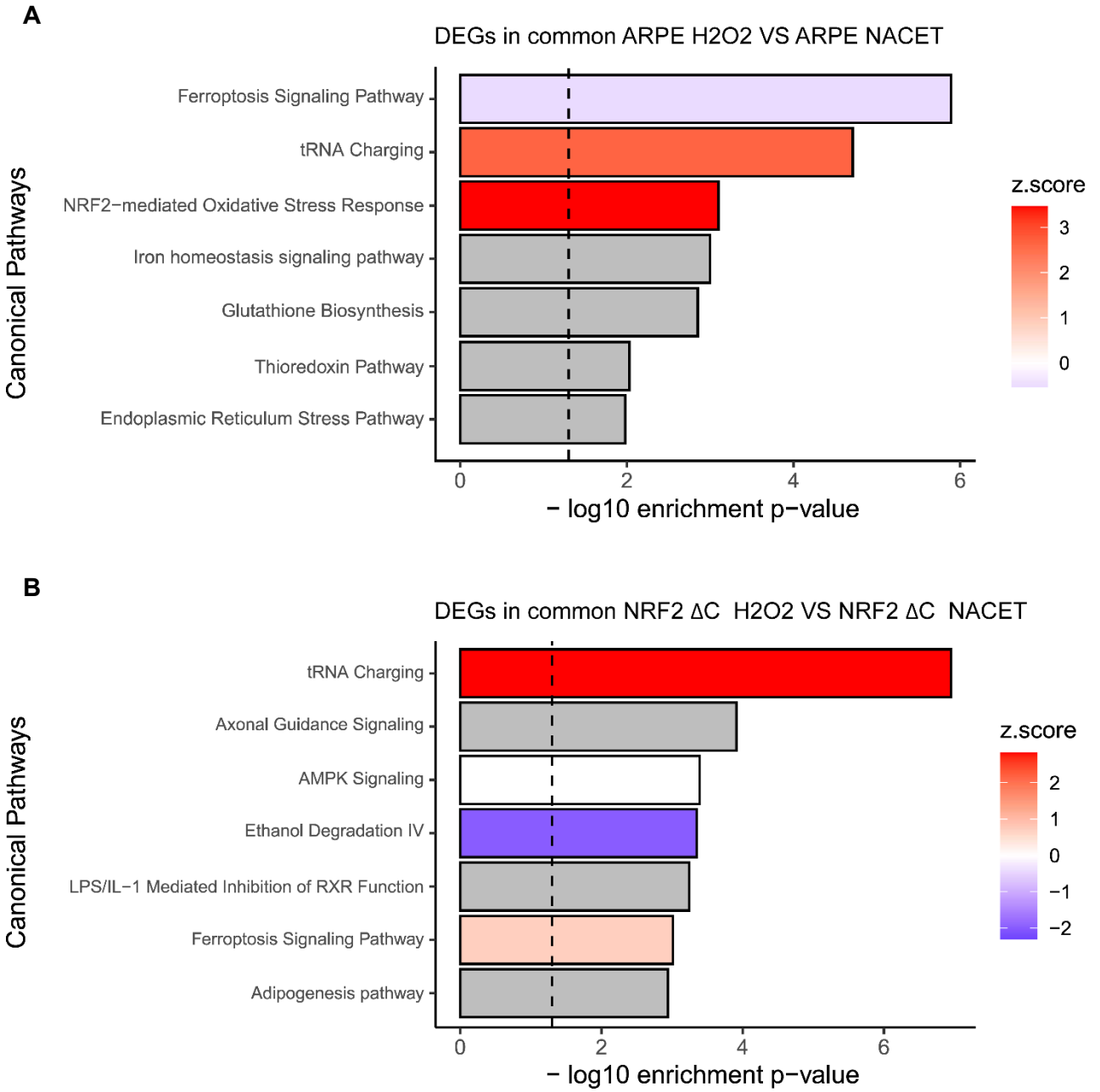

Figure 33. IPA of DEGs in common between H_2O_2 and NACET, both in (A) ARPE-19 (ARPE Ctrl VS ARPE H2O2 compared to ARPE Ctrl VS ARPE NACET) and (B) NRF2 ΔC cells (NRF2 ΔC Ctrl VS NRF2 ΔC H2O2 compared to NRF2 ΔC Ctrl VS NRF2 ΔC NACET). Enrichment p-value (x-axis) and activation z-score (color code) were calculated by IPA. The group mentioned before "VS" is the base group

4.4 Intracellular cysteine level is linked to NRF2 expression

To characterize the molecular mechanism underlying the NRF2 stabilization by NACET, we compare the effect of NACET, NAC and Cysteine on this process. By Western blot analysis, we demonstrated that NAC did not induces an increase of NRF2 expression in RPE cells, while cysteine, even if at lower level, allowed a NRF2 upregulation (Figure 34). Furthermore, to demonstrate that NACET and cysteine trigger the NRF2 pathway induction with a specific mechanism and not as a consequence of

a general reductive stress, we treated the cells with the reductive compound DTT, and did not observe any activation but, on the contrary, a decrease in the basal level of NRF2 expression.

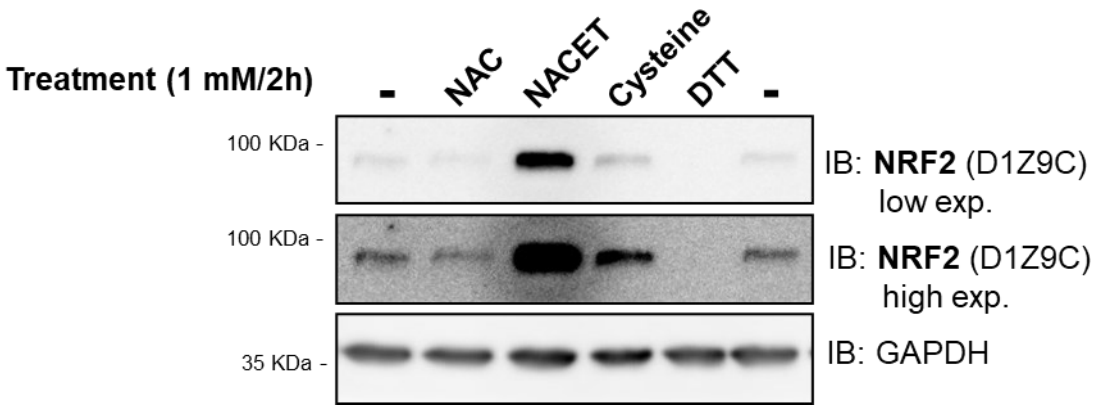

Figure 34 Cysteine, but not reductive stress or NAC, induces NRF2 expression in RPE cells. Confluent ARPE-19 cells were treated for 2 hours with 1 mM NAC, NACET, cysteine or DTT, in DMEM/F12 or in DMEM without cysteine and methionine where reported. The whole cell lysates were analysed by western blot with anti-NRF2 (D1Z9C) antibody and anti-GAPDH antibody for the loading control. The low and the high exposition of the immunoblot for the NRF2 100 kDa isoform was reported to better appreciate the differences in the induction levels.

This observation, together with the knowledge that NACET, but not NAC, can passively cross the plasma membrane and that Cysteine can be actively transported inside the cell by the system X_c^-, strongly suggest that NRF2 can be stabilized by the increased intracellular levels of NACET, Cysteine or some of their downstream metabolites, such as GSH or γ-glutamylcysteine. To better characterize the induction mechanism under study, we pretreated ARPE-19 cells with the inhibitor Buthionine Sulfoximine (BSO). BSO targets γ-glutamylcysteine ligase (GCL), the enzyme involved in the first rate-limiting step of the GSH biosynthesis (Figure 35 A). As shown in Figure 35 C, the BSO-mediated GCL inhibition, induced a stronger NRF2 upregulation after NACET treatment in comparison to what happened in ARPE-19 cells treated with only NACET, suggesting that a metabolite upstream of γ-glutamylcysteine was responsible of this effect. To verify the efficacy of the inhibitor, ARPE-19 cells were treated as before, lysed by TCA-EDTA solution and analysed by HPCL to measure the intracellular levels of the metabolites of interest (Figure 36 B). As shown, cysteine and NAC intracellular levels were significantly increased after NACET treatment, but only cysteine levels were further increased in presence of BSO, suggesting that the intracellular increase of cysteine plays a critical role in the NRF2 upregulation.

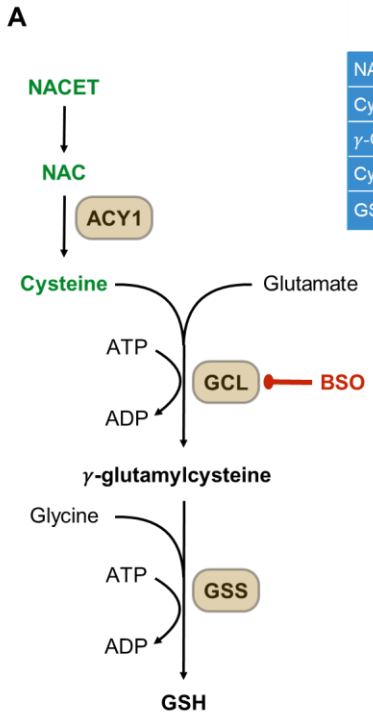

B

Intracellular thiols (nmol/mg prot)

	-	NACET 15'	NACET 1h	BSO 45'	BSO 1.5 h	NACET 15' +BSO 45'	NACET 1h +BSO 1.5h
NAC	0	10.2±2.4	9.6±1.9	0	0	9.4±1.0	9.4±0.3
Cys	1.7±0.1	3.4±0.7	3.6±1.1*	1.9±0.1	1.8±0.2	4.6±1.5**	4.4±1.1**
γ-GluCys	0.06±0.02	0.05±0.01	0.05±0.01	0.04±0.01	0.03±0.012	0.05±0.01	0.08±0.01
CysGly	0.19±0.07	0.25±0.1	0.26±0.12	0.22±0.01	0.20±0.02	0.17±0.02	0.17±0.01
GSH	108.5±7.6	103.7±12.6	107.2±14.5	110.3±2.3	104.7±16.1	117.7±12.8	101.8±7.2

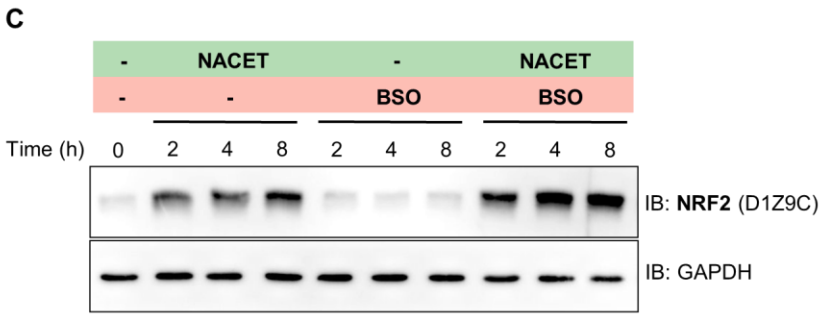

Figure 35. Cysteine accumulation is linked to the NRF2 activation. A) Schematic representation of the GSH synthesis pathway (see text for details). B) Confluent ARPE-19 cells were pre-treated for 30' with 100 μM BSO and then incubated with 0.2 mM NACET for the indicated time points. The whole cell lysates were analysed by western blot with anti-NRF2 (D1Z9C) antibody, Anti-GAPDH antibody was used for the loading control. C) ARPE-19 cells treated as in (B), were lysed by TCA-EDTA solution and the intracellular thiols were measured by HPLC (γ–GluCys: γ-glutamilcysteine; CysGly: cysteinylglycine). Thiol concentrations are normalized for the total protein content and expressed in nmol/mg protein. Measurements are the means ± SD of the independent experiments.

4.5 Critical KEAP1 cysteine residues are cysteinylated by cysteine

Once determined that cysteine can be responsible for the activation of NRF2, we wondered whether KEAP1 can act as cysteine sensor and, eventually, which KEAP1 stress sensor residue is involved. To address this point, we incubated in vitro the recombinant purified KEAP1 with increasing amount of free cysteine and determine by mass spectrometry that some critical KEAP1 cysteine residues are modified by cysteinylation, with cysteine 583 the more sensible one (Figure 36).

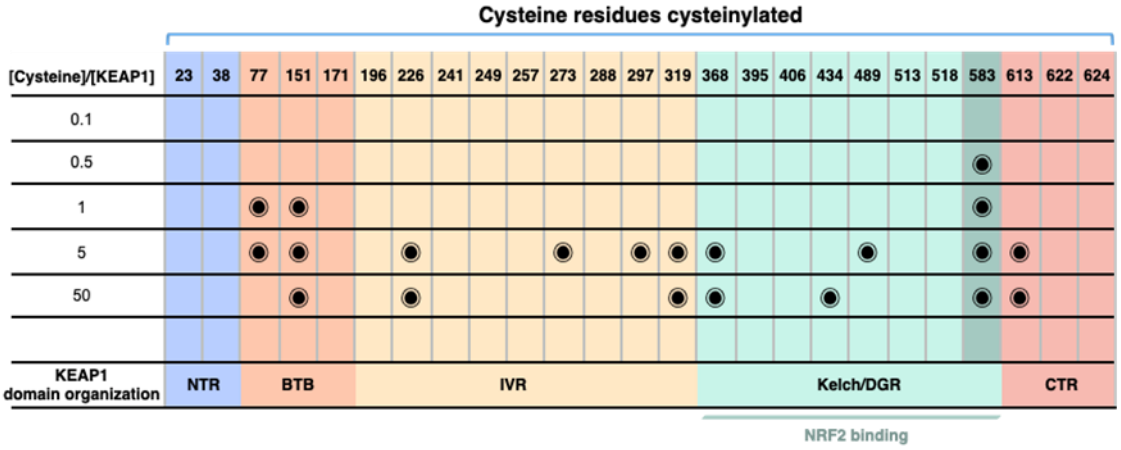

Figure 36. KEAP1 is cysteinylated in sensor residues by free cysteine. Recombinant human KEAP1 was incubated with decreasing concentration of freshly prepared cysteine. The cysteinylated cysteine residues observed by mass spectrometry are indicated by black dots. Lowering the cysteine/KEAP1 ratio, only the most reactive, and supposed specific, residues presented the modification

The data reported strongly suggested that cysteine can react with the cytoplasmatic negative regulator of the NRF2-ARE signaling pathway KEAP1, and that this cysteinylation can mediate the disengagement of NRF2, its stabilization and, consequently, its nuclear translocation and activity as transcriptional regulator. However, further analysis will be carried out in cellular context to confirm the identity of the KEAP1 sensor cysteine residues involved in this activation mechanism.

4.6 System X_c^- in the NRF2 stabilization

To confirm the SLC7A11 upregulation by NACET treatment observed in whole transcriptomic analysis, we performed a time-course treatment with 1 mM NACET on ARPE-19 cells and analysed the expression of SLC7A11 by means of RT-qPCR. NACET induced a rapid increase in *SLC7A11* mRNA level, with maximal of activation at 6 hours post-treatment (Figure 37).

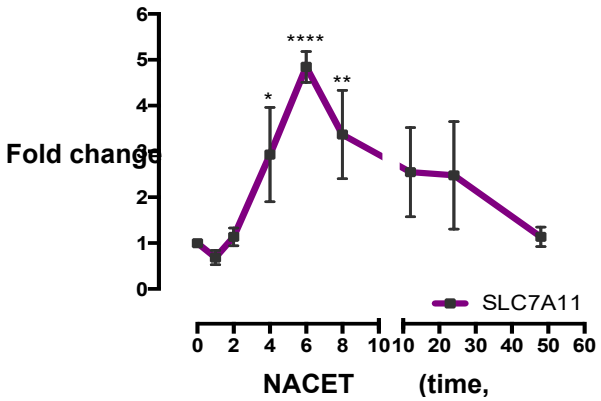

Figure 37. NACET induces SLC7A11 mRNA in ARPE-19 cells. Confluent ARPE-19 cells were treated with 1 mM NACET and total mRNA was extracted at the indicated time points. The expression of SLC7A11 was analysed by RT-qPCR and represented as fold change relative to untreated cell condition. mRNA levels were normalized to the expression of GAPDH as internal control. Results are represented as means ± SD of three independent experiments. * $p<0.05$, ** $p < 0.01$ and **** $p < 0.0001$.

The NACET-dependent SLC7A11 induction was confirmed also at the protein level, with an increase of the expression of two isoforms of about 110 and 40 kDa (Figure 38).

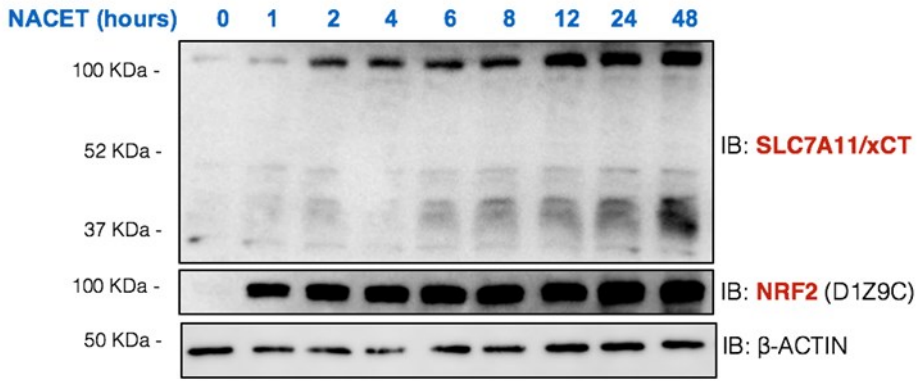

Figure 38. NACET induces SLC7A11 expression in ARPE-19 cells. Confluent ARPE-19 cells were treated with 1 mM NACET at the indicated time points, and whole cell lysates were analysed by western blot with anti-NRF2 (D1Z9C) and anti-SLC7A11 antibodies, β-ACTIN was used as loading control.

Because we demonstrated that cysteine induces NRF2 stabilization, we wondered whether the cystine/glutamate antiporter SLC7A11/xCT was not only a target, but also a mediator of this activation mechanism. To investigate this point, we transduced ARPE-19 cells with a lentiviral particles for the overexpression of SLC7A11/xCT, or GFP as control, and then we treated the cell culture with cystine, glutamine (freshly prepared, since at physiological pH glutamine is unstable and tends to degrade to ammonium and pyroglutamate), as intracellular precursor of L-glutamate, or directly L-glutamate, that added in the extracellular environment acts as a cystine/glutamate antiporter inhibitor (Figure 39). Overexpression of SLC7A11/xCT was sufficient to increase the cystine-mediated NRF2 induction, and this effect was enhanced by glutamine and inhibited by of L-glutamate, as expected if cystine-mediated induction of NRF2 was mediated by the system X_c^-. All

together, these results strongly suggest the involvement of SLC7A11/xCT in the cysteine/cystine-dependent NRF2 pathway activation.

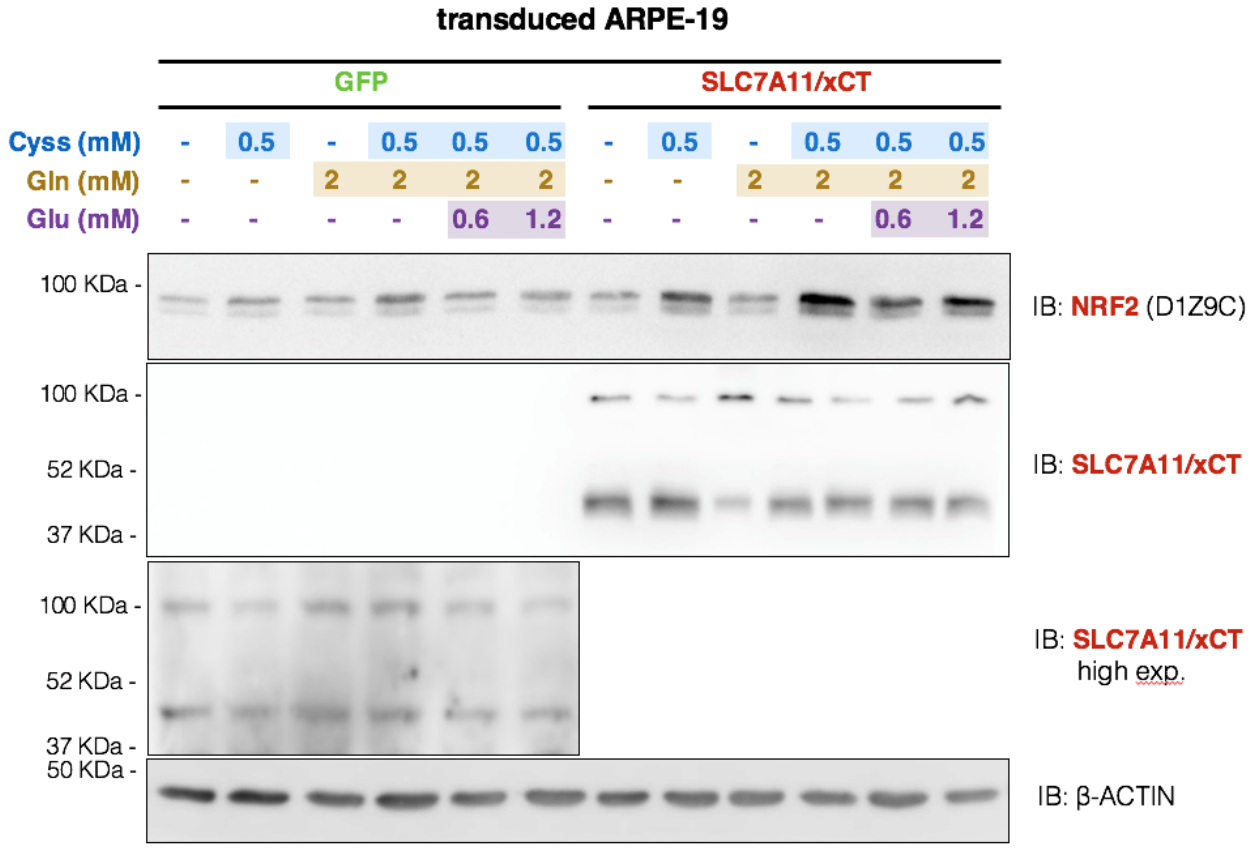

Figure 39. SLC7A11/xCT is involved in cysteine/cystine-dependent NRF2 pathway activation. Confluent ARPE-19 cells were infected with lentiviral particles for the overexpression of SLC7A11 or GFP as negative and infection control; after 16 hours the medium was chanced and the cells were treated with 0.5 mM cystine (Cyss), 2 mM glutamine (Gln), and L-glutamate (Glu) as indicated for another 24 hours. The whole cell lysates were analysed by western blot with anti-NRF2 (D1Z9C), anti-SLC7A11 antibodies. β-ACTIN was used as loading control. ARPE-19 cells express very low basal levels of SLC7A11/xCT; thus two different expositions were necessary to show the protein in GFP and SLC7A11/xCT transduced cells. For higher expression the filter was cut out to avoid dazzling by overexpressed protein signal.

4.7 NACET-induced NRF2 expression is not cell-context dependent

To demonstrate that NACET does not induces NRF2 expression in a cell-context dependent manner, we repeated the treatment in 2 primary cell cultures, human fibroblasts (Fibrob.) and human umbilical vein endothelial cells (HUVEC), and in 10 tumoral or immortalized cell lines of different tissue origins: HK-2 (immortalized kidney epithelial cells), Panc-1 (epithelioid pancreas carcinoma), HT-29 (epithelioid colorectal adenocarcinoma), U-2 OS (osteosarcoma), HeLa (cervical adenocarcinoma), RD (Rhabdomyosarcoma), MCF7 (breast cancer adenocarcinoma), T98G (glioblastoma), and A549 (lung carcinoma).

As shown in (Figure 40), NACET treatment results in the induction of NRF2 expression, confirming our hypothesis. An exception was represented by T98G and A549 cells, which however showed constitutive high levels of NRF2 expression.

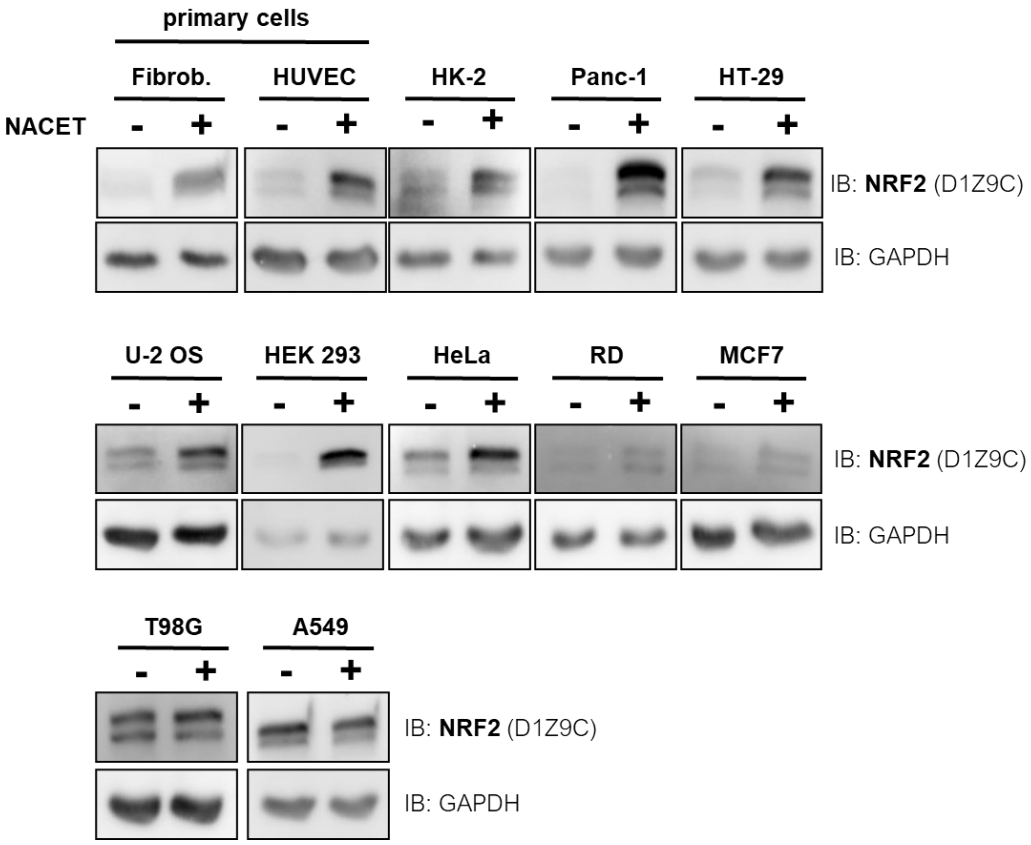

Figure 40. NACET-induced NRF2 expression is not cell-context dependent. The indicated cell lines or primary cells were treated with 1 mM NACET for 6 hours, the whole cell lysates were analysed by western blot with anti-NRF2 (D1Z9C) and anti-GAPDH antibodies. The latter was used for the loading control.

4.8 NACET treatment on young and old mouse retinas

In light of the data presented, as well as the recent observation that NACET reaches the ocular tissues following oral administration (Tosi et al., 2021), and with the aim to suggest NACET as therapeutic and preventive agent for AMD, we wanted to deep investigate NACET effects *in vivo* on young and old mouse retina. Therefore, we watered young (8-20 weeks) and old (80-110 weeks) C57BL/6J mice with NACET-supplemented water and after 5 days we sacrificed the mice for eye dissection and retina collection. One of the retinas of each mouse has been used to measure the concentration of Cys and GSH through HPLC analysis, while the other retina has been used for RNA-seq analysis (Figure 41).

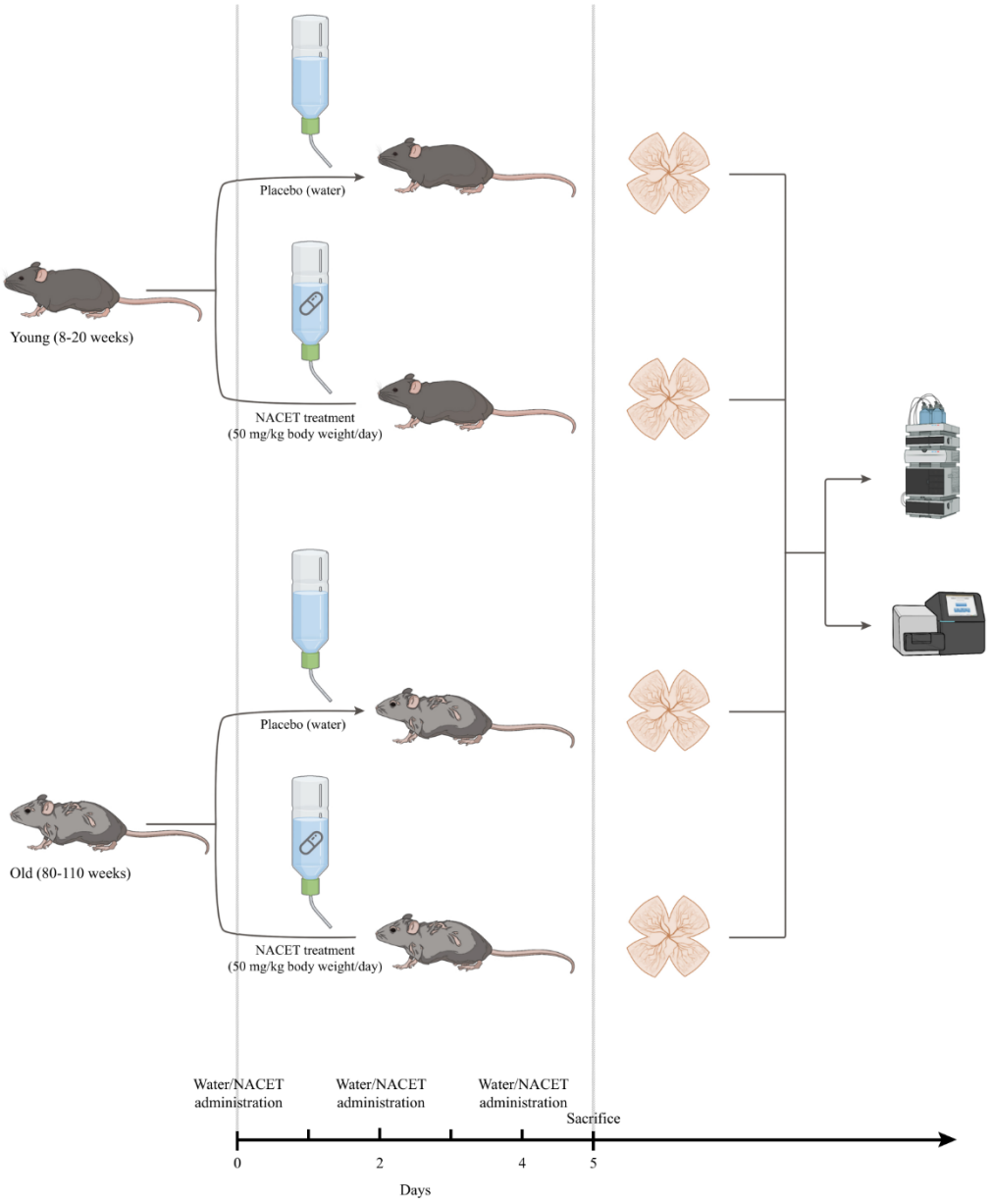

Figure 41. NACET treatment scheme of young (8-20 weeks) and old (80-110 weeks) C57BL6/J mice.

We measured the cysteine and glutathione levels in young and old mouse retina, through HPLC analysis (Figure 42). Cys and GSH levels were significantly higher in retinas of old as compared to young mise, as well as in mice orally administrated with NACET, regardless of age. This suggests an

increased request of antioxidant response by the aged retina and that NACET can increase the natural GSH antioxidant system of the retina.

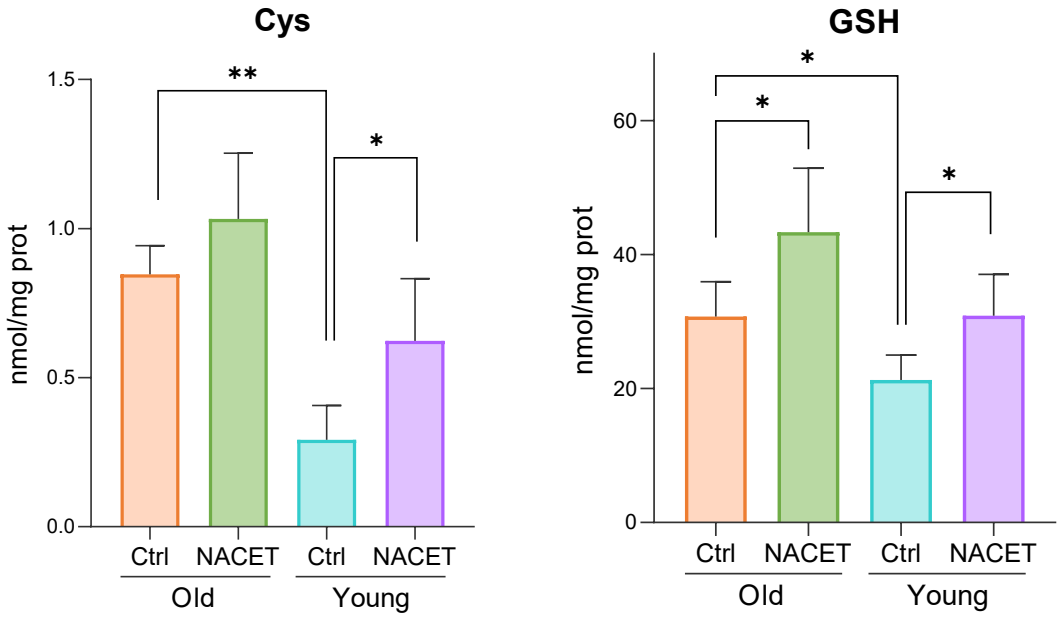

Figure 42. Cys and GSH concentration levels in young and old mouse retina. Results are represented as means ± SD of biological replicates, * $p<0.05$, and ** $p < 0.01$.

Furthermore, we performed a transcriptome analysis on young and old mouse retinas following NACET treatment. To determinate the relationship between all retina samples, we conducted the Principal Component Analysis (Figure 43). The PC2 accounted for 25.6% of the expression variance and showed a separation of the samples based on aging related differences, which result diminished in presence of NACET treatment. The PC1 accounted for 45.4% of the expression variance and separated the samples as consequence of NACET treatment, displaying that young and old have a different transcriptome response to NACET treatment.

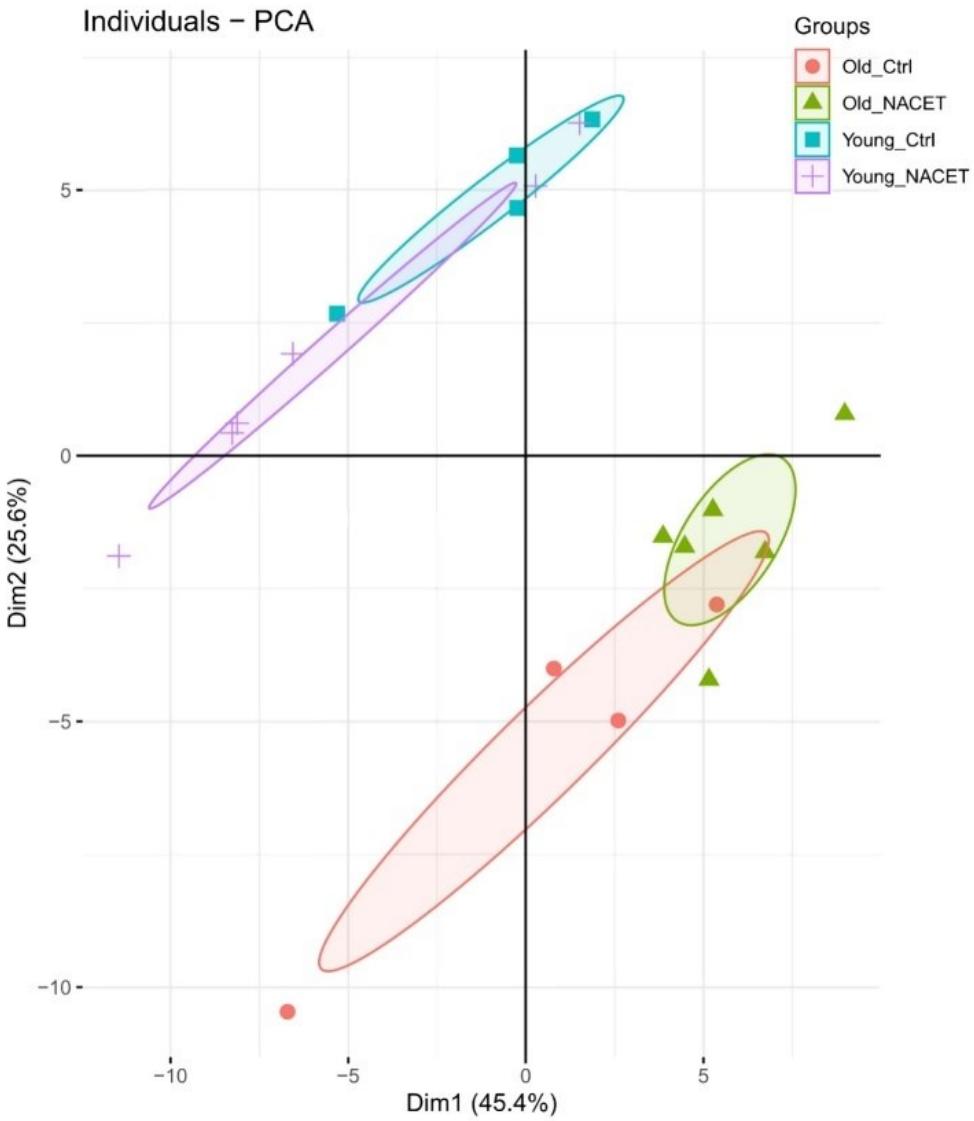

Figure 43. Principal Component Analysis (PCA) of normalized RNA-seq data of young and old mouse retina following NACET treatment.

Upon comparing the expression pattern between young and old control groups, we detected 719 DEGs and the numbers of up- and down-regulated genes were 410 and 309, respectively. No significant changes have been found between young control and young NACET, while we identified 376 DEGs comparing old control versus old NACET, among them 185 up-regulated and 191 down-regulated (Figure 44).

The IPA of DEGs reveals that calcium, STAT3, ephrin receptor and TGF signaling pathways are among the most enriched pathways in young versus old mouse retina (Figure 45A), while ER stress pathway and unfolded protein response are the functions associated with the highest rated network in the comparison between control and NACET treated old mice (Figure 45B). Moreover, in the Figure 46A are shown the putative upstream regulators of the identified differentially regulated pathways found in the comparison of retina transcriptomes between young versus old, among them several are

known to be involved in inflammation and senescence-associated secretory phenotype (SASP)-related genes, such as tumor necrosis factor-α (TNF-α), Interferon gamma (IFN-γ), and Toll-like receptor (TLR). While in the Figure 46B are shown the regulators of the comparison between old versus old NACET-treated mice. Interestingly, in the latter the NFE2L2 regulator is evidently upregulated in NACET treated mice, confirming the data obtained *in vitro* in RPE cells.

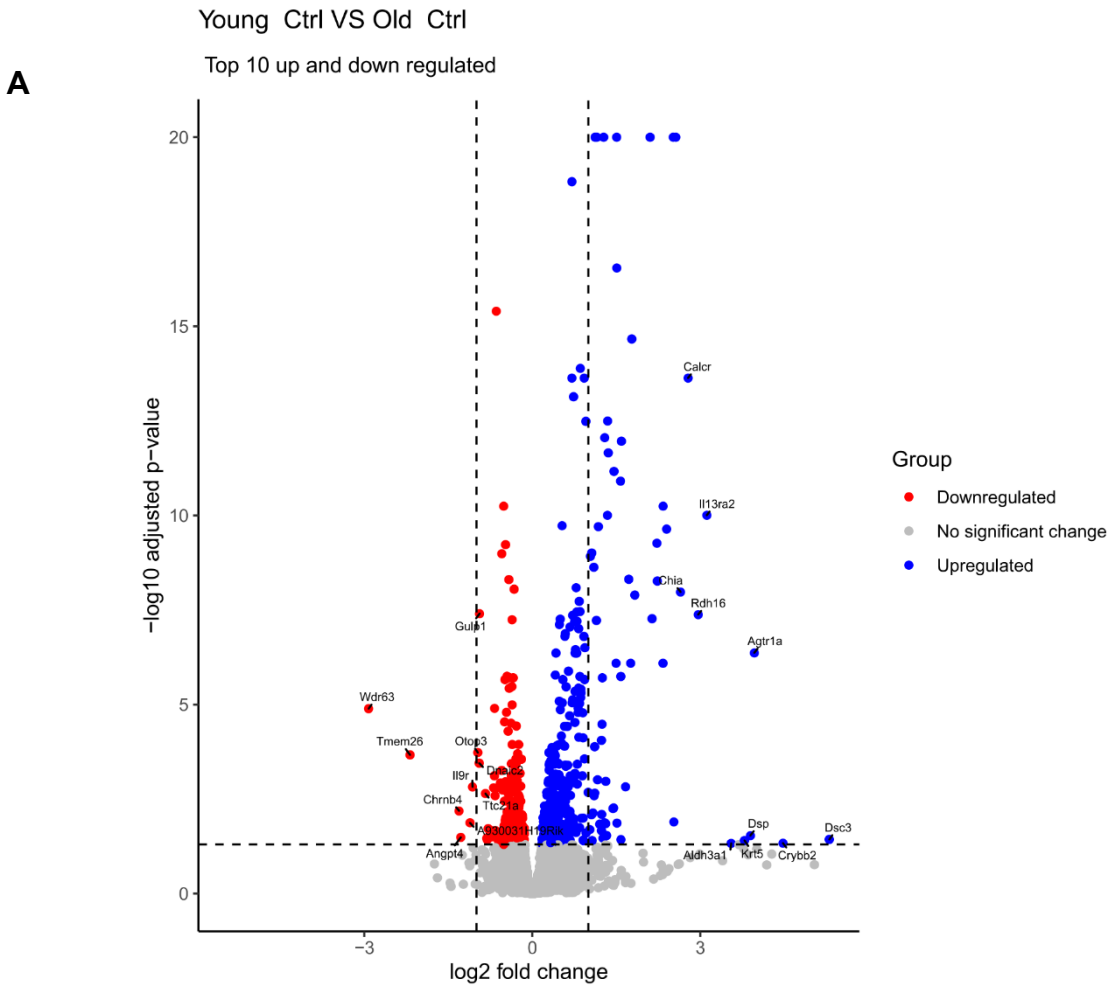

B

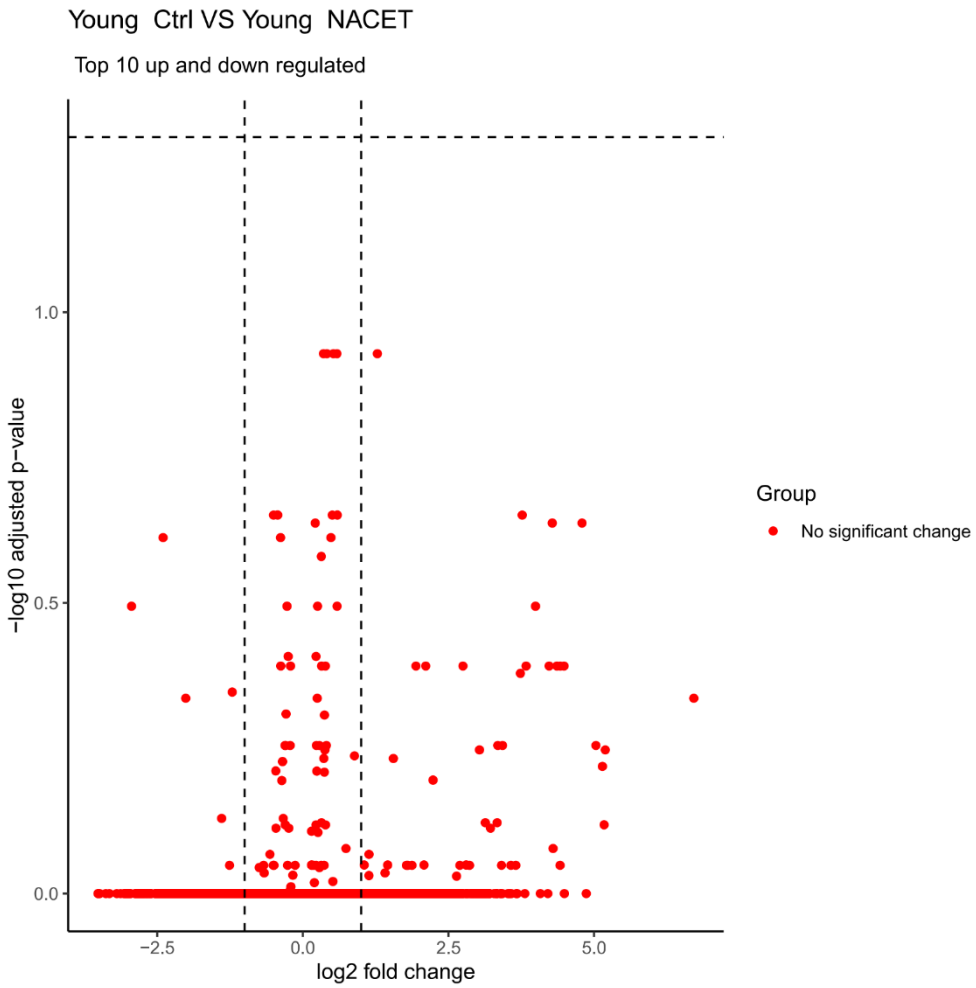
Young Ctrl VS Young NACET
Top 10 up and down regulated
−log10 adjusted p−value
1.0
0.5
0.0
−2.5
0.0
2.5
5.0
log2 fold change
Group
No significant change

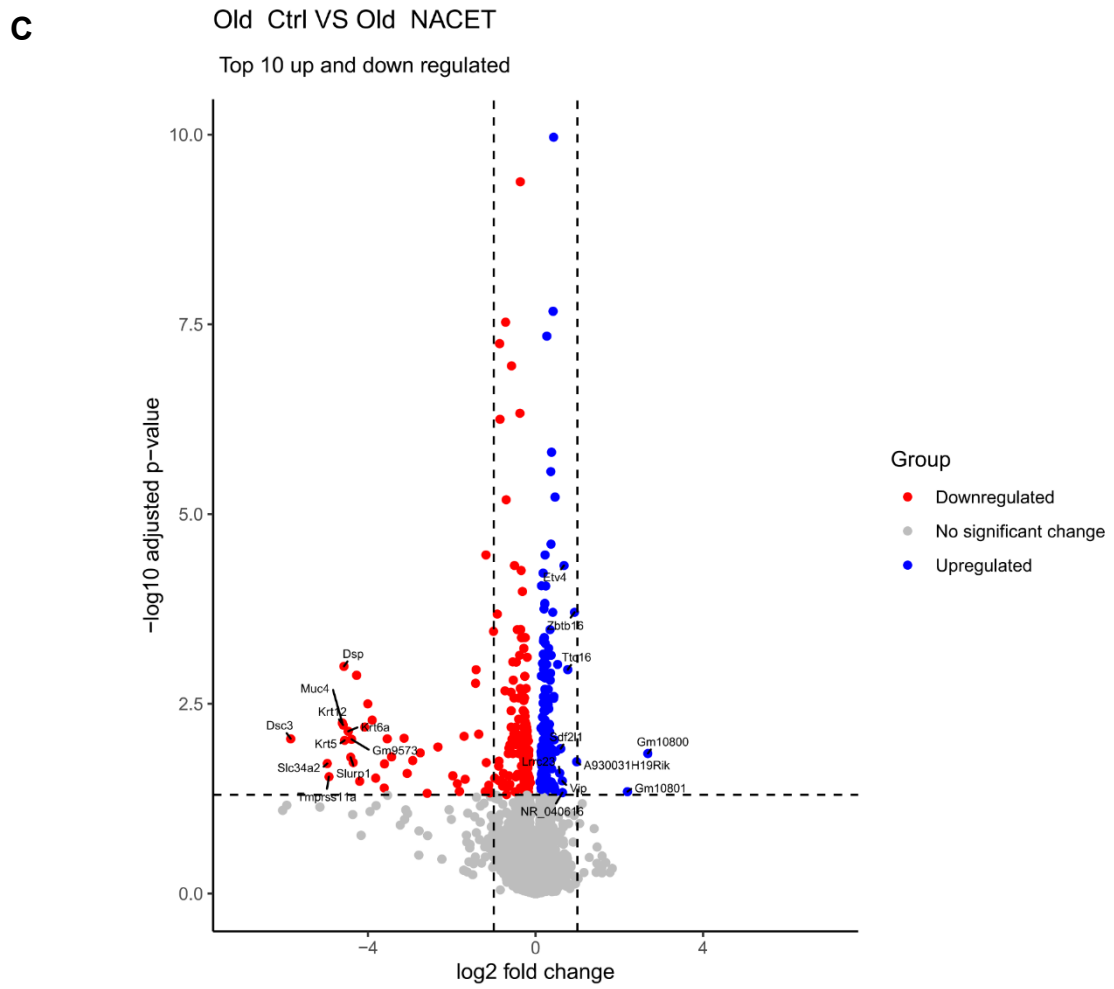

Figure 44. Volcano plot representation of differential expression analysis of genes in young and old mouse retina, indicating the top 10 up- and down-regulated genes. (A) Volcano plot displays that there are 719 DEGs between young ctrl and old ctrl, and the numbers of up- and down-regulated genes in old ctrl are 410 and 309, respectively. B) Volcano plot of young ctrl VS young NACET shows no significant changes between the two groups, while (C) volcano plot of old ctrl VS old NACET displays that there are 376 DEGs, and the numbers of up- and down-regulated genes in old NACET are 185 and 191, respectively. The group mentioned before “VS" is the base group.

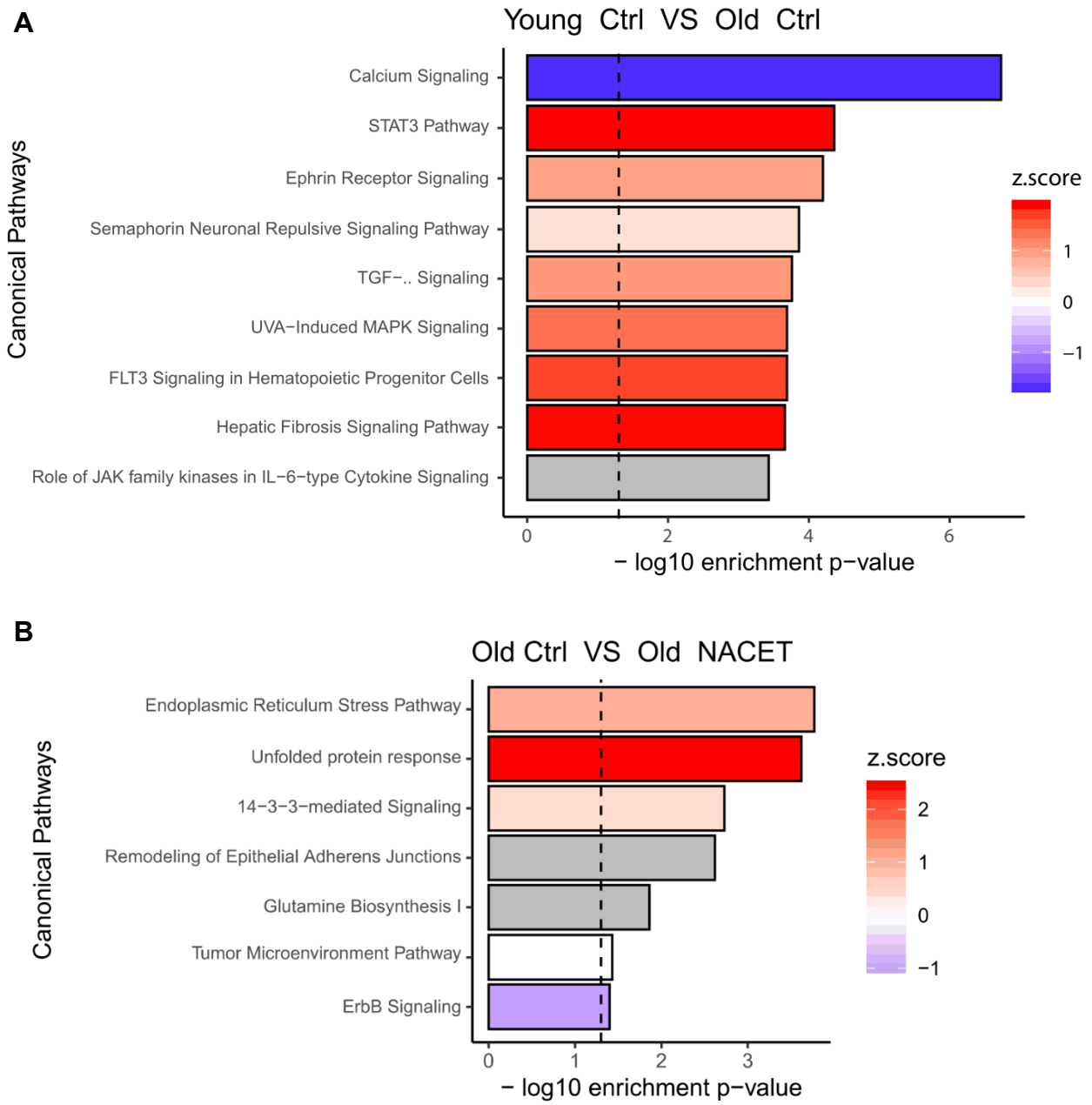

Figure 45. IPA of DEGs of young and old mouse retina. A) Analysis of DEGs of young ctrl compared to old ctrl and of (B) old ctrl compared to old NACET retina. Enrichment p-value (x-axis) and activation z-score (color code) were calculated by IPA. The group mentioned before “VS" is the base group.

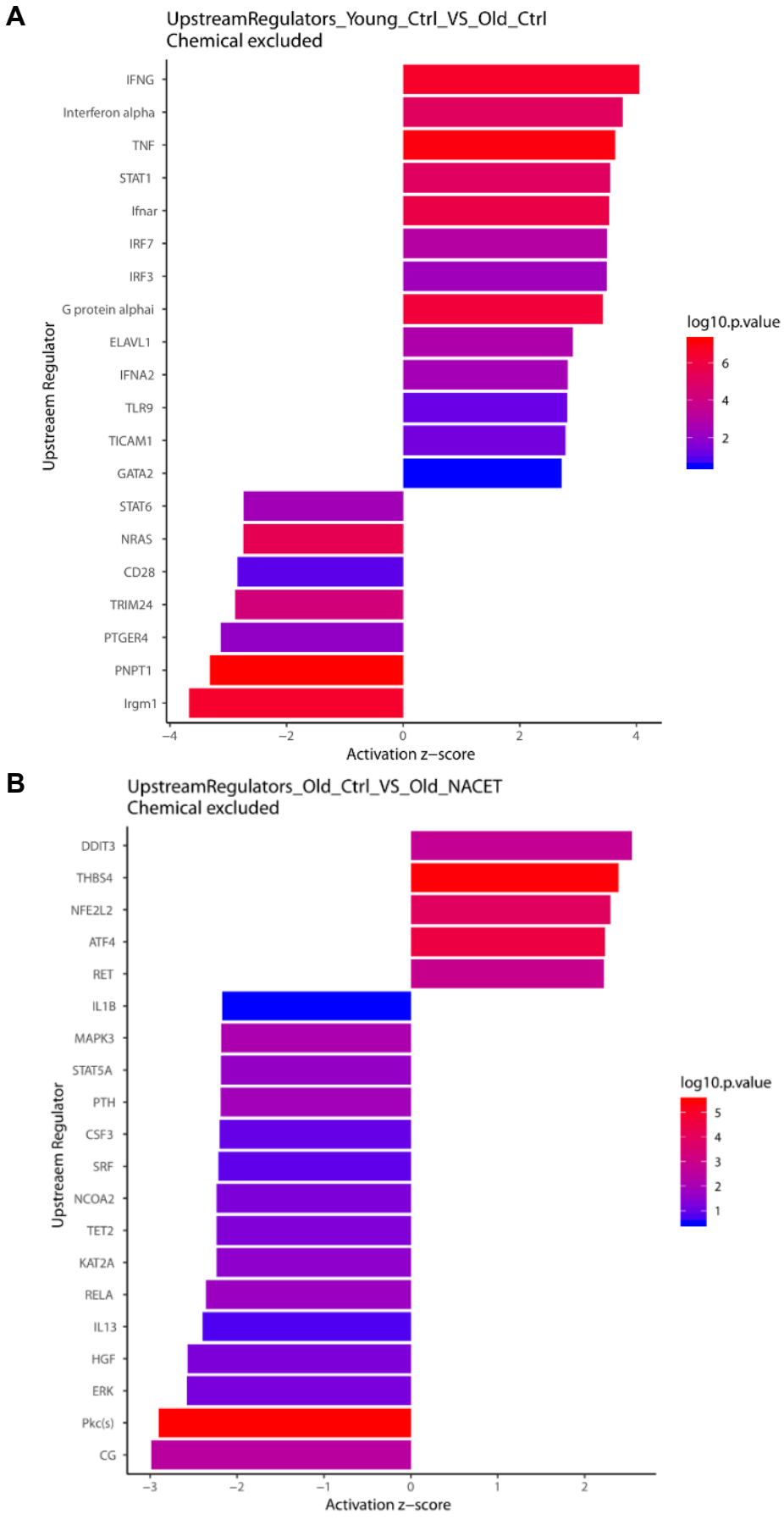

Figure 46. Top 20 Upstream regulators (chemical excluded) of DEGs of young and old mouse retina. Enrichment p-value (color code) and activation z-score (x-axis) were calculated by IPA. The group mentioned before “VS" is the base group.

Since aging related differences are reduced in the presence of NACET (Figure 43), we focused our analysis on DEGs having an opposite expression trend between the two comparisons: young control versus old control and old control versus old NACET (Figure 47). In a simpler manner, the overlaps genes showed in the Venn diagrams (29+28) are indicating the number of genes rescued by NACET treatment. So overall, 57 DEGs have been rescued (Table 5). IPA of these DEGs shows that unfolded protein response is the function with the highest rated network (Figure 48).

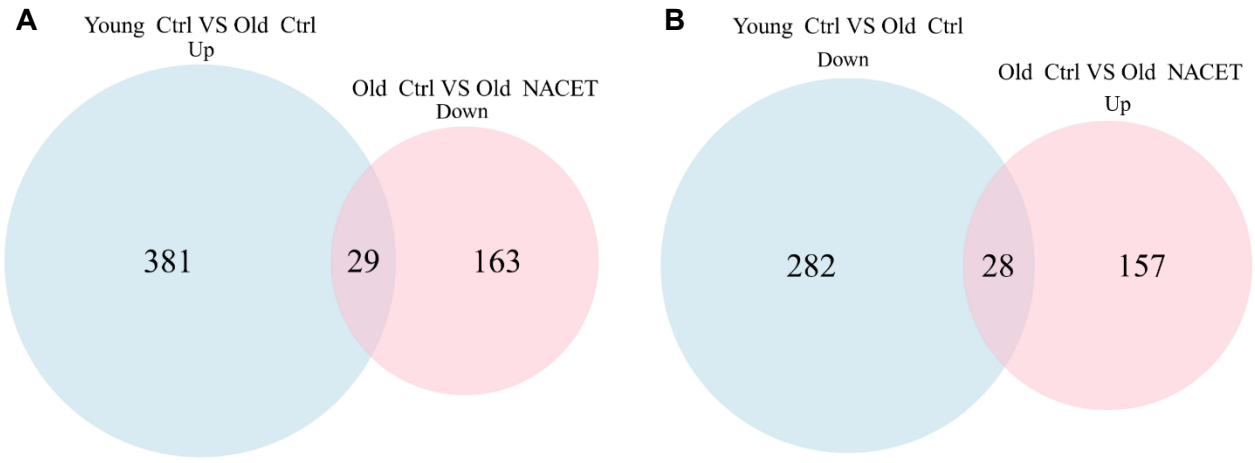

Figure 47. Representation of DEGs directly rescued by NACET treatment in old mouse retina. (A) Venn Diagram summarizes the overlap of the up-regulated genes found in the comparison between young control versus old control and the down-regulated genes found in in the comparison between old control versus old NACET. (B) Venn diagram shows the overlap of the down-regulated genes found in the comparison between young control versus old control and the up-regulated genes found in in the comparison between old control versus old NACET. The group mentioned before “VS" is the base group.

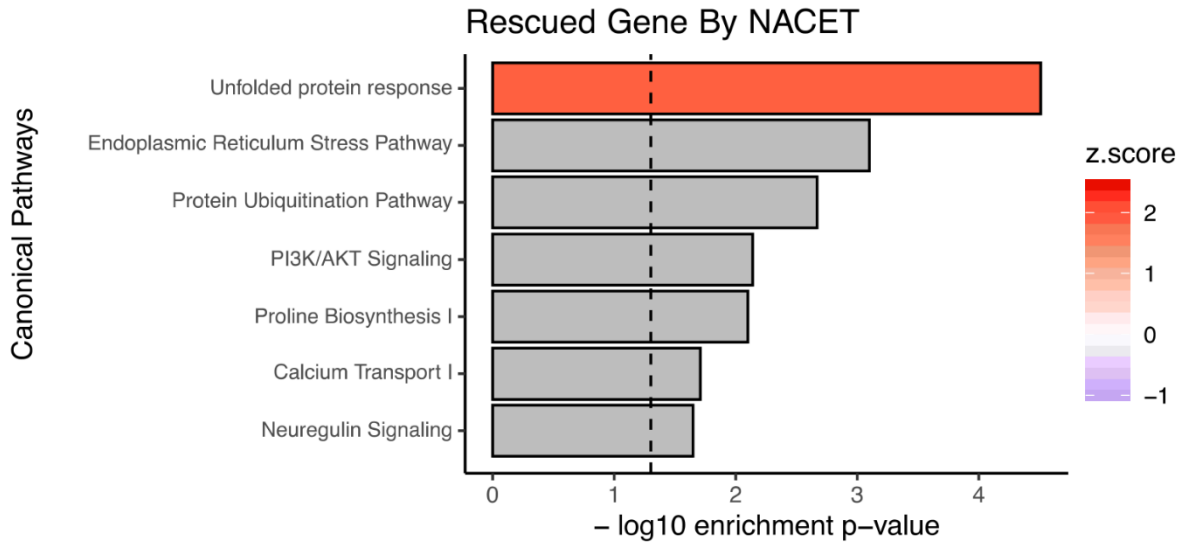

Figure 48. Analysis of DEGs directly rescued by NACET treatment in old mouse retina. Enrichment p-value (x-axis) and activation z-score (color code) were calculated by IPA. The group mentioned before “VS" is the base group.

Symbol	Gene ID	Full name	AGING*	NACET*
Cep83os	67723	Centrosomal protein 83, opposite strand	0,258	-0,297
A930031H19Rik	77835	RIKEN cDNA A930031H19 gene	-1,115	0,980
Aldh18a1	56454	Aldehyde dehydrogenase 18 family, member A1	-0,390	0,465
Ank2	109676	Ankyrin-2	-0,185	0,107
Ankrd13b	268445	Ankyrin repeat domain 13b	-0,243	0,200
Zfand4	67492	Zinc finger, AN1-type domain 4	0,640	-0,587
Ap1m1	11767	Adaptor-related protein complex AP-1, mu subunit 1	-0,218	0,221
Ap3b2	11775	Adaptor-related protein complex 3, beta 2 subunit	-0,220	0,127
Atp11b	76295	ATPase, class VI, type 11B	0,326	-0,225
Atp2a2	11938	ATPase, Ca++ transporting, cardiac muscle, slow twitch 2	-0,178	0,181
Bag6	224727	BCL2-associated athanogene 6	-0,219	0,133
Bcl2	12043	B cell leukemia/lymphoma 2	0,422	-0,381
Btc	12223	Betacellulin, epidermal growth factor family member	0,498	-0,365
C430042M11Rik	320021	RIKEN cDNA C430042M11 gene	0,392	-0,339
Calr	12317	Calreticulin	-0,284	0,368
Clic6	209195	Chloride intracellular channel 6	0,900	-0,326
Clpb	20480	ClpB caseinolytic peptidase B	-0,207	0,222
D630045J12Rik	330286	RIKEN cDNA D630045J12 gene	-0,434	0,209
Drosha	14000	Drosha, ribonuclease type III	-0,181	0,142
Dsc3	13507	Desmocollin-3	5,302	-5,845
Dsp	109620	Desmoplakin	3,893	-4,574
Mir670hg	414123	MIR670 host gene (non-protein coding)	-0,388	0,384
Fbxw8	231672	F-box and WD-40 domain protein 8	-0,262	0,197
Gca	227960	Grancalcin	0,412	-0,256
Gm10742	100038486	Predicted gene 10742	0,580	-0,264
Gm14412	102640477	Predicted gene 14412	0,557	-0,582
Gm6245	621629	Predicted gene 6245	0,424	-0,350
H2-K1	14972	Histocompatibility 2, K1, K region	0,542	-0,230
Hsp90ab1	15516	Heat shock protein 90 alpha (cytosolic), class B member 1	-0,222	0,224
Hspa5	14828	Heat shock protein 5	-0,325	0,380
Hspa8	15481	Heat shock protein 8	-0,246	0,430
Htra1	56213	HtrA serine peptidase 1	-0,528	0,355
Cilk1	56542	Ciliogenesis associated kinase 1	0,241	-0,212
Il13ra2	16165	Interleukin 13 receptor, alpha 2	3,116	-0,881
Irf6	54139	Interferon regulatory factor 6	1,590	-0,614
Krt5	110308	Keratin-5	3,788	-4,557
Lrfn2	70530	Leucine Rich Repeat And Fibronectin Type III Domain Containing 2	-0,367	0,359
Ly75	17076	Lymphocyte antigen 75	2,102	-0,515
Mars	216443	Methionine-tRNA synthetase 1	-0,225	0,224
Mfap3l	71306	Microfibrillar-associated protein 3-like	0,196	-0,195
Mib2	76580	Mindbomb E3 ubiquitin protein ligase 2	-0,237	0,228
Mrtfa	223701	Myocardin related transcription factor A	-0,333	0,239
Thap12	72981	THAP domain containing 12	0,186	-0,144
Ptpn20	19256	Protein tyrosine phosphatase, non-receptor type 20	0,843	-1,184
Rell1	100532	RELT-like 1	0,533	-0,469
Reln	19699	Reelin	-0,479	0,163
Rft1	328370	RFT1 homolog	0,291	-0,284
Rimbp3	239731	RIMS binding protein 3	0,574	-0,295
Scg2	20254	Secretogranin II	-0,232	0,235
Slc1a4	55963	Solute carrier family 1 (glutamate/neutral amino acid transporter), member 4	-0,376	0,288
Slc29a4	243328	Solute carrier family 29 (nucleoside transporters), member 4	0,932	-0,650
Spata6	67946	Spermatogenesis associated 6	0,394	-0,396
Spc25	66442	SPC25, NDC80 kinetochore complex component, homolog (S. cerevisiae)	-0,645	0,316
Tec	21682	Tec protein tyrosine kinase	1,356	-0,471
Tuba4a	22145	Tubulin, alpha 4A	-0,275	0,246
Vgf	381677	VGF nerve growth factor inducible	-0,475	0,527
Zfp949	71640	Zinc finger protein 949	0,318	-0,181

**log2 fold change*

Table 5. List of DEGs rescued by NACET treatment in aged mouse retina.

5 DISCUSSION

Oxidative stress plays a major role in AMD pathogenesis and progression, and several known or potential antioxidant compounds have been tested to investigate their effects on AMD. Most of the enzymatic antioxidant defences (e.g., SODs, catalase, and the enzymes responsible for glutathione metabolism) are regulated at transcriptional level by the transcription factor nuclear factor erythroid 2-related factor 2 (NRF2), which allows the maintenance of redox homeostasis (Bellezza et al., 2018; Nakagami, 2016).

In this study, we used as an antioxidant agent N-acetyl-L-cysteine ethyl ester (NACET), a derivative molecule of the well-known N-acetyl-L-cysteine (NAC). NACET has an improved lipophilicity and bioavailability compared to NAC (Giustarini et al., 2012), and it has been demonstrated that NACET but not NAC, predisposes RPE cells to oxidative stress resistance and increases the intracellular levels of reduced GSH in RPE cells *in vitro*, and in rats' eyes after oral administration (Tosi et al., 2021). Therefore, since the use of NACET to treat oxidative stress-related retinal diseases, such as AMD, is promising, we decided to deeply investigate the effects of NACET both *in vitro* and *in vivo*, on RPE cell line and mouse retina, respectively.

Initially, we conducted a transcriptome analysis on ARPE-19 cells treated with NAC or NACET, and surprisingly, RNA-seq data analysis showed that 32 out of 41 genes serum-independently upregulated only by NACET were NRF2 direct targets and that 21 of them were described to be involved in oxidative stress response. It is noteworthy to underline that NRF2 signaling is impaired in aging, thereby determining retinal cell death (Bellezza, 2018).

We confirmed, through Western blot analysis and RT-qPCR, that NACET induces the activation of NRF2 pathway, as well as its target genes. Moreover, by using CRISPR genome editing technique, we generated an RPE cell line expressing an endogenous defective form of NRF2 and unequivocally pointed out NRF2 as indispensable mediator of NACET-dependent transcriptional activation of several genes involved in oxidative stress response, such as genes involved in glutathione synthesis and utilization (e.g., GCLM, MGST1), thioredoxin metabolism (e.g., TXN, TXNRD1), and heme and iron homeostasis (e.g., HMOX1).

Since we have used NACET by relying on its propriety of being a precursor of GSH, we expected a decrease in antioxidant gene expression, while an increased was observed. However, because high concentrations of cysteine can be toxic to the cell especially in neuronal cells (Wang & Cynader, 2001), we hypothesized that the observed NRF2 activation is a response of an increase of intracellular level of cysteine with the aim to convert it to GSH, the major source and buffer of cysteine levels,

and keep concentrations of free cysteine within a narrow window in the micromolar range (Kohl et al., 2019). Our data demonstrated that the supplementation of cysteine in culture medium is *per se* capable of inducing NRF2 protein stabilization, while the use of DTT as alternative reductive stressor does not, excluding reductive stress as a cause of NRF2 induction. Moreover, the inhibitor Buthionine Sulfoximine (BSO), that targets γ-glutamylcysteine ligase (GCL), the enzyme involved in the first rate-limiting step of the GSH biosynthesis, enhanced NACET-induced NRF2 activation together with an increase of intracellular free cysteine level. Finally, by *in vitro* experiments, we demonstrate that KEAP1, the cellular sensor and negative regulator of NRF2, reacts directly with cysteine through key regulatory residues. Therefore, even if other aimed experiments are needed, our data strongly suggest that KEAP1 senses the altered levels of free cysteine by the cysteinylation of its key cysteine residues, and thereby disengagement and stabilization of NRF2, that intervenes in restoring the cellular homeostasis. From the point of view of AMD therapy, NACET could be a potent antioxidant agent not only as cell permeable GSH precursor, but also as an inducer of the KEAP1-NRF2 oxidative defence pathway.

However, even though we identified this effect in a specific cell line of retinal pigment epithelial cells, this result is not cell specific. In fact, we reproduced it in numerous human cell types, including primary, immortalized, and tumoral cells, the latter originating from a broad range of tissues. Many tumors increase uptake and dependence on glucose, cystine or glutamine, and overexpression of SLC7A11/xCT and/or alteration of KEAP1/NRF2 pathway occur in cancer cells to satisfy the metabolic requirements for growth and survival (Cloer et al., 2019; W. L. Wu & Papagiannakopoulos, 2020). Moreover, increased cystine uptake is necessary to sustain the high demand of GSH synthesis by the in cancer cells, that use it to counter the high degree of oxidative stress in tumoral environment and eventually for conjugation and detoxification of chemotherapy (Cloer et al., 2019; W. Lin et al., 2020; S. Wu et al., 2019). Our findings shed also new light to forced cystine uptake by cancer cells: cysteine could serve as GSH precursor but also to sustain NRF2-KEAP1-ARE pathway activation, that protects them from genotoxic chemo- and radiotherapies, as well as from oxidative stress.

As age is the strongest demographic risk factor associated with AMD (Heesterbeek et al., 2020), to deeply investigate NACET effects on retina during aging, we treated young and old mice with NACET-supplemented water for 5 days. In the retina of both young and old mice, the cysteine and GSH levels slightly increase after NACET treatment, thereby demonstrating that NACET can reach the neural layer of the retina and be effective in increasing one of the main antioxidant defences of the cell.

RNA-seq data analysis showed a different gene expression pattern between young and old mouse retinas caused by aging related differences. Senescence-associated secretory phenotype (SASP) arising from chronic senescence is a master and protracted source of the chronic inflammation typical of aging and age related disease, such as AMD (Lee et al., 2021; Sharma et al., 2014). Among the upstream regulators found dysregulated in aging retina, several are related to inflammation- and SASP, such as tumor necrosis factor-α (TNF-α), Interferon gamma (IFN-γ), and toll-like receptor (TLR).

According to this, it is interesting to note that the genes coding for interleukin-13 receptor subunit alpha-2, *Il13ra2*, and lymphocyte antigen 75, *LY75*, are two of the 57 DEGs in aging retina whose expression is rescued by NACET. IL13Rα2 is a transmembrane receptor which binds the anti-inflammatory cytokine Interleukin-19 (IL-13) with very high affinity. Due to its very short cytoplasmic region lacking signaling motifs IL-13Rα2 acts as a "decoy" receptor, sequestering IL-13 and thereby preventing excessive IL-13 signaling via the signaling receptor complex IL-13Rα1 and IL-4Rα (Chandriani et al., 2014; Kawakami et al., 2001). In the context of AMD, photosensitization of N-retinylidene-N-retinylethanolamine (named A2E), a well-known fluorophore of lipofuscin, affects the microenvironment of the retina by inducing the expression of several SASP factors including IL13Rα2, thereby contributing to create a pro-inflammatory environment that drives retina senescence and degeneration (J. Wang et al., 2018).

L75 is another marker of immune activation, expressed on the surface of various immune cells, including B cells, T cells monocytes, and NK cells (W. Jiang et al., 1995; Kato et al., 2006). In aging mice, at the mRNA level, LY75 is overexpressed in the RPE/choroid complex and the retina, suggesting the involvement of inflammation and immune activation in pathogenesis of age-related macular degeneration (H. Chen et al., 2008; M. Chen et al., 2010) and the potential application of NACET for the recovery of the healthy status of the retina.

Another five genes differentially regulated in aged retinas and rescued by NACET (*Aldh18a1*, *Ap3b2*, *Atp2a2*, *D630045J12Rik*, *Rimbp3*) are correlated with retinopathy (Assoum et al., 2016; De Bruijn et al., 2018; Rappaport et al., 2017; Shinde et al., 2016; Wolthuis et al., 2014). In particular, *Atp2a2*, also known as Sarcoplasmic/endoplasmic reticulum calcium ATPase 2 (SERCA2), is downregulated in the retina of old mice and upregulated following NACET treatment. SERCA2 is the main subtype of SERCA in the retina, and plays an important role in maintaining Ca^{2+} homeostasis by transporting cytoplasmic Ca^{2+} into ER and sarcoplasmic reticulum (Krizaj, 2005). In ARPE-19 cells, SERCA2 overexpression significantly decreased ER stress-related apoptosis and inflammation (L. Jiang et al., 2020). Moreover, the irreversible oxidation of cysteine 674 (C674) in SERCA2 is increased in the

type 1 diabetic retinal vasculature and replacement of C674 by serine, to represent the partial irreversible oxidation of C674, causes retinopathy in the mouse by mitochondrial mediated apoptosis (Liu et al., 2021).

The ER is an essential intracellular organelle responsible for protein synthesis and folding, and calcium homeostasis. Perturbation of ER functions result in accumulation of unfolded or misfolded proteins that cause an increase in ROS, enhancing oxidative stress and the activation of an unfolded protein response (UPR) in photoreceptors cells. These pathways, involved in endogenous antioxidant defence, if chronically stimulated, determine the activation of pro-apoptotic programs associated with oxidative stress and pro-inflammatory signalling in the retina, leading to retinal degeneration (Domènech & Marfany, 2020; Ni & Lee, 2007; Zhang et al., 2014), and chronic ER-stress is considered a primary pathogenic mechanism leading to AMD (Libby & Gould, 2010).

However, mild UPR upregulates ER chaperones that increase the protein-folding capacity of ER and promote the degradation of misfolded proteins, thereby protecting photoreceptor cells against cell death from oxidative stress and various stimuli (Mendes et al., 2009). From this point of view, it is noteworthy to point out that the transcripts of four genes (*Hspa8*, *Hspa5*, *Hsp90ab1*, and *Calr*) downregulated in aged retina and rescue by NACET code for molecular chaperones. Molecular chaperones include diverse families of multidomain proteins that facilitate and regulate protein folding, unfolding or disaggregation within the cells (Saibil, 2013). Interestingly, mutations in molecular chaperones have been found in inherited retinal dysfunction and degeneration (Kosmaoglou et al., 2008), HSP90α deficiency causes retinal degeneration (Y. Wu et al., 2020) and the expression of HSPA5 plays an important role in maintaining cone photoreceptor structural integrity and is drastically reduced in the donor eyes from atrophic AMD patients (Chintalapudi et al., 2016).

In recent years the high temperature requirement A1 (HTRA1), which results upregulated in aged retina followed NACET treatment, is the subject of drug discovery efforts in AMD because of the prevalence of high-frequency *HTRA1* variants in affected subjects (Yang et al., 2006). However, its precise role in AMD pathology remains controversial (Grassmann et al., 2017; Kanda et al., 2010). Gerhardt and colleagues hypothesized that HTRA1 is implicated in UPR, upregulated by ER and essential for RPE survival under conditions of proteotoxicity. In fact, in a subset of AMD patients, deleterious substitutions in *HTRA1* lower the ER stress threshold of RPE, and cause the collapse of proteome homeostasis, which may be an event that contributes to RPE degeneration (Gerhardt et al. (2017).

In our model, other interesting transcripts downregulated in aged retina and rescued by NACET treatment code for nerve growth factor inducible (VGF) and reelin (RELN). VGF is a polypeptide induced by neurotrophic factors and involved in neurite growth and neuroprotection. VGF is highly expressed in several types of neurons in the retina (Snyder & Salton, 1998) and has been proposed as a treatment of RGCs degeneration because it has protective effects on RGCs in the optic nerve crush (ONC) model (Takeuchi et al., 2018). Moreover, it may be a potential new therapeutic target for Amyotrophic Lateral Sclerosis (ALS) because it protects neuronal cells against ER stress-induced cell death (Shimazawa et al., 2010). RELN is a large secreted glycoprotein that plays a pivotal role for the positioning of neurons throughout brain development (Rice et al., 2001) and interestingly age-related reduction in rod and cone functions has been observed in knock-out mice for both reelin receptors: apolipoprotein E receptor 2 (ApoER2) and very low-density lipoprotein receptor VLDLR (Trotter et al., 2011).

To maintain the correct cell functions and avoid extensive ROS production with further mitochondrial damage and ROS release, damaged and dysfunctional mitochondria must be removed form cells via mitophagy, a mitochondrial-specific type of autophagy (Markaki et al., 2021). The aged retina is characterized by impaired mitophagy, which is linked to AMD pathogenesis (Kaarniranta et al., 2020). In young subjects RPE mitigate ROS generation by the elimination of dysfunctional mitochondria, via the PINK1 Parkin-derived pathway of mitophagy, and by increasing antioxidant defences via NRF2 activation. While in the elderly both the mitophagic process and NRF2 activation are impaired thus causing retinal cell death (Bellezza, 2018). In this context, we identified *Bcl2* and *Bag6* as two important transcripts that showed opposite regulation in aging and following NACET treatment. In addition to its most famous role as anti-apoptotic molecule, BCL2 suppressed mitophagy through inhibition of Parkin (PRKN) translocation to depolarized mitochondria (Hollville et al., 2014), while BAG6 acts as promoter of mitophagy by leading to the activation of the PINK1/PRKN pathway and to the phospho-ubiquitination of mitochondrial proteins (Ragimbeau et al., 2021), thereby suggesting a therapeutic role of NACET to restore age-dependent BCL2 upregulation and BAG6 downregulation.

Lastly, an interesting gene upregulated in aged retina and rescued by NACET, is betacellulin (BTC), a member of the epidermal growth factor (EGF) family that plays an important role in the development of increased retinal vascular permeability in diabetic mice (Anand-Apte et al., 2010).

Taken together our study demonstrated for the first time that NACET activates the NRF2 pathway and thereby it decreases oxidative stress not only as cysteine/GSH precursor but also by modulating the expression of important antioxidant genes, such as those coding for key enzymes involved in the

GSH synthesis (Figure 49). Furthermore, oral administration of NACET in mice has shown that NACET can reach the retina, increase antioxidant defences, and reduce factors related to senescence and inflammation. In conclusion, although preclinical experiments are ultimately required in animal models of the disease, our data show that NACET is a promising antioxidant agent for prevention and therapy of AMD.

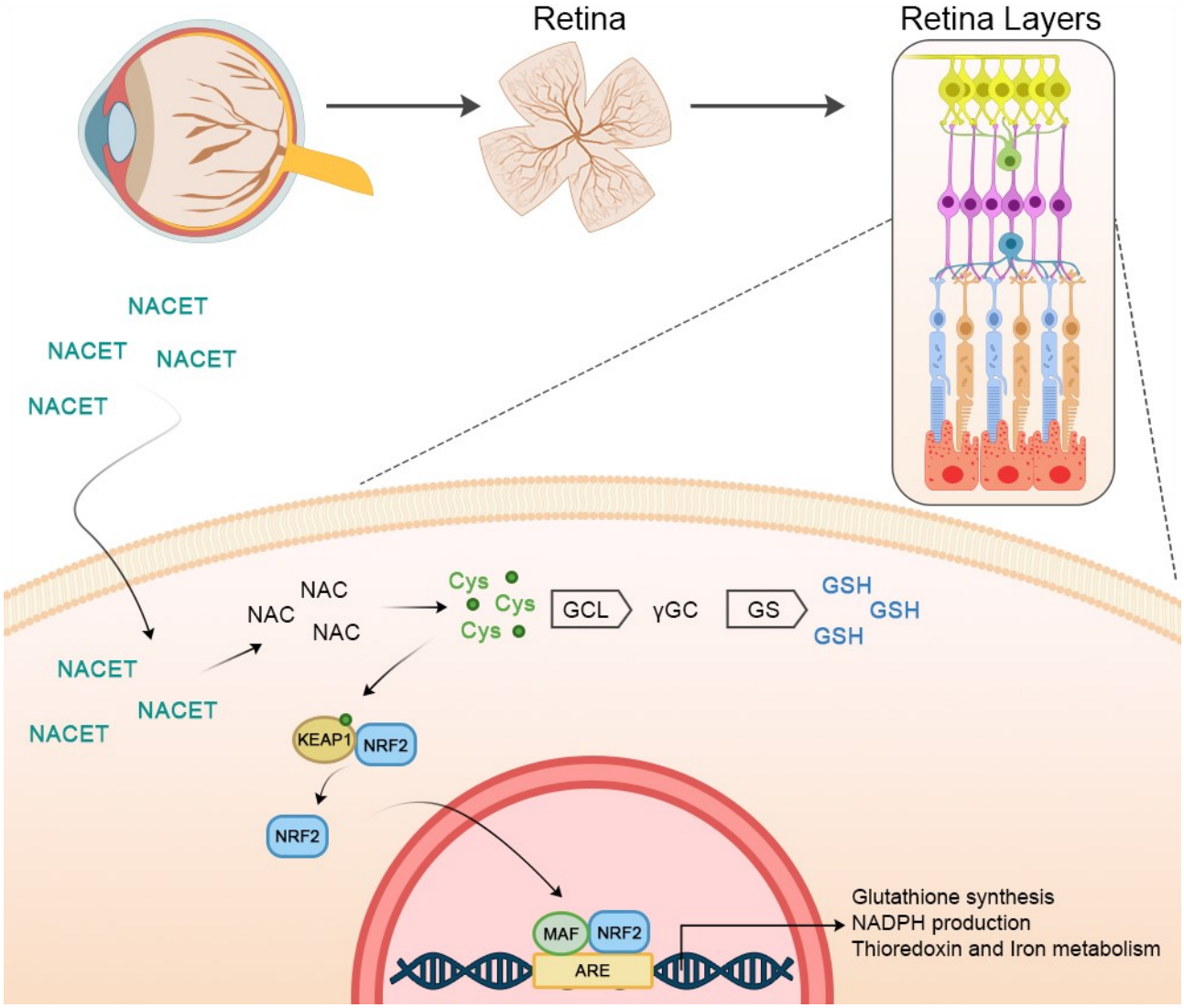

Figure 49. Mechanisms of Nrf2-ARE pathway activation by NACET in neural retina. NACET enters the cell, where it is de-esterified to NAC, that is de-acetylated to cysteine. Cys participates to GSH synthesis and causes NRF2 pathway activation. NRF2 disassociated from KEAP1 translocates into the nucleus and binds to ARE in the promoter regions of various detoxification and anti-antioxidant genes.

6 REFERENCES

Al-Zamil, W. M., & Yassin, S. A. (2017). Recent developments in age-related macular degeneration: A review. *Clinical Interventions in Aging*, *12*, 1313–1330. https://doi.org/10.2147/CIA.S143508

Anand-Apte, B., Ebrahem, Q., Cutler, A., Farage, E., Sugimoto, M., Hollyfield, J., & Folkman, J. (2010). Betacellulin induces increased retinal vascular permeability in mice. *PLoS ONE*, *5*(10). https://doi.org/10.1371/journal.pone.0013444

Ananth, S., Miyauchi, S., Thangaraju, M., Jadeja, R. N., Bartoli, M., Ganapathy, V., & Martin, P. M. (2020). Selenomethionine (Se-Met) induces the cystine/glutamate exchanger SLC7A11 in cultured human retinal pigment epithelial (RPE) cells: Implications for antioxidant therapy in aging retina. *Antioxidants*, *10*(1), 1–17. https://doi.org/10.3390/antiox10010009

Anders, S., Pyl, P. T., & Huber, W. (2015). HTSeq-A Python framework to work with high-throughput sequencing data. *Bioinformatics*, *31*(2), 166–169. https://doi.org/10.1093/bioinformatics/btu638

Assoum, M., Philippe, C., Isidor, B., Perrin, L., Makrythanasis, P., Sondheimer, N., Paris, C., Douglas, J., Lesca, G., Antonarakis, S., Hamamy, H., Jouan, T., Duffourd, Y., Auvin, S., Saunier, A., Begtrup, A., Nowak, C., Chatron, N., Ville, D., … Thevenon, J. (2016). Autosomal-Recessive Mutations in AP3B2, Adaptor-Related Protein Complex 3 Beta 2 Subunit, Cause an Early-Onset Epileptic Encephalopathy with Optic Atrophy. *American Journal of Human Genetics*, *99*(6), 1368–1376. https://doi.org/10.1016/j.ajhg.2016.10.009

Bellezza, I. (2018). Oxidative stress in age-related macular degeneration: NRF2 as therapeutic target. *Frontiers in Pharmacology*, *9*(NOV), 1–7. https://doi.org/10.3389/fphar.2018.01280

Bellezza, I., Giambanco, I., Minelli, A., & Donato, R. (2018). Nrf2-Keap1 signaling in oxidative and reductive stress. *BBA - Molecular Cell Research*, *1865*(5), 721–733. https://doi.org/10.1016/j.bbamcr.2018.02.010

Blasiak, J. (2020). Senescence in the pathogenesis of age-related macular degeneration. *Cellular and Molecular Life Sciences*, *77*(5), 789–805. https://doi.org/10.1007/s00018-019-03420-x

Blasiak, J., Pawlowska, E., Sobczuk, A., Szczepanska, J., & Kaarniranta, K. (2020). The aging stress response and its implication for amd pathogenesis. *International Journal of Molecular Sciences*, *21*(22), 1–22. https://doi.org/10.3390/ijms21228840

Bono, S., Feligioni, M., & Corbo, M. (2021). Impaired antioxidant KEAP1-NRF2 system in amyotrophic lateral sclerosis: NRF2 activation as a potential therapeutic strategy. *Molecular Neurodegeneration*, *16*(1), 1–26. https://doi.org/10.1186/s13024-021-00479-8

Bridges, C. C., Kekuda, R., Wang, H., Prasad, P. D., Mehta, P., Huang, W., Smith, S. B., & Ganapathy, V. (2001). Structure, function, and regulation of human cystine/glutamate transporter in retinal pigment epithelial cells. *Investigative Ophthalmology and Visual Science*, *42*(1), 47–54.

Caceres, P. S., & Rodriguez-Boulan, E. (2020). Retinal pigment epithelium polarity in health and blinding diseases. *Current Opinion in Cell Biology*, *62*, 37–45. https://doi.org/10.1016/j.ceb.2019.08.001

Carpi-Santos, R., & Calaza, K. C. (2018). Alterations in System xc− Expression in the Retina of Type 1 Diabetic Rats and the Role of Nrf2. *Molecular Neurobiology*, *55*(10), 7941–7948. https://doi.org/10.1007/s12035-018-0961-8

Chakravarthy, U., Evans, J., & Rosenfeld, P. J. (2010). Age related macular degeneration. *BMJ (Online)*, *340*(7745), 526–530. https://doi.org/10.1136/bmj.c981

Chandriani, S., DePianto, D. J., N'Diaye, E. N., Abbas, A. R., Jackman, J., Bevers, J., Ramirez-Carrozzi, V., Pappu, R., Kauder, S. E., Toy, K., Ha, C., Modrusan, Z., Wu, L. C., Collard, H. R., Wolters, P. J., Egen, J. G., & Arron, J. R. (2014). Endogenously Expressed IL-13Rα2 Attenuates IL-13–Mediated Responses but Does Not Activate Signaling in Human Lung Fibroblasts. *The Journal of Immunology*, *193*(1), 111–119. https://doi.org/10.4049/jimmunol.1301761

Chen, H., Liu, B., Lukas, T. J., & Neufeld, A. H. (2008). The aged retinal pigment epithelium/choroid: A potential substratum for the pathogenesis of age-related macular degeneration. *PLoS ONE*, *3*(6). https://doi.org/10.1371/journal.pone.0002339

Chen, M., Muckersie, E., Forrester, J. V., & Xu, H. (2010). Immune activation in retinal aging: A gene expression study. *Investigative Ophthalmology and Visual Science*, *51*(11), 5888–5896. https://doi.org/10.1167/iovs.09-5103

Chintalapudi, S. R., Wang, X. F., Li, H., Lau, Y. H. C., Williams, R. W., & Jablonski, M. M. (2016). Genetic and immunohistochemical analysis of HSPA5 in mouse and human retinas. *Molecular Vision*, *22*(November), 1318–1331. http://www.molvis.org/molvis/v22/1318

Cloer, E. W., Goldfarb, D., Schrank, T. P., Weissman, B. E., & Major, M. B. (2019). Nrf2 activation in cancer: From DNA to protein. *Cancer Research*, *79*(5), 889–898. https://doi.org/10.1158/0008-5472.CAN-18-2723

Cuadrado, A. (2015). Structural and functional characterization of Nrf2 degradation by glycogen synthase kinase 3/β-TrCP. *Free Radical Biology and Medicine*, *88*(Part B), 147–157. https://doi.org/10.1016/j.freeradbiomed.2015.04.029

Cuollo, L., Antonangeli, F., Santoni, A., & Soriani, A. (2020). The Senescence-Associated Secretory Phenotype and Age-Related Diseases. *Biology*, *9*(485), 1–16. https://doi.org/10.3390/biology9120485

De Bruijn, S. E., Verbakel, S. K., De Vrieze, E., Kremer, H., Cremers, F. P. M., Hoyng, C. B., Ingeborgh Van Den Born, L., & Roosing, S. (2018). Homozygous variants in KIAA1549, encoding a ciliary protein, are associated with autosomal recessive retinitis pigmentosa. *Journal of Medical Genetics*, *55*(10), 705–712. https://doi.org/10.1136/jmedgenet-2018-105364

Domènech, E. B., & Marfany, G. (2020). The relevance of oxidative stress in the pathogenesis and therapy of retinal dystrophies. *Antioxidants*, *9*(4), 1–22. https://doi.org/10.3390/antiox9040347

Dun, Y., Mysona, B., Van Ells, T., Amarnath, L., Shamsul Ola, M., Ganapathy, V., & Smith, S. B. (2006). Expression of the cystine-glutamate exchanger (xc-) in retinal ganglion cells and regulation by nitric oxide and oxidative stress. *Cell and Tissue Research*, *324*(2), 189–202. https://doi.org/10.1007/s00441-005-0116-x

Dunn, K. C., Aotaki-Keen, A. E., Putkey, F. R., & Hjelmeland, L. M. (1996). ARPE-19, a human retinal pigment epithelial cell line with differentiated properties. *Experimental Eye Research*, *62*(2), 155–170. https://doi.org/10.1006/exer.1996.0020

Finkel, T., & Holbrook, N. J. (2000). Oxidants, Oxidative Stress and Biology of Ageing. *Insight Review Articles*, *408*(November), 239–247. https://doi.org/10.1038/35041687

Franceschini, C., Bonafè, M., Valensin, S., Olivieri, F., De Luca, M., Ottaviani, E., & De Benedictis, G. (2000). *Inflamm-aging An Evolutionary Perspective on Immunosenescence.PDF* (p. Annals of the New York Academy of Sciences 908(1):). https://doi.org/10.1111/j.1749-

6632.2000.tb06651.x

Fritsche, L. G., Igl, W., Bailey, J. N. C., Grassmann, F., Sengupta, S., Bragg-Gresham, J. L., Burdon, K. P., Hebbring, S. J., Wen, C., Gorski, M., Kim, I. K., Cho, D., Zack, D., Souied, E., Scholl, H. P. N., Bala, E., Lee, K. E., Hunter, D. J., Sardell, R. J., … Heid, I. M. (2016). A large genome-wide association study of age-related macular degeneration highlights contributions of rare and common variants. *Nature Genetics*, *48*(2), 134–143. https://doi.org/10.1038/ng.3448

Gerhardt, M. J., Marsh, J. A., Morrison, M., Kazlauskas, A., Khadka, A., Rosenkranz, S., DeAngelis, M. M., Saint-Geniez, M., & Jacobo, S. M. P. (2017). Erratum: ER stress-induced aggresome trafficking of HtrA1 protects against proteotoxicity (Journal of molecular cell biology (2017) 9 6 (516-532)). *Journal of Molecular Cell Biology*, *9*(6), 533. https://doi.org/10.1093/jmcb/mjx040

Giustarini, D., Galvagni, F., Dalle Donne, I., Milzani, A., Severi, F. M., Santucci, A., & Rossi, R. (2018). N-acetylcysteine ethyl ester as GSH enhancer in human primary endothelial cells: A comparative study with other drugs. *Free Radical Biology and Medicine*, *126*(June), 202–209. https://doi.org/10.1016/j.freeradbiomed.2018.08.013

Giustarini, D., Milzani, A., Dalle-Donne, I., Tsikas, D., & Rossi, R. (2012). N-Acetylcysteine ethyl ester (NACET): A novel lipophilic cell-permeable cysteine derivative with an unusual pharmacokinetic feature and remarkable antioxidant potential. *Biochemical Pharmacology*, *84*(11), 1522–1533. https://doi.org/10.1016/j.bcp.2012.09.010

Gorgoulis, V., Adams, P. D., Alimonti, A., Bennett, D. C., Bischof, O., Bishop, C., Campisi, J., Collado, M., Evangelou, K., Ferbeyre, G., Gil, J., Hara, E., Krizhanovsky, V., Jurk, D., Maier, A. B., Narita, M., Niedernhofer, L., Passos, J. F., Robbins, P. D., … Demaria, M. (2019). Cellular Senescence: Defining a Path Forward. *Cell*, *179*(4), 813–827. https://doi.org/10.1016/j.cell.2019.10.005

Grassmann, F., Heid, I. M., Weber, B. H. F., Fritsche, L. G., Igl, W., Bailey, J. N., Grassmann, F., Sengupta, S., Bragg-Gresham, J. L., Burdon, K. P., Hebbring, S. J., Wen, C., Gorski, M., Kim, I. K., Cho, D., Zack, D., Souied, E., Scholl, H. P., Bala, E., … Heid, I. M. (2017). Recombinant haplotypes narrow the ARMS2/HTRA1 association signal for age-related macular degeneration. *Genetics*, *205*(2), 919–924. https://doi.org/10.1534/genetics.116.195966

Habib, E., Linher-Melville, K., Lin, H. X., & Singh, G. (2015). Expression of xCT and activity of system xc- are regulated by NRF2 in human breast cancer cells in response to oxidative stress. *Redox Biology*, *5*(March), 33–42. https://doi.org/10.1016/j.redox.2015.03.003

Handa, J. T., Rickman, C. B., Dick, A. D., Gorin, M. B., Miller, J. W., Toth, C. A., Uef, M., Zarbin, M., & Farrer, L. A. (2019). A systems biology approach towards understanding and treating non-neovascular age-related macular degeneration. *Nature Communications*, *10*, 1–11. https://doi.org/10.1038/s41467-019-11262-1

Heesterbeek, T. J., Lorés-Motta, L., Hoyng, C. B., Lechanteur, Y. T. E., & den Hollander, A. I. (2020). Risk factors for progression of age-related macular degeneration. *Ophthalmic and Physiological Optics*, *40*(2), 140–170. https://doi.org/10.1111/opo.12675

Hejtmancik, J. F., & Nickerson, J. M. (2015). Molecular Biology of Eye Disease. *Progress in Molecular Biology and Translational Science*, *134*, xix–xx. https://doi.org/10.1016/S1877-1173(15)00179-9

Hollville, E., Carroll, R. G., Cullen, S. P., & Martin, S. J. (2014). Bcl-2 family proteins participate in mitochondrial quality control by regulating parkin/PINK1-dependent mitophagy. *Molecular*

Cell, *55*(3), 451–466. https://doi.org/10.1016/j.molcel.2014.06.001

Jaramillo, M. C., & Zhang, D. D. (2013). The emerging role of the Nrf2 – Keap1 signaling pathway in cancer. *Genes & Development*, *27*(20), 2179–2191. https://doi.org/10.1101/gad.225680.113

Jiang, L., Wang, C., & Shen, X. (2020). LncRNA GAS5 suppresses ER stress-induced apoptosis and inflammation by regulating SERCA2b in HG-treated retinal epithelial cell. *Molecular Medicine Reports*, *22*(2), 1072–1080. https://doi.org/10.3892/mmr.2020.11163

Jiang, W., Swiggard, W. J., Heufler, C., Peng, M., Mirza, A., Steinman, R. M., & Nussenzweig, M. C. (1995). The receptor DEC-205 expressed by dendritic cells and thymic epithelial cells is involved in antigen processing. In *Nature* (Vol. 375, Issue 6527, pp. 151–155). https://doi.org/10.1038/375151a0

Kaarniranta, K., Uusitalo, H., Blasiak, J., Felszeghy, S., Kannan, R., Kauppinen, A., Salminen, A., Sinha, D., & Ferrington, D. (2020). Mechanisms of mitochondrial dysfunction and their impact on age-related macular degeneration. *Progress in Retinal and Eye Research*, *79*, 1–46. https://doi.org/10.1016/j.preteyeres.2020.100858

Kanda, A., Stambolian, D., Chen, W., Curcio, C. A., Abecasis, G. R., & Swaroop, A. (2010). Age-related macular degeneration-associated variants at chromosome 10q26 do not significantly alter ARMS2 and HTRA1 transcript levels in the human retina. Molecular Vision, 16(March), 1317–1323. http://www.molvis.org/molvis/v16/a145

Kato, M., McDonald, K. J., Khan, S., Ross, I. L., Vuckovic, S., Chen, K., Munster, D., MacDonald, K. P. A., & Hart, D. N. J. (2006). Expression of human DEC-205 (CD205) multilectin receptor on leukocytes. *International Immunology*, *18*(6), 857–869. https://doi.org/10.1093/intimm/dxl022

Kauppinen, A. (2020). Introduction to the multi-author review on macular degeneration. *Cellular and Molecular Life Sciences*, *77*(5), 779–780. https://doi.org/10.1007/s00018-019-03418-5

Kawakami, K., Taguchi, J., Murata, T., & Puri, R. K. (2001). The interleukin-13 receptor α2 chain: An essential component for binding and internalization but not for interleukin-13-induced signal transduction through the STAT6 pathway. *Blood*, *97*(9), 2673–2679. https://doi.org/10.1182/blood.V97.9.2673

Kohl, J. B., Mellis, A. T., & Schwarz, G. (2019). Homeostatic impact of sulfite and hydrogen sulfide on cysteine catabolism. *British Journal of Pharmacology*, *176*(4), 554–570. https://doi.org/10.1111/bph.14464

Kosmaoglou, M., Schwarz, N., Bett, J. S., & Cheetham, M. E. (2008). Molecular chaperones and photoreceptor function. *Progress in Retinal and Eye Research*, *27*(4), 434–449. https://doi.org/10.1016/j.preteyeres.2008.03.001

Krämer, A., Green, J., Pollard, J., & Tugendreich, S. (2014). Causal analysis approaches in ingenuity pathway analysis. *Bioinformatics*, *30*(4), 523–530. https://doi.org/10.1093/bioinformatics/btt703

Krizaj, D. (2005). Serca isoform expression in the mammalian retina. *Experimental Eye Research*, *81*(6), 690–699. https://doi.org/10.1016/j.exer.2005.04.007

Kularatne, R. N., Bulumulla, C., Catchpole, T., Takacs, A., Christie, A., Stefan, M. C., & Csaky, K. G. (2020). Protection of human retinal pigment epithelial cells from oxidative damage using cysteine prodrugs. *Free Radical Biology and Medicine*, *152*(December 2019), 386–394. https://doi.org/10.1016/j.freeradbiomed.2020.03.024

Lambert, N. G., ElShelmani, H., Singh, M. K., Mansergh, F. C., Wride, M. A., Padilla, M., Keegan, D., Hogg, R. E., & Ambati, B. K. (2016). Risk factors and biomarkers of age-related macular degeneration. *Progress in Retinal and Eye Research*, *54*, 64–102. https://doi.org/10.1016/j.preteyeres.2016.04.003

Lee Ann, R. A. (2012). Clinical Anatomy and Physiology of the Visual System. In *Clinical Anatomy and Physiology of the Visual System*. https://doi.org/10.1016/C2009-0-56108-9

Lee, K. S., Lin, S., Copland, D. A., Dick, A. D., & Liu, J. (2021). Cellular senescence in the aging retina and developments of senotherapies for age-related macular degeneration. *Journal of Neuroinflammation*, *18*(1), 1–17. https://doi.org/10.1186/s12974-021-02088-0

Lehmann, G. L., Benedicto, I., Philp, N. J., & Rodriguez-Boulan, E. (2014). Plasma membrane protein polarity and trafficking in RPE cells: Past, present and future. *Experimental Eye Research*, *126*, 5–15. https://doi.org/10.1016/j.exer.2014.04.021

Libby, R. T., & Gould, D. B. (2010). Endoplasmic reticulum stress as a primary pathogenic mechanism leading to age-related macular degeneration. *Advances in Experimental Medicine and Biology*, *664*, 403–409. https://doi.org/10.1007/978-1-4419-1399-9_46

Lim, L. S., Mitchell, P., Seddon, J. M., Holz, F. G., & Wong, T. Y. (2012). Age-related macular degeneration. *The Lancet*, *379*(9827), 1728–1738. https://doi.org/10.1016/S0140-6736(12)60282-7

Lin, H., Qiao, Y., Yang, H., Nan, Q., Qu, W., Feng, F., Liu, W., Chen, Y., & Sun, H. (2020). Small molecular Nrf2 inhibitors as chemosensitizers for cancer therapy. *Future Medicinal Chemistry*, *12*(3), 243–267. https://doi.org/10.4155/fmc-2019-0285

Lin, W., Wang, C., Liu, G., Bi, C., Wang, X., Zhou, Q., & Jin, H. (2020). SLC7A11/xCT in cancer: biological functions and therapeutic implications. *American Journal of Cancer Research*, *10*(10), 3106–3126. https://www.ncbi.nlm.nih.gov/pmc/articles/PMC7642655

Liu, G., Wu, F., Wu, H., Wang, Y., Jiang, X., Hu, P., & Tong, X. (2021). Inactivation of cysteine 674 in the sarcoplasmic/endoplasmic reticulum calcium ATPase 2 causes retinopathy in the mouse. *Experimental Eye Research*, *207*(April), 108559. https://doi.org/10.1016/j.exer.2021.108559

Lo, J. Y., Spatola, B. N., & Curran, S. P. (2017). WDR23 regulates NRF2 independently of KEAP1. *PLoS Genetics*, *13*(4), 1–26. https://doi.org/10.1371/journal.pgen.1006762

Love, M. I., Huber, W., & Anders, S. (2014). Moderated estimation of fold change and dispersion for RNA-seq data with DESeq2. *Genome Biology*, *15*(12), 550. https://doi.org/10.1186/s13059-014-0550-8

Marazita, M. C., Dugour, A., Marquioni-Ramella, M. D., Figueroa, J. M., & Suburo, A. M. (2016). Oxidative stress-induced premature senescence dysregulates VEGF and CFH expression in retinal pigment epithelial cells: Implications for Age-related Macular Degeneration. *Redox Biology*, *7*, 78–87. https://doi.org/10.1016/j.redox.2015.11.011

Marí, M., Colell, A., Morales, A., Von Montfort, C., Garcia-Ruiz, C., & Fernández-Checa, J. C. (2010). Redox control of liver function in health and disease. *Antioxidants and Redox Signaling*, *12*(11), 1295–1331. https://doi.org/10.1089/ars.2009.2634

Markaki, M., Tsagkari, D., & Tavernarakis, N. (2021). Mitophagy mechanisms in neuronal physiology and pathology during ageing. *Biophysical Reviews*, *13*(6), 955–965. https://doi.org/10.1007/s12551-021-00894-7

Martis, R. M., Knight, L. J., Donaldson, P. J., & Lim, J. C. (2020). Identification, Expression, and

Roles of the Cystine/Glutamate Antiporter in Ocular Tissues. *Oxidative Medicine and Cellular Longevity*, *2020*. https://doi.org/10.1155/2020/4594606

Mendes, C. S., Levet, C., Chatelain, G., Dourlen, P., Fouillet, A., Dichtel-Danjoy, M. L., Gambis, A., Ryoo, H. D., Steller, H., & Mollereau, B. (2009). ER stress protects from retinal degeneration. *EMBO Journal*, *28*(9), 1296–1307. https://doi.org/10.1038/emboj.2009.76

Miller, J. W., Bagheri, S., Vavvas, D. G., Service, R., Eye, M., & Medical, H. (2017). Advances in Age-related Macular Degeneration Understanding and Therapy. *US Ophthalmic Rev.*, *10*(2), 119–130. https://doi.org/10.17925/USOR.2017.10.02.119.Advances

Murali, A., Krishnakumar, S., Subramanian, A., & Parameswaran, S. (2020). Bruch's membrane pathology: A mechanistic perspective. *European Journal of Ophthalmology*, *30*(6), 1195–1206. https://doi.org/10.1177/1120672120919337

Nakagami, Y. (2016). Nrf2 Is an Attractive Therapeutic Target for Retinal Diseases. *Oxidative Medicine and Cellular Longevity*, *2016*. https://doi.org/10.1155/2016/7469326

Ni, M., & Lee, A. S. (2007). ER chaperones in mammalian development and human diseases. *FEBS Letters*, *581*(19), 3641–3651. https://doi.org/10.1016/j.febslet.2007.04.045

Nissen, M. H., & Röpke, C. (2005). The Biology of the Eye. In *Advances in Organ Biology* (Vol. 10, pp. 291–305). https://doi.org/10.1016/S1569-2590(05)10011-1

Niture, S. K., Khatri, R., & Jaiswal, A. K. (2014). Regulation of Nrf2—an update. *Free Radical Biology and Medicine*, *66*, 36–44. https://doi.org/10.1016/j.freeradbiomed.2013.02.008

Park, J. Y., Kim, S., Sohn, H. Y., Koh, Y. H., & Jo, C. (2019). TFEB activates Nrf2 by repressing its E3 ubiquitin ligase DCAF11 and promoting phosphorylation of p62. *Scientific Reports*, *9*(1), 1–12. https://doi.org/10.1038/s41598-019-50877-8

Ragimbeau, R., El Kebriti, L., Sebti, S., Fourgous, E., Boulahtouf, A., Arena, G., Espert, L., Turtoi, A., Gongora, C., Houédé, N., & Pattingre, S. (2021). BAG6 promotes PINK1 signaling pathway and is essential for mitophagy. *FASEB Journal*, *35*(2). https://doi.org/10.1096/fj.202000930R

Rappaport, N., Twik, M., Plaschkes, I., Nudel, R., Stein, T. I., Levitt, J., Gershoni, M., Morrey, C. P., Safran, M., & Lancet, D. (2017). MalaCards: An amalgamated human disease compendium with diverse clinical and genetic annotation and structured search. *Nucleic Acids Research*, *45*(D1), D877–D887. https://doi.org/10.1093/nar/gkw1012

Reuter, S., Gupta, S. C., Chaturvedi, M. M., & Aggarwal, B. B. (2010). Oxidative stress, inflammation, and cancer: How are they linked? *Free Radical Biology and Medicine*, *49*(11), 1603–1616. https://doi.org/10.1016/j.freeradbiomed.2010.09.006

Rice, D. S., Nusinowitz, S., Azimi, A. M., Martínez, A., Soriano, E., & Curran, T. (2001). The Reelin Pathway modulates the structure and function of retinal synaptic circuitry. *Neuron*, *31*(6), 929–941. https://doi.org/10.1016/S0896-6273(01)00436-6

Saibil, H. (2013). Chaperone machines for protein folding, unfolding and disaggregation. *Nature Reviews Molecular Cell Biology*, *14*(10), 630–642. https://doi.org/10.1038/nrm3658

Sharma, K., Sharma, N. K., & Anand, A. (2014). Why AMD is a disease of ageing and not of development: Mechanisms and insights. *Frontiers in Aging Neuroscience*, *6*(JUL), 1–11. https://doi.org/10.3389/fnagi.2014.00151

Shihan, M. H., Novo, S. G., Le Marchand, S. J., Wang, Y., & Duncan, M. K. (2021). A simple method for quantitating confocal fluorescent images. *Biochemistry and Biophysics Reports*, *25*, 100916.

https://doi.org/10.1016/j.bbrep.2021.100916

Shimazawa, M., Tanaka, H., Ito, Y., Morimoto, N., Tsuruma, K., Kadokura, M., Tamura, S., Inoue, T., Yamada, M., Takahashi, H., Warita, H., Aoki, M., & Hara, H. (2010). An Inducer of VGF protects cells against ER stress-induced cell death and prolongs survival in the mutant SOD1 animal Models of Familial ALS. *PLoS ONE*, *5*(12). https://doi.org/10.1371/journal.pone.0015307

Shinde, V., Kotla, P., Strang, C., & Gorbatyuk, M. (2016). Unfolded protein response-induced dysregulation of calcium homeostasis promotes retinal degeneration in rat models of autosomal dominant retinitis pigmentosa. *Cell Death and Disease*, *7*, 1–11. https://doi.org/10.1038/cddis.2015.325

Simmons, A. B., & Fuerst, P. G. (2018). Analysis of Retinal Vascular Plexuses and Interplexus Connections. In *Methods in Molecular Biology* (pp. 317–330). https://doi.org/10.1007/978-1-4939-7720-8_22

Snyder, S. E., & Salton, S. R. J. (1998). Expression of VGF mRNA in the adult rat central nervous system. *Journal of Comparative Neurology*, *394*(1), 91–105. https://doi.org/10.1002/(SICI)1096-9861(19980427)394:1<91::AID-CNE7>3.0.CO;2-C

Sung, C. H., & Chuang, J. Z. (2010). The cell biology of vision. *Journal of Cell Biology*, *190*(6), 953–963. https://doi.org/10.1083/jcb.201006020

Takeuchi, H., Inagaki, S., Morozumi, W., Nakano, Y., Inoue, Y., Kuse, Y., Mizoguchi, T., Nakamura, S., Funato, M., Kaneko, H., Hara, H., & Shimazawa, M. (2018). VGF nerve growth factor inducible is involved in retinal ganglion cells death induced by optic nerve crush. *Scientific Reports*, *8*(1), 1–13. https://doi.org/10.1038/s41598-018-34585-3

Taylor, D. J., Hobby, A. E., Binns, A. M., & Crabb, D. P. (2016). How does age-related macular degeneration affect real-world visual ability and quality of life? A systematic review. *BMJ Open*, *6*(12), 1–13. https://doi.org/10.1136/bmjopen-2016-011504

Tonelli, C., Chio, I. I. C., & Tuveson, D. A. (2018). Transcriptional Regulation by Nrf2. *Antioxidants and Redox Signaling*, *29*(17), 1727–1745. https://doi.org/10.1089/ars.2017.7342

Tosi, G. M., Giustarini, D., Franci, L., Minetti, A., Imperatore, F., Caldi, E., Fiorenzani, P., Aloisi, A. M., Sparatore, A., Rossi, R., Chiariello, M., Orlandini, M., & Galvagni, F. (2021). Superior properties of N-acetylcysteine ethyl ester over n-acetyl cysteine to prevent retinal pigment epithelial cells oxidative damage. *International Journal of Molecular Sciences*, *22*(2), 1–12. https://doi.org/10.3390/ijms22020600

Trapnell, C., Roberts, A., Goff, L., Pertea, G., Kim, D., Kelley, D. R., Pimentel, H., Salzberg, S. L., Rinn, J. L., & Pachter, L. (2012). Differential gene and transcript expression analysis of RNA-seq experiments with TopHat and Cufflinks. *Nature Protocols*, *7*(3), 562–578. https://doi.org/10.1038/nprot.2012.016

Trotter, J. H., Klein, M., Jinwal, U. K., Abisambra, J. F., Dickey, C. A., Tharkur, J., Masiulis, I., Ding, J., Locke, K. G., Rickman, C. B., Birch, D. G., Weeber, E. J., & Herz, J. (2011). ApoER2 function in the establishment and maintenance of retinal synaptic connectivity. *Journal of Neuroscience*, *31*(40), 14413–14423. https://doi.org/10.1523/JNEUROSCI.3135-11.2011

Wang, J., Feng, Y., Han, P., Wang, F., Luo, X., Liang, J., Sun, X., Ye, J., Lu, Y., & Sun, X. (2018). Photosensitization of A2E triggers telomere dysfunction and accelerates retinal pigment epithelium senescence article. *Cell Death and Disease*, *9*(2). https://doi.org/10.1038/s41419-017-0200-7

Wang, J., Shanmugam, A., Markand, S., Zorrilla, E., Ganapathy, V., & Smith, S. B. (2015). Sigma 1 receptor regulates the oxidative stress response in primary retinal Müller glial cells via NRF2 signaling and system xc−, the Na+-independent glutamate–cystine exchanger. *Free Radical Biology and Medicine*, *86*(3), 25–36. https://doi.org/10.1016/j.freeradbiomed.2015.04.009

Wang, X. F., & Cynader, M. S. (2001). Pyruvate released by astrocytes protects neurons from copper-catalyzed cysteine neurotoxicity. *Journal of Neuroscience*, *21*(10), 3322–3331. https://doi.org/10.1523/jneurosci.21-10-03322.2001

Wolthuis, D. F. G. J., Van Asbeck, E., Mohamed, M., Gardeitchik, T., Lim-Melia, E. R., Wevers, R. A., & Morava, E. (2014). Cutis laxa, fat pads and retinopathy due to ALDH18A1 mutation and review of the literature. *European Journal of Paediatric Neurology*, *18*(4), 511–515. https://doi.org/10.1016/j.ejpn.2014.01.003

Wu, S., Lu, H., & Bai, Y. (2019). Nrf2 in cancers: A double-edged sword. *Cancer Medicine*, *8*(5), 2252–2267. https://doi.org/10.1002/cam4.2101

Wu, T., Zhao, F., Gao, B., Tan, C., Yagishita, N., Nakajima, T., Wong, P. K., Chapman, E., Fang, D., & Zhang, D. D. (2014). Hrd1 suppresses Nrf2-mediated cellular protection during liver cirrhosis. *Genes and Development*, *28*(7), 708–722. https://doi.org/10.1101/gad.238246.114

Wu, W. L., & Papagiannakopoulos, T. (2020). The Pleiotropic Role of the KEAP1/NRF2 Pathway in Cancer. *Annual Review of Cancer Biology*, *4*, 413–435. https://doi.org/10.1146/annurev-cancerbio-030518-055627

Wu, Y., Zheng, X., Ding, Y., Zhou, M., Wei, Z., Liu, T., & Liao, K. (2020). The molecular chaperone Hsp90α deficiency causes retinal degeneration by disrupting Golgi organization and vesicle transportation in photoreceptors. *Journal of Molecular Cell Biology*, *12*(3), 216–229. https://doi.org/10.1093/jmcb/mjz048

Yang, Z., Camp, N. J., Sun, H., Tong, Z., Gibbs, D., Cameron, D. J., Chen, H., Zhao, Y., Pearson, E., Li, X., Chien, J., DeWan, A., Harmon, J., Bernstein, P. S., Shridhar, V., Zabriskie, N. A., Hoh, J., Howes, K., & Zhang, K. (2006). A variant of the HTRA1 gene increases susceptibility to age-related macular degeneration. *Science*, *314*(5801), 992–993. https://doi.org/10.1126/science.1133811

Zhang, S. X., Sanders, E., Fliesler, S. J., & Wang, J. J. (2014). Endoplasmic reticulum stress and the unfolded protein responses in retinal degeneration. *Experimental Eye Research*, *125*(716), 30–40. https://doi.org/10.1016/j.exer.2014.04.015

Zuo, L., Prather, E. R., Stetskiv, M., Garrison, D. E., Meade, J. R., Peace, T. I., & Zhou, T. (2019). Inflammaging and oxidative stress in human diseases: From molecular mechanisms to novel treatments. *International Journal of Molecular Sciences*, *20*(18). https://doi.org/10.3390/ijms20184472